

Detection and isotopic characterisation of methane emissions

An integrated approach developing and applying mobile
methods and stationary measurements



Mag. Mounir Takriti

**This thesis is submitted for the degree of Doctor of
Philosophy**

September 2018

Lancaster Environment Centre

Für Mutti

Declaration

This thesis has not been submitted in support of an application for another degree at this or any other university. It is the result of my own work and includes nothing that is the outcome of work done in collaboration except where specifically indicated. Many of the ideas in this thesis were the product of discussions with my supervisors, Sue Ward, Peter Wynn, and Niall McNamara.

Statement of authorship

This thesis has been prepared in the alternative format, as a set of three papers, presented in Chapters 2–4, as intended for submission to peer-reviewed journals. Chapter 2 and Chapter 4 have co-authors in addition to my supervisory team. Please find below details of these publications with information regarding my contributions, as certified by the signature of all co-authors.

Chapter 2 is intended for submission as:

Takriti, M., Wynn, P., Elias, D., Ward, S., McNamara, N. (2018). Mobile methane measurements: Effects of instrument specifications on data interpretation, reproducibility, and isotopic precision. In preparation.

M Takriti was involved in planning the instrumental setup, planned the experiment, assembled and built the experimental equipment, carried out the full sampling, performed the full data analysis, developed the model and wrote the manuscript.

Chapter 3 is intended for submission as:

Takriti, M., Wynn, P., Ward, S., McNamara, N. (2018). Isotopic characterisation and mobile detection of methane emissions in North West England. In preparation. M Takriti was responsible for planning, setup of experimental equipment, sampling, data analysis, and writing of the manuscript.

Chapter 4 is intended for submission as:

Takriti, M., Chadwick, A., Rose, R., Dodd, B., Oakley, S., Wynn, P., McNamara, N., Ward, S. (2018). Large seasonal and interannual variations in CH₄ emissions do not affect carbon and hydrogen isotopes from an ombrotrophic peat bog. In preparation.

M Takriti was involved in planning the experiment and performed all the isotopic data collection, part of the flux data collection, performed all flux and isotopic data analysis and wrote the manuscript which incorporated data, methodology and analysis from co-authors.

Yours sincerely



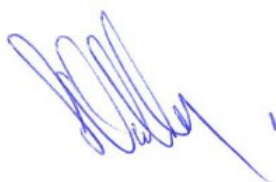
Alexander Chadwick



Rob Rose



Beverly Dodd



Simon Oakley



Dafydd Elias



Sue Ward



Peter Wynn



Niall McNamara

Abstract

Methane (CH₄) is a powerful greenhouse gas which is formed through both microbial and geological processes. Emissions of CH₄ originate from natural sources, such as wetlands, and from anthropogenic sources, such as agriculture, fossil fuel infrastructure, and landfills. Due to anthropogenic activity, atmospheric concentrations of CH₄ have increased by 160% since preindustrial times and are responsible for around 20% of total radiative forcing. Considerable uncertainties over the contribution of different sources remain, due to large spatial and temporal variability and because emission sources are often co-located in the landscape, hindering accurate attribution of emissions. Thus, understanding regional CH₄ sources is important for reducing fugitive emissions and to better constrain atmospheric CH₄ budgets. Stable isotope analysis is a powerful method for constraining methane budgets as source categories differ in their isotopic signatures.

My aim in this thesis was to develop and apply isotope-based methods to characterise, and attribute CH₄ emissions. I developed a system for mobile isotopic CH₄ measurements and used instrument comparisons and model simulations to evaluate system performance. My findings have implications for the interpretation and comparability of data and provide a framework for optimising sampling strategies (Chapter 2). I used dual-isotope sampling and mobile measurements to characterise and identify emission sources in North West England prior to the start of shale gas exploration. My results show that dual isotope analysis can distinguish between microbial emission sources in the region and provide evidence for offshore emissions. Mobile measurements identified fugitive emissions from landfills and gas pipelines (Chapter 3). To investigate seasonal variations in wetland isotopic signatures, I performed a 2.5-year monitoring study at an ombrotrophic peat bog. Despite large changes in emission fluxes over time and, I found constant isotopic signatures throughout the sampling period (Chapter 4).

The work presented in this thesis provides insights for evaluating novel methods for CH₄ emission measurements and contribute to the understanding of emission sources needed to effectively constrain CH₄ budgets and reduce emissions.

Acknowledgements

This PhD project was funded through a Lancaster University Faculty for Science and Technology studentship, and was conducted in collaboration with the Centre for Ecology and Hydrology. Additional funding was received through an FST early career small grant awarded to by the research committee to S Ward, as well as an Ecological Continuity Trust small grant awarded to M Takriti.

This thesis would not have been possible without the support of many people who provided advice, guidance, encouragement, and help.

Thank you to my supervisors, Sue, Peter, and Niall, for your unwavering support, mentoring, and encouragement over these last four years. It was an amazing journey.

Thank you to Roger Timmis, for the many contacts and for always keeping me in the loop, to Laura Smith, David Elphinstone, Ray Walker, Richard Phillips, Richard Miller, Rob Petley-Jones, and Phil Mason, for arranging access to field sites.

Thank you to all the people who helped me with fieldwork, James, Radim, Maria, Dee, Simon, Arlette, Yanan. A special thank you to Rob, Bev, and Alex, for carrying that “ultraportable” analyser up that hill so many times.

Thank you to all the people I have shared an office with over the years, Katharine, Sam, Wallace, Kasia, Guy, Rosanne, Craig, Gabi, Yasmin, it was an amazing time with you all. To Annette, Kelly, Daff, the Lab Group, the PGR office, the A-Team, and all the people and institutions that keep LEC and CEH running, provide support, and make it an amazing place, thank you. Thank you, Natalie, for your incredible support on the final straight.

Contents

1 INTRODUCTION	1
1.1 Methane sources	3
1.1.1 Methane source attribution.....	4
1.1.2 Natural gas.....	7
1.1.3 Microbial methanogenesis.....	8
1.1.4 Wetlands.....	9
1.1.5 Waste treatment.....	11
1.1.6 Ruminant livestock.....	13
1.2 Methods for estimating CH ₄ emissions.....	13
1.2.1 Closed chamber flux measurements.....	14
1.2.2 Eddy covariance.....	15
1.2.3 Radial plume mapping.....	16
1.2.4 Differential absorption LiDAR.....	18
1.2.5 Tracer release.....	18
1.2.6 Inverse Gaussian plume models.....	19
1.2.7 Plume scanning.....	21
1.3 Source identification at local to regional scales.....	22
1.4 Thesis overview	23
1.4.1 Thesis aims	23
1.4.2 Study approach and summary of findings.....	24
1.4.3 Thesis structure.....	26
1.5 References.....	27
2 MOBILE METHANE MEASUREMENTS.....	40
2.1 Abstract.....	40
2.2 Introduction	41
2.3 Materials and methods.....	43
2.3.1 Methane measurements.....	43
2.3.2 Coordinates and wind data	45
2.3.3 Laboratory testing	46
2.3.4 Standard calibration and drift check	46
2.3.5 Field data collection	46
2.3.6 Data analysis.....	47
2.3.7 Isotope precision model.....	48
2.4 Results and discussion	50
2.4.1 Dual instrument measurements	50
2.4.2 Isotope precision model.....	54
2.5 Conclusions	58
2.6 References.....	59
2.7 Supplementary material	62
2.7.1 Supplementary figures	62
2.7.2 Isotope precision model source code.....	66

3 ISOTOPIC CHARACTERISATION AND MOBILE DETECTION OF METHANE EMISSIONS..... 69

3.1 Abstract.....	69
3.2 Introduction	70
3.3 Methods	72
3.3.1 <i>Study area</i>	72
3.3.2 <i>Background air sampling</i>	73
3.3.3 <i>Characterisation of emission sources</i>	73
3.3.4 <i>Mobile measurements</i>	75
3.3.5 <i>Data analysis</i>	77
3.4 Results	79
3.4.1 <i>Background air sampling</i>	79
3.4.2 <i>Fylde isotopic source characterisation</i>	80
3.4.3 <i>Wetland sites</i>	83
3.4.4 <i>Mobile CH₄ source identification and land use</i>	85
.....	89
3.5 Discussion	90
3.5.1 <i>Background air sampling</i>	90
3.5.2 <i>Fylde isotopic source characterisation</i>	91
3.5.3 <i>Wetland sites</i>	91
3.5.4 <i>Mobile CH₄ source identification</i>	92
3.5.5 <i>Land use</i>	94
3.5.6 <i>Conclusion</i>	94
3.6 References.....	96
3.7 Supplementary material	101
3.7.1 <i>Supplementary tables</i>	101
3.7.2 <i>Supplementary figures</i>	103

4 LARGE SEASONAL AND INTERANNUAL VARIATIONS IN METHANE EMISSIONS DO NOT AFFECT CARBON AND HYDROGEN ISOTOPES FROM AN OMBROTROPHIC PEAT BOG..... 107

4.1 Abstract.....	107
4.2 Introduction	108
4.3 Methods	111
4.3.1 <i>Study area</i>	111
4.3.2 <i>Flux measurements</i>	111
4.3.3 <i>Isotope measurements</i>	112
4.3.4 <i>Soil moisture, water level, temperature, and water chemistry</i>	112
4.3.5 <i>Methane production and oxidation potential</i>	113
4.3.6 <i>Statistical analysis</i>	113
4.4 Results	114
4.4.1 <i>Methane fluxes and environmental factors</i>	114
4.4.2 <i>Isotope signatures</i>	120
4.4.3 <i>Peat incubations</i>	122
4.5 Discussion	124
4.5.1 <i>Fluxes and environmental drivers</i>	124
4.5.2 <i>Isotope signatures</i>	126
4.5.3 <i>Conclusions</i>	127
4.6 References.....	129

4.7 Supplementary material	136
4.7.1 <i>Supplementary tables</i>	136
4.7.2 <i>Supplementary figures</i>	138
5 GENERAL DISCUSSION	142
5.1 Mobile measurements	142
5.2 Emission source characterisation.....	143
5.2.1 <i>Dual isotope source signatures</i>	143
5.3 Future research	144
5.3.1 <i>Wetland ecosystems</i>	144
5.3.2 <i>Mobile emission measurements and isotopic characterisation</i>	145
5.4 References.....	147

List of Tables

Table 2.1 Number of CH ₄ peaks counted during mobile surveys at different thresholds with two gas analysers and the number of peaks whose $\delta^{13}\text{CH}_4$ signature could be estimated with a precision of < 5 ‰.....	53
Table 2.2 Mean standard error for the slope of a Miller-Tans plot for 1,000 runs of a Monte Carlo simulation with the shown instrument and plume parameters. Precision = 1 SD of isotopic precision for a single measurement, r = number of measurement cycles over which gas in the cavity is replaced, np = measurement cycles, peak height = max peak concentration above background.	57
Table 3.1 Stable isotope ratios of mixed air collected at a coastal and an inland location. Wind speed and direction show mean values during the sampling period.....	80
Table 3.2 Stable isotope signatures of CH ₄ emission source categories in the study area, n.a. indicates samples lost due to technical errors. Landfill phases refer to individual cells of the landfill.....	81
Table 3.3 Major CH ₄ plumes identified in the study area with $\delta^{13}\text{C}$ signature SE < 6.0 ‰.	82
Table 3.4 Flux rates measured for different vegetation types in a reed bed (Leighton Moss) and a lowland raised bog (Roudsea Wood).	83
Table 4.1 Spearman rank correlations of CH ₄ flux and soil parameters. * p < 0.05, ** p < 0.01, *** p < 0.001, n.s. not significant, n.a. indicates non-monotonic relationships between variables.	119

List of Figures

Figure 1.1 Scheme of variations in $\delta^{13}\text{C}$ and $\delta^2\text{H}$ associated with methane oxidation and production mechanisms. Taken from Flanagan et al. (2005).....	9
Figure 1.2 Vertical RPM setup, taken from U.S. EPA (2011).....	17
Figure 1.3 Example of a vertical RPM concentration gradient map. The x-axis represents the cross wind distance (TDL to tower in meters). Note that the concentration decreases with height. Sensor located on lower left. Taken from Goldsmith et al. (2012).	17
Figure 1.4 Schematic overview of tracer release method. Taken from Mønster et al. (2014).	19
Figure 1.5 CH_4 concentration from gas pipe leaks in Washington, DC. The four sampling heights are represented by the vertical boundaries of the image and the two dashed lines. Taken from Jackson et al. (2014). Insert shows a plume whose centre is above the sampling height.	22
Figure 2.1 Schematic of mobile system. Dotted line shows a temporary connection between the reference gas cylinder and the air inlet only used during drift checks.	45
Figure 2.2 Graphical representation of isotope precision model. a) Initial peak with true peak height (maximum concentration above background) and given peak length n_p relative to the number of measurement cycles (represented by points); b) representation of the instrument optical cavity and the gas concentration in it. Blue line represents instrument laser and therefore the length over which concentration is measured. c) broadened peak as measured by the instrument with random noise added (grey overlay).....	49
Figure 2.3 Concentration of a 3.03 ppm CH_4 standard gas as measured on a G2201-i isotopic gas analyser and an Ultraportable Greenhouse Gas Analyzer connected in series. Solid lines show measurements where the standard gas was connected for 120 s and both instruments reached stable readings. Dashed lines show measurements where the standard gas was connected for 10 s. Horizontal lines indicate rise times at which 90% (T_{90}) or 100% (T_{100}) of the final concentration have been reached for the UGGA.	51

Figure 2.4 Mobile CH ₄ measurements made simultaneously by a G2201-i isotopic gas analyser and a UGGA greenhouse gas analyser connected in series. Only data points above background concentration for at least one of the analysers are shown.....	51
Figure 2.5 Maximum peak concentration above background for CH ₄ peaks measured either by a G2201-i or a UGGA (n = 230). Peaks recorded by both analysers were matched if they overlapped temporally. In case of multiple overlapping peaks, the highest peak was selected.....	52
Figure 2.6 Scatter plot of peak CH ₄ areas (n = 230) measured across four mobile surveys as measured by a G2201-i isotopic gas analyser and a UGGA greenhouse gas analyser connected in series.	54
Figure 3.1 Miller-Tans plots of δ ¹³ C signatures of vegetated plots, dominated by mosses or grasses, and plots with nascent vegetation at Leighton Moss reed bed and vegetated plots, dominated by heather or mosses, at Roudsea Wood lowland raised bog. Regressions calculated using York’s method.	84
Figure 3.2 Miller-Tans plots of δ ² H signatures of vegetated plots and plots with nascent vegetation at Leighton Moss reed bed and vegetated plots at Roudsea Wood lowland raised bog. Regressions calculated using York’s method.	85
Figure 3.3 Map of mobile measurements in the Fylde area. Map insert highlights the study area within the UK. Symbol width indicates CH ₄ concentration as measured by a Picarro G2201- <i>i</i> isotopic gas analyser. Colour indicates 30 s running mean measured δ ¹³ C values grouped by standard deviations from the mean. Numbered items refer to CH ₄ emission plumes listed in Table 3.3 and drilling sites: 1 Jameson Rd landfill, 2 Preston Lancaster New Rd, 3 Newton Dr, 4 Garstang Rd, Roseacre Wood drilling site, 6) Preston New Rd drilling site, 7 Midgeland Farm landfill.	87
Figure 3.4 Map of mobile measurements around Lancaster and Morecambe Bay. Symbol width indicates CH ₄ concentration as measured by a Picarro G2201- <i>i</i> isotopic gas analyser. Colour indicates 30 s running mean measured δ ¹³ C values grouped by standard deviations from the mean. The high concentration measurement in Lancaster city centre is in Cable St, see Table 3.3.	88

Figure 3.5 Map of mobile measurements around Barrow-in-Furness. Symbol width indicates CH ₄ concentration as measured by a Picarro G2201- <i>i</i> isotopic gas analyser. Colour indicates 30 s running mean measured δ ¹³ C values grouped by standard deviations from the mean. 1 Roose Rd, 2 Rampside Gas Terminal with emissions measured at Rampside Rd, see Table 3.3.....	89
Figure 3.6 Miller-Tans plot for elevated CH ₄ data across land use types, excluding stationary measurements (n = 4,134). A separate regression was calculated for known emissions from landfill sites (n = 161).....	90
Figure 4.1 CH ₄ flux rates from five sampling plots in an ombrotrophic peat bog. Green shading indicates periods with above average flux rates.	116
Figure 4.2 Box plot of CH ₄ fluxes across five plots. Different letters below boxes indicate significant differences at p < 0.05.....	117
Figure 4.3 Mean air temperature and soil temperature at 30 cm depth. Soil temperature data missing from January 22 to March 18 2015 due to instrument failure.	117
Figure 4.4 Mean water table levels from five dipwells located near the CH ₄ flux sampling plots.....	118
Figure 4.5 Relationship between CH ₄ flux and soil temperature.	118
Figure 4.6 Relationship between CH ₄ flux rates and mean water table levels.....	119
Figure 4.7 Miller-Tans plot showing the source signature of ¹³ CH ₄ in an ombrotrophic peat bog from 2015 to 2017. The source signature is the slope of a York-regression (n = 77). Data points marked with x were excluded because of non-normality of residuals. Dashed line shows model with all data points included.....	121
Figure 4.8 Miller-Tans plot showing the source signature of ² H-CH ₄ in an ombrotrophic peat bog from 2015 to 2017. The source signature is the slope of a York-regression (n = 60). Data points marked with x were excluded because of non-normality of residuals. Dashed line shows model with all data points included.....	122

Figure 4.9 Potential CH₄ A) production and B) oxidation within the peat profile of three replicate peat cores. Sampling dates of peat cores shown at top of panels. Note that flux rates for A) are plotted on an inverse hyperbolic sine scale for comparability.123

Figure 5.1 Dual-isotope samples collected during this PhD project from different sources plotted against CH₄ formation mechanisms as adapted from Whiticar (1999). Reed bed sites with a dot represent possible combinations of $\delta^{13}\text{C}$ and $\delta^2\text{H}$ shown in Figures 4.7 & 4.8.144

1

Introduction

On Earth, carbon (C) is continuously cycled between the atmosphere, biosphere, hydrosphere, and geosphere. The hydrocarbon methane (CH_4) is a central component of this C cycle. It is the most reduced form of C, and its cycling is closely linked to that of carbon dioxide (CO_2), the most oxidised form of C. Through photosynthesis in the terrestrial and marine biosphere, C is removed from the atmosphere and fixed in organic compounds. Eventually, this C is returned to the atmosphere through the breakdown of organic matter. Depending on environmental conditions, mainly the availability of oxygen, most C will be converted into either CH_4 or CO_2 . In the atmosphere, both CH_4 and CO_2 act as greenhouse gases (GHGs) and are the main drivers of anthropogenic climate change.

CH_4 affects the climate by absorbing infrared radiation at $3.3 \mu\text{m}$ and $7.7 \mu\text{m}$, but it also affects the abundance of other GHGs in the atmosphere through its role in atmospheric chemistry (Dean et al., 2018). CH_4 is a precursor of ozone (O_3), which is both a GHG and an air pollutant, and its oxidation in the stratosphere produces water vapour, the most abundant GHG (Dean et al., 2018; Monks et al., 2015). Eventually, when CH_4 is oxidised, either by reaction with the OH radical in the atmosphere, or by microbes in soils or aquatic systems, its C atom becomes part of CO_2 , contributing to its pool in the atmosphere.

Since the start of the industrial revolution in the 18th century, the C cycle has experienced massive perturbations due to anthropogenic activity. Atmospheric CH_4 concentrations have increased from around 700 ppb in 1750 to 1840 ppb in 2016, an increase of over 160 % (Ciais et al., 2013; Dlugokencky, 2018). By comparison, atmospheric concentrations of CO_2 have increased from 277 ppm to 403 ppm in 2016, an increase of 45 % (Le Quéré

et al., 2018). Absolute concentrations of CH₄ in the atmosphere are therefore two orders of magnitude below CO₂. However, the global warming potential (GWP) of CH₄, a measure of globally-averaged radiative forcing over a given time period, relative to the radiative forcing of the same amount of CO₂, is 32 over a 100-year timeframe (Etminan et al., 2016). Over a 20-year timeframe, the GWP is 86, and since pre-industrial times CH₄ has contributed around 20 % to global warming induced by long-lived greenhouse gases (Kirschke et al., 2013; Myhre et al., 2013).

The lifetime of CH₄ in the atmosphere is approximately 10 years, depending on atmospheric chemistry (Myhre et al., 2013). By comparison, CO₂ emissions affect atmospheric concentrations for decades to millennia (Joos et al., 2013). Because of its short atmospheric lifetime, CH₄ emission reductions could reduce climate warming over the coming decades, as well as improve air quality (D. T. Shindell et al., 2012; West et al., 2006). To achieve such emission reductions, a thorough understanding of the CH₄ cycle, including both natural and anthropogenic sources, is needed.

The main sources of CH₄ emissions are well-known and can be separated into two categories: thermogenic CH₄ formed during the breakdown of organic matter under high temperature and pressure under rock formations, and microbially-produced CH₄, formed by methanogenic archaea. The latter is mainly produced in anaerobic conditions in wetlands and rice paddies, the gastrointestinal tract of ruminants and termites, and during waste treatment and storage. Other sources include combustion processes (pyrogenic methane) and various abiotic processes (Etiope and Sherwood Lollar, 2013; Myhre et al., 2013). Despite this knowledge, many unknowns about the CH₄ cycle remain. Growth rates of atmospheric CH₄ decreased in the 1990s, concentrations stabilised between 1999 and 2006, and have since started to increase again. The causes for both the stabilisation and renewed increase are debated in the literature, with changes in the atmospheric OH sink, wetland emissions, agricultural emissions, biomass burning, and fossil fuel emissions all variously implied (Bergamaschi et al., 2013; Franco et al., 2016; Kirschke et al., 2013; Nisbet et al., 2016; Saunio et al., 2016a; Schaefer et al., 2016; Turner et al., 2017; Worden et al., 2017).

The overarching aim of this thesis is the development and application of stable isotope-based approaches for detection, characterisation, and source attribution of CH₄ emissions in the landscape. In this chapter, I discuss principles of CH₄ source attribution as well as formation mechanisms. I further review both natural and anthropogenic emission sources

and their contribution to the CH₄ cycle. Finally, I present an overview of methods employed for the detection, quantification, and source attribution of CH₄ emissions at the landscape level.

1.1 Methane sources

Atmospheric methane originates from numerous sources (Figure 1.1), but can be broadly grouped into four main categories, based on the process of CH₄ formation (Etiope and Sherwood Lollar, 2013; Kirschke et al., 2013): 1) microbial CH₄ produced by methanogenic archaea; 2) thermogenic CH₄, produced from the breakdown of organic matter in sedimentary rocks; 3) pyrogenic CH₄, produced during incomplete combustion of biomass; 4) abiotic CH₄, produced through chemical reactions that do not directly involve organic matter. The last category includes a variety of chemical processes that occur on a small scale globally (Etiope and Sherwood Lollar, 2013). For the purposes of this thesis, this review will focus on sources of CH₄ emissions in temperate environments which contribute significantly to the global CH₄ budget. This includes thermogenic emissions, i.e. natural gas, and microbial emissions associated with natural wetlands, agriculture, and waste management.

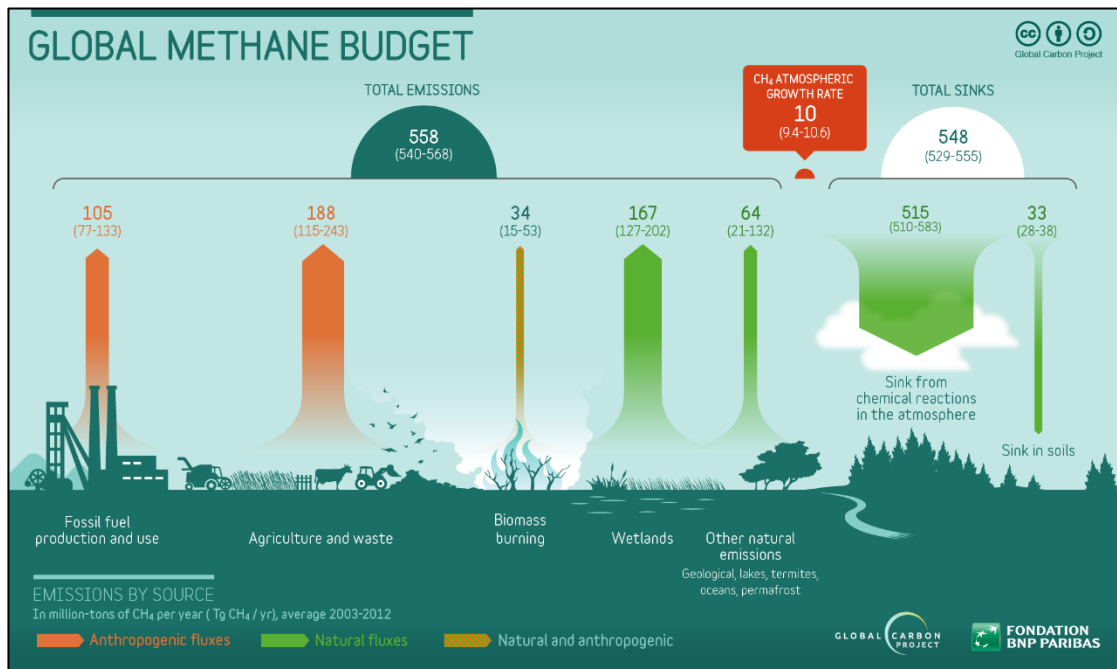


Figure 1.1 The global CH₄ budget, taken from Saunois et al. (2016b).

1.1.1 Methane source attribution

Unless CH₄ emissions can be measured directly at the source, identifying their origin can be ambiguous as often a multitude of different sources contribute to total emissions in a given catchment. Three approaches have been developed to attribute CH₄ emissions to specific sources: 1) based on the radiocarbon signature of CH₄; 2) based on the stable isotope signature of CH₄; 3) based on the ratio between CH₄ and other gaseous hydrocarbons in naturally occurring gas mixtures.

1.1.1.1 Radiocarbon

Methane from geological reservoirs can be identified via its ¹⁴CH₄ (radiomethane) signature. The ¹⁴C isotope has a half-life of around 5,730 years; geological sources are thus fully depleted in ¹⁴C (Cicerone and Oremland, 1988). Naturally occurring ¹⁴C originates in the atmosphere, where neutrons formed through cosmic rays react with ¹⁴N to form ¹⁴C which is oxidised to ¹⁴CO₂. Atmospheric ¹⁴CO₂, cycled through the biosphere, is the source of both biogenic and pyrogenic ¹⁴CH₄. The continued release of ¹⁴C depleted C from fossil fuels reduces the ¹⁴C/¹²C ratio in the atmosphere, known as the Suess Effect (Keeling, 1979). Radiomethane ratios have therefore been used to estimate the contribution of geological sources, i.e. fossil methane, to global methane emissions (Cicerone and Oremland, 1988; Lassey et al., 2007a, 2007b; Quay et al., 1999).

There are, however, two anthropogenic sources of ¹⁴CH₄: One is the ¹⁴CO₂ created during atmospheric nuclear weapons tests between 1954 and their ban in 1963 (Lassey et al., 2007b). The second source is ¹⁴CH₄ released from nuclear power plants where ¹⁴C is formed from ¹⁴N, ¹⁷O, and ¹³C through neutron irradiation (Povinec et al., 1986). In pressurized water reactors, the presence of hydrogen means that most of the ¹⁴C is vented in its reduced form. While this source is inconsequentially small in terms of total CH₄ emissions, the ¹⁴CH₄ content of emissions can be around 70 %, it is poorly constrained, and limits the accuracy with which the contribution of fossil emissions can be determined (Lassey et al., 2007a, 2007b).

1.1.1.2 Stable isotopes

The three primary mechanisms of CH₄ formation, microbial, thermogenic, and pyrogenic, differ in the ratios of their stable C (¹³C/¹²C) and H (²H/¹H) isotope ratios. While isotopes of the same element are nearly identical in their chemical properties, they differ in mass. Due to these differences in mass, chemical, biological, and physical processes can

fractionate isotopes, i.e. lead to the enrichment of one isotope relative to the other. Generally, lighter isotopes will react more readily because of lower energy costs and higher velocity. This often leads to particularly strong fractionation in biological processes, where enzymes preferentially catalyse reactions with substrates with lighter isotopic composition. Different C and H fractionation factors are thus associated with each CH₄ formation mechanism, giving each source type a distinct isotopic signature. The ability to distinguish between source categories, and even between individual metabolic pathways of biogenic CH₄ formation, has made isotopic analysis the primary tool for source attribution of CH₄ emissions (Whiticar, 1999). Stable isotope ratios of substances with a natural abundance of heavy and light isotopes, where the vast majority of the substance consists of the light isotopes, are typically expressed using the delta (δ) notation (Slater et al., 2001). Using the stable isotope ratios of ¹³C and ¹²C, reported in parts per thousand (permille, ‰) as an example:

$$\delta^{13}\text{C} = \left(\left(\frac{\frac{^{13}\text{C}}{^{12}\text{C}}_{\text{Sample}}}{\frac{^{13}\text{C}}{^{12}\text{C}}_{\text{Standard}}} \right) - 1 \right) \times 1000$$

where the values are referenced to the international standard Vienna Pee Dee Belemnite (VPDB) for C and Vienna Standard Mean Ocean Water (VSMOW) for H.

There are ten stable isotopologues (isotopic compositions) of CH₄, given by the possible combinations of the stable isotopes ¹²C, ¹³C, ¹H, and ²H (deuterium, D) in a CH₄ molecule. Conventional isotopic analysis effectively measures the relative abundance of the three most abundant isotopologues, ¹²CH₄, ¹³CH₄, and ¹²CH₃D (Stolper et al., 2014b). Current research on CH₄ emissions, including the research present in this thesis, mainly focuses on the measurement of these isotopologues. However, recent advances in analytical technology have allowed for “clumped” isotope analysis of CH₄, i.e. of multiply substituted isotopologues, such as ¹³CH₃D and ¹²CH₂D₂ (Ono et al., 2014; Stolper et al., 2014b). Under equilibrium conditions, there is a higher concentration of clumped isotopologues compared to a random distribution of isotopes among all isotopologues. This is because distributions with a higher concentration of clumped isotopes are thermodynamically favoured as they have a lower zero-point energy (Wang et al., 2004). The concentration of clumped isotopes is a function of formation temperature under equilibrium conditions (Stolper et al., 2014b). This is because the entropy of a system increases with temperature.

The entropy, and therefore disorder, is maximised when isotopes are distributed randomly among all isotopologues. The abundance of multiply substituted isotopologues thus decreases with temperature (Stolper et al., 2014b).

The study of CH₄ isotopologues will likely increase our understanding of CH₄ biogeochemistry. For example, Stolper et al. (2014a) have calibrated a clumped isotope geo-thermometer, which allows differentiation between thermogenic CH₄ with formation temperatures between ~100 and 230 °C and biogenic CH₄ with formation temperatures < 80 °C (Killops and Killops, 2013; Stolper et al., 2014a).

1.1.1.3 Hydrocarbon ratios

While there are both microbial and non-microbial origins of CH₄, the heavier gaseous hydrocarbons ethane and propane have no known significant microbial sources, but are co-released with CH₄ from thermogenic and pyrogenic sources (Simpson et al., 2012).

Oil and natural gas are formed through the thermal degradation (“cracking”) of kerogens, solid hydrocarbons in sedimentary rocks, at high pressure. Higher pressure and temperature lead to more complete cracking and progressively lighter hydrocarbons, ending with the formation of CH₄. The CH₄ content of natural gas is thus an indicator of its thermal maturity. Mature (dry) gas has a very high CH₄ content and is heavily enriched in ¹³CH₄. Wet gas is still mostly CH₄ but contains a higher proportion of ethane and propane which are typically more enriched in ¹³C than CH₄ (Jackson et al., 2013; Simpson et al., 2012). Generally, thermogenic CH₄ has ratios of CH₄ to ethane plus propane ($C_1/(C_2+C_3)$) < 50 (Whiticar, 1999).

Methane and other light hydrocarbons, including ethane and propane, are also released at low ratios during incomplete combustion of organic matter (Andreae and Merlet, 2001). The main sources are the burning of organic fuels, as well as biomass and soil carbon during wildfires, and slash-and-burn farming (Kirschke et al., 2013).

The fact that heavier alkanes are co-released with CH₄ during extraction and distribution of natural gas and biomass burning, but not from biogenic sources, has been used as a tool for source attribution, both for identifying the source of local emissions (e.g. Hakala, 2014; Jackson et al., 2014) and for constraining global fugitive emissions (Schwietzke et al., 2014a, 2014b).

1.1.2 Natural gas

Natural gas generally refers to a mixture of gases of geological origin whose main component is CH₄. Natural gas is primarily thermogenic in origin, although a significant portion of natural gas in geological formations can be of microbial rather than thermogenic origin, as microbes decompose organic matter in buried sediments, coal seams, or organic-rich shales (Katz, 2011; Martini et al., 1996).

Isotopic signatures of natural gas can vary widely, but are typically in the range of -60 ‰ to -30 ‰ for $\delta^{13}\text{C}$, and -340 ‰ to -150 ‰ for $\delta^2\text{H}$, depending on source type and location (Sherwood et al., 2017). This variability is due to factors including differences in the thermal maturity (see section 1.1.1.3), the isotopic signature of the source material, the contribution of microbial gas, or diffusive processes (Prinzhofer and Pernaton, 1997; Sherwood et al., 2017; Stolper et al., 2015).

Natural gas is mainly emitted to the atmosphere through anthropogenic activities. However, Kvenvolden and Rogers (2005) have argued that around 45 Tg CH₄ yr⁻¹ are emitted through geological seepage, corresponding to over 5 % of the total CH₄ budget (Kirschke et al., 2013). Emissions of natural gas occur during the extraction, crushing, and processing of coal, oil extraction and gas flaring, and, primarily, from extraction, processing, and distribution of natural gas (Dlugokencky et al., 2011; Miller et al., 2013). Globally, fugitive emissions from fossil fuels are estimated to account for roughly one third of total anthropogenic emissions (Kirschke et al., 2013). Emissions from the fossil fuel industry are a function of both the amount of fuels extracted, and the technology and practices used in extraction, processing, transfer, and distribution.

Natural gas is considered as a “bridge fuel” during the transition to a decarbonised economy, as it emits less CO₂ per unit of energy released than other fossil fuels (Brandt et al., 2014). Production of natural gas in the United States has increased by around 50 % over the last two decades, particularly from unconventional sources such as shale gas (EIA, 2018). This has led to concerns that reductions in CO₂ emissions achieved from the use of natural gas are offset by increased fugitive emissions of CH₄ (Howarth, 2014), which have increased during the last decade (Franco et al., 2016). The medium and long-term climate impacts of substituting natural gas for other fossil fuels, whether it leads to a reduction or an increase in radiative forcing, depend on the fraction of produced CH₄ released into the atmosphere (Allen, 2014). There is a very high level of uncertainty surrounding the

proportion of fugitive emissions from the natural gas supply chain, with estimates ranging from 0.2 % to 10 % due to differences in extraction, processing and transport, regional levels of regulation, and estimation methodologies used (Balcombe et al., 2017). A large portion of total emissions originate from so-called super-emitters, a small percentage of sites in the natural gas supply chain with atypically high emissions, mainly due to malfunction or equipment failure (Zavala-Araiza et al., 2015). In addition, distribution pipelines that deliver natural gas to end-users can be prone to leaks and emit significant quantities of CH₄ (McKain et al., 2015). Efforts to curb fugitive emissions therefore depend on effective methods of surveying and monitoring natural gas infrastructure to rapidly detect and control emissions.

1.1.3 Microbial methanogenesis

Methanogenesis is the final step in the degradation of organic matter under anoxic conditions. It is exclusively performed by archaea from the phylum euryarchaeota. In the presence of inorganic oxidants, such as sulphate, methanogenesis is outcompeted by other metabolic pathways, such as bacterial sulphate reduction, which have a higher redox potential. This limits CH₄ production in sulphate rich environments under anoxic conditions, such as marine sediments (Whiticar, 1999).

Due to isotopic fractionation during methanogenesis, microbial CH₄ is typically more heavily depleted in ¹³C (δ¹³C of -70 to -45 ‰) than thermogenic (-60 ‰ to -30 ‰) and pyrogenic (-32 to -13‰) CH₄. Similarly, ²H of microbial CH₄ is also more heavily depleted (δ²H of -440 to -290 ‰) than thermogenic (-340 ‰ to -150 ‰) and pyrogenic (-230 to -195 ‰) CH₄ (Sherwood et al., 2017). However, fewer studies have included measurements of δ²H than δ¹³C.

There are two major metabolic pathways for biological CH₄ formation with the following net reactions:



Reaction (1) occurs during acetate fermentation (acetoclastic methanogenesis), which is considered the dominant pathway in most terrestrial and freshwater environments (Conrad, 2005; Valentine et al., 2004). Reduction of CO₂ (hydrogenotrophic

methanogenesis, reaction (2)) is considered the dominant pathway in deep marine sediments where the pool of sulphate and organic substrates is depleted (Whiticar, 1999). However, McCalley et al. (2014) found that hydrogenotrophic methanogenesis accounted for up to 75% of CH₄ emissions in a Swedish permafrost peatland.

Carbon and hydrogen isotope effects differ for the two pathways: acetate fermentation leads to higher $\delta^{13}\text{C}$ but lower $\delta^2\text{H}$ values of CH₄ compared to CO₂ reduction (Figure 1.3).

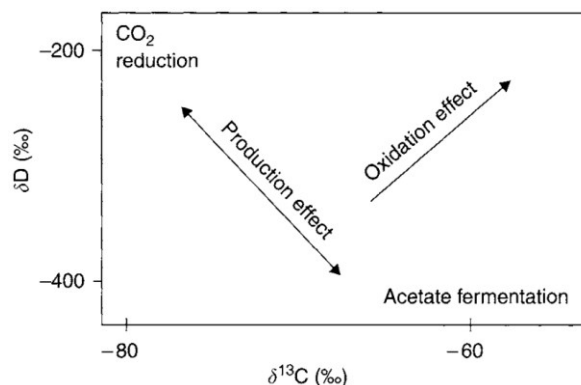


Figure 1.3 Scheme of variations in $\delta^{13}\text{C}$ and $\delta^2\text{H}$ associated with methane oxidation and production mechanisms. Taken from Flanagan et al. (2005).

Microbial methanogenesis occurs in both natural systems, primarily wetlands, and as a result of anthropogenic activities, mainly agriculture and waste management.

1.1.4 Wetlands

Wetlands are the largest source of atmospheric CH₄, with estimates ranging from 142 Tg to 284 Tg CH₄ yr⁻¹, or around one third of total emissions (Kirschke et al., 2013). Wetlands thus represent a large source of uncertainty in the global CH₄ budget, partly due to a high uncertainty in their global land cover as well as high spatial and temporal variability (Dean et al., 2018; Giri et al., 2005; Papa et al., 2010; Poulter et al., 2017). Variability in wetland emissions due to variations in climate are the main driver of interannual variability in global CH₄ emissions (Stocker et al., 2013). The increase in atmospheric CH₄ levels in recent years has partly been attributed to increased emissions from wetlands due to increased temperatures in northern high latitudes and increased rainfall over tropical wetlands (Kirschke et al., 2013).

Emission rates from wetlands are highly variable depending on the ecosystem in question and the microhabitat within a given ecosystem (Limpens et al., 2008). Estimates for mean

rates during the growing season range from 42 mg CH₄ m⁻² day⁻² in swamps to 96mg CH₄ m⁻² day⁻¹ in bogs (Turetsky et al., 2014). CH₄ emission rates at any given point in time depend on both the rate of methanogenesis in the anaerobic lower parts of the soil and methanotrophy by CH₄ oxidising bacteria in the upper aerobic part, as well as transport to the atmosphere via three main pathways: diffusion, ebullition, and plant-mediated transport.

As with methanogens, methanotrophs discriminate against the heavy ¹³C and ²H isotopes, leading to an isotopic enrichment of the remaining CH₄. However, the isotopic signature of CH₄ released from wetlands is typically in the range of biological sources with δ¹³C values in the range of -48 to -70 ‰ (Sherwood et al., 2017) and as low as -95 ‰ in ombrotrophic peat bogs (Hornibrook and Bowes, 2007) and arctic wetlands (McCalley et al., 2014).

The main factors controlling rates of CH₄ production in wetlands are water table depth, vegetation structure, and temperature (Turetsky et al., 2014). Water table depth determines the size of the aerobic and anaerobic zones and therefore the balance between methanogenesis and methanotrophy. Decreasing water tables reduce the anaerobic zone of CH₄ production while simultaneously increasing the depth of the aerobic zone through which CH₄ passes before escaping to the atmosphere, facilitating oxidation (Whalen, 2005). In peatlands, water table depth also affects the rate of diffusion from the peat to the atmosphere as the rate of diffusion is lower in saturated peat below the water table (Lai, 2009).

Vegetation affects CH₄ production in multiple ways. Under anaerobic conditions, both substrate availability and quality appear to be major constraints on methanogenesis (Mer and Roger, 2001; Whalen, 2005). Plants provide substrates for methanogenesis through root exudates and litter. Rates of CH₄ production are therefore often correlated with plant productivity (Mer and Roger, 2001). Plants can also facilitate CH₄ emissions by acting as a conduit for gas through the aerobic zone, thereby by-passing the aerobic methane oxidising layers and reducing substrate availability to methanotrophs. This is particularly the case for plants with aerenchymous tissues, such as many sedges, which are associated with higher CH₄ emissions (Turetsky et al., 2014; Ward et al., 2013). Part of CH₄ can also be released through ebullition, i.e. the formation of gas bubbles from standing water or peat (Lai, 2009; McEwing et al., 2015). Ebullition events can be triggered by a drop in hydrostatic or

atmospheric pressure, or an increase in temperature and subsequent increase of pressure in gas bubbles formed below the surface (Lai, 2009).

Cultivable methanogens are mostly mesophiles with temperature optima between 30 and 40°C, and CH₄ production in high latitude ecosystems is likely limited by temperature (Whalen, 2005). Furthermore, diurnal patterns in CH₄ emissions have been shown to follow temperature. This may be due in part to changes in the relative activity of methanogens and methanotrophs, as methanotrophy appears to be less sensitive to temperature than methanogenesis (Mer and Roger, 2001).

CH₄ emissions from wetlands are subject to strong seasonal variations, particularly in high latitude ecosystems. For example, Whalen and Reeburgh (1992) found that emission rates varied between 0 and > 600 mg m⁻² day⁻¹ in Alaskan tundra sites over the course of a season, with highest rates observed in mid-summer. However, while less often investigated, non-growing season CH₄ fluxes contribute significantly to total annual emissions (Treat et al., 2018).

Seasonal changes in temperature, water level and plant activity are likely to change the balance between methanogenesis and methanotrophy, and therefore may change the isotopic signature of emitted CH₄. Studies examining seasonal variations in isotopic signatures of CH₄ emissions are rare, however. Popp and Chanton (1999) found little seasonal variation in emitted ¹³CH₄ from a Canadian fen over a three-year study period, except for a single time period where water levels dropped below the peat surface, resulting in a ¹³C enrichment of emissions. McCalley et al. (2014) found variations of around 10 ‰ in δ¹³C over the course of a one-year study in Swedish permafrost peatlands, while Fisher et al. (2017) have found increasingly depleted values from summer to autumn in a Finnish peatland.

1.1.5 Waste treatment

1.1.5.1 Landfills

Landfills, together with waste waters and livestock manure, contribute an estimated 67 to 90 Tg yr⁻¹ to global CH₄ emissions and are one of the main anthropogenic sources, along with fossil fuels, enteric fermentation of livestock, and rice paddies (Stocker et al., 2013). CH₄ is emitted as part of landfill gas, a mixture that mainly consists of CH₄ (around 45 to

60 %) and CO₂, which is produced after initial aerobic and non-methanogenic phases in landfills (Bergamaschi et al., 1998; US EPA, 2017).

Production of CH₄ in landfills is highly variable, depending on factors such as organic matter content, temperature, and moisture (Goldsmith et al., 2012; US EPA, 2017). Modern landfills in industrialised countries are routinely equipped with gas collection systems and collected gas is either flared or used for heat or electricity generation. However, substantial amounts of CH₄ may still be released through the landfill cover. Goldsmith et al. (2012) found rates ranging from 1 to 200 g CH₄ m⁻² day⁻¹ at 20 different landfills in the United States with higher emissions in more humid, warmer climates, while Chanton and Liptay (2000) found emission rates as high as 9000 g CH₄ m⁻² day⁻¹ in a Florida landfill. One of the main determinants of emission rates is the landfill cover type. As with the aerobic zone in wetlands, landfill cover soil provides a suitable environment for CH₄ oxidisers. Based on stable isotope signatures of emitted CH₄, up to 80% of the produced CH₄ may be oxidised during its transport through the cover soil (Bergamaschi et al., 1998). The residual CH₄ emitted can therefore be highly enriched in ¹³C, with values as high as -40 ‰, which puts it in the range of thermogenic CH₄ (Chanton and Liptay, 2000). Other studies report isotope values from landfills ranging from -50 ‰ to -62 ‰ for δ¹³C and -312 ‰ to 273 ‰ for δ²H (Bergamaschi et al., 1998; Liptay et al., 1998; Sherwood et al., 2017; Zazzeri et al., 2017). Zazzeri et al. (2017) report a typical δ¹³C value of -58 ‰ for emissions from landfills and waste water treatment in the UK. However, while CH₄ production in a landfill is largely independent of environmental factors, oxidation rates can be subject to seasonal variation, with higher rates found during the summer when soils are warmer and microbial activity is higher (Chanton and Liptay, 2000). The properties of the cover soil can also affect oxidation rates, with better aerated sandy soils or soils with an organic cover showing higher oxidation rates than soils with high clay content (Chanton and Liptay, 2000; Goldsmith et al., 2012).

1.1.5.2 Waste water treatment and biogas plants

Anaerobic conditions, and therefore the potential for methanogenesis, exist at various stages during the collection and treatment of sewage. Emission sources and rates will be highly dependent on the specific construction and the technologies used in the plant in question. For example, Yoshida et al. (2014) found emission rates between 4.99 and 92.3 kg CH₄ h⁻¹ at a Danish waste water treatment plant (WWTP). WWTPs often use anaerobic digesters to reduce the carbon content of sewage sludge while producing CH₄ to power

plant processes. Several studies have identified anaerobic digesters as the main sources of CH₄ emissions in WWTPs (Daelman et al., 2012; Yoshida et al., 2014), while significant leakage can also occur from other structures such, as oxic tanks and digested sludge (Oshita et al., 2014; Wang et al., 2011). Anaerobic digestion is also used to produce biogas for energy production from plant material and/or manure in biogas plants. Liebetrau et al. (2013) found emission rates ranging from around 2 to 25 g CH₄ kWh⁻¹ in German biogas plants.

Little information is available on the isotopic composition of fugitive CH₄ emissions from waste treatment. Besides the values reported by Zazzeri et al. (2017) above, Townsend-Small et al. (2012) found δ¹³C and δ²H from manure biofuel to be around -51.2 ‰ and -303 ‰ respectively. The relatively high δ¹³C values were attributed to the high microbial activity in the closed digester. The same study found values of -46.6 ‰ and -298 ‰ for δ¹³C and δ²H from WWTPs.

1.1.6 Ruminant livestock

CH₄ emissions from livestock, particularly cows, and to a lesser extent sheep and goats, are among the largest anthropogenic CH₄ sources, contributing between 87 and 94 Tg CH₄ yr⁻¹ (Stocker et al., 2013). Enteric fermentation in the rumen of these animals leads to H₂ production, the substrate for hydrogenotrophic methanogenesis (Wright and Klieve, 2011), through which a single dairy cow can produce over 300g CH₄ day⁻¹ (Laubach and Kelliher, 2004). For a sheep, the rate is as high as 25g CH₄ day⁻¹ (Judd et al., 1999). CH₄ production rates as well as their isotopic signature depend on diet. Cows fed with maize were found to have higher CH₄ δ¹³C values (-57.4 ‰) than those fed with C₃ plants (-67.7 ‰), reflecting the differences in the isotopic composition of C₃ and C₄ plants (Klevenhusen et al., 2009).

Around 10 % of the total CH₄ emissions associated with livestock originate from the decomposition of manure, rather than enteric fermentation (Janssens-Maenhout et al., 2017) (see also section 1.1.5.2). The isotopic signature of manure is also dependent on the C source (Klevenhusen et al., 2010) and may therefore also depend on the feed used.

1.2 Methods for estimating CH₄ emissions

Accurately quantifying emissions on local to regional scales is crucial to implementing emission reduction measures. However, there is a high degree of uncertainty about the contribution of individual sources, and the accuracy of emission inventories is often

challenged by top-down emission estimates (Hsu et al., 2010; Kirschke et al., 2013; Levin et al., 1999; Lowry et al., 2001; Miller et al., 2013). Part of this uncertainty is due to the heterogeneous nature of CH₄ sources, which are difficult to accurately capture, and tracing total emissions to their individual sources is challenging.

The scarcity of accurate data available for CH₄ emissions is partly due to limitations in analytical technology. While, for example, gas analysers suitable for continuous measurements of CO₂ in the field have existed for several decades (Desjardins and Lemon, 1974), due to the comparatively low atmospheric concentrations of CH₄, analysis has been mainly performed using gas chromatography (GC). While accurate, GC analysis is comparatively labour-intensive, slow, and precludes the use of a number of methods for measuring CH₄ fluxes in the field, which require portable and high-frequency sensors.

Due to advances in optical sensors over the past decades, there has been an increase in the number of approaches available for measurement and source attribution of CH₄ (e.g. Fan et al., 1992; Kormann et al., 2001; Thoma et al., 2009). A comprehensive review of these methods is beyond the scope of this text, and there are a number of reviews available covering a range of technologies and applications. See for example U.S. EPA, (2011) and U.S. EPA, (2007) for a technical compilation and evaluation of optical remote sensing methods, Babilotte et al. (2010) and Babilotte (2011) for a method comparison for estimating fugitive landfill emissions, and Christen (2014) for a review of atmospheric measurement techniques.

This review will therefore limit itself to giving an overview of methods currently employed to estimate CH₄ emission fluxes of both natural and anthropogenic sources, by describing their functioning principles, and highlighting some of their applications and limitations. It will furthermore discuss approaches currently available for CH₄ source attribution at local to regional scales.

1.2.1 Closed chamber flux measurements

Chamber flux measurements are widely used to measure CH₄ emissions from soils (e.g. Whalen, 2005) and active (uncovered) landfill sites (e.g. Bergamaschi et al., 1998). The principle of applying a sealed chamber to measure gas fluxes from a surface has also been applied to technical components. For example, Liebetrau et al. (2013) have used chambers sealed with airtight foil to measure leaks from equipment at biogas plants. Floating

chambers have been used to measure fluxes from digesters (Liebetrau et al., 2013; Wang et al., 2011), storage tanks (Oshita et al., 2014), and oxidation ponds (Detweiler et al., 2014) at biogas plants and WWTPs.

There are two main types of chamber measurement systems: closed static chamber (CSC) and closed dynamic chamber (CDC) systems. With CSC systems, sampling is typically performed manually, and samples are analysed at a laboratory. To accurately measure soil fluxes using CSC systems, appropriate sampling procedures need to be adopted as the headspace gas concentration may be affected by incubation period (Heinemeyer and McNamara, 2011), chamber placement, and headspace mixing (Christiansen et al., 2011). By comparison, CDC systems can be automated, are connected in a closed loop to a gas analyser, and analysis is performed *in-situ*. While enabling a higher sampling frequency, this method is costlier. Its application in field studies may also be limited by the current analytical capabilities of portable gas analysers, which are unable to perform, for example, dual-isotope analysis of CH₄.

Chamber flux measurements are commonly used for assessing treatment effects in experimental studies and for estimating emissions from entire ecosystems. The latter, however, can be challenging due to the high variability in many natural ecosystems. For example, Lessard et al. (1994) estimated that an average of 137 sampling sites would be needed to determine the CH₄ flux in a forest soil within 10 % of its true value.

1.2.2 Eddy covariance

The eddy covariance technique is the most commonly used micrometeorological technique for the measurement of gas fluxes. Due to surface friction, air movements near the ground are dominated by turbulent motions (eddies). The eddy covariance technique is based on the measurement of vertical movement of parcels of air through such turbulent motions. Air movement is measured by a sonic anemometer mounted on a tower. The concentration of CH₄ (or other trace gas) is measured by a high frequency gas analyser, which allows the vertical flux of CH₄ to be calculated. The source area (footprint) of the measured flux depends on a number of factors: the height of the tower (ranging from \approx 1 m to $>$ 100 m), the surface roughness (height of surface structures such as vegetation or buildings), turbulence intensity, wind speed and direction, and atmospheric thermal stability (Velasco and Roth, 2010).

Eddy covariance systems can hence have footprints ranging from less than 100 m to several km and can provide continuous flux measurements with a high temporal resolution. The recent development of instrumentation that allows measurement of isotopic ratios in CH₄ fluxes (isoflux) may provide further insights into CH₄ cycling (Santoni et al., 2012).

One of the main limitations of the eddy covariance technique is that measured surfaces must be homogenous and the emission sources evenly distributed. This makes the technique unsuitable, for example, for estimating emissions from technical structures such as natural gas infrastructure.

1.2.3 Radial plume mapping

1.2.3.1 Vertical radial plume mapping

Radial plume mapping (RPM) is an optical remote sensing (ORS) method to measure emission fluxes from source areas. An ORS instrument, usually a tuneable diode laser (TDL) or open path Fourier transform infrared (OP-FTIR) spectrometer, is mounted on an aiming platform. The optical beam is alternately directed at mirrors positioned on a vertical plane at different heights on a tower and different distances from the sensor on the ground (Figure 1.4). The ORS instrument scans each of the mirrors, giving a path integrated concentration (PIC) measurement. Concentration gradient maps are calculated from the PIC measurements (Figure 1.5) and, in combination with meteorological data, the emission flux can be calculated.

Path lengths of 300 m and, under ideal meteorological conditions, accurate source measurements of areas <75% of plane length are possible. Emission flux estimates become less accurate for large area sources, as is often the case for landfill sites (Thoma et al., 2010), and for complex terrain, such as slopes (U.S. EPA, 2011).

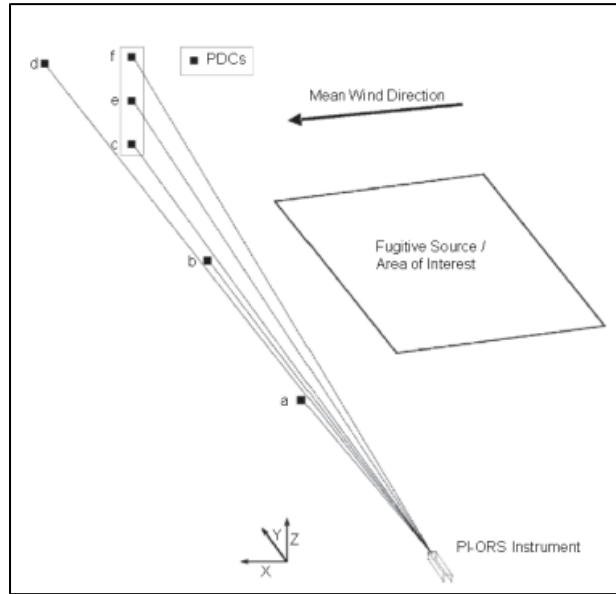


Figure 1.4 Vertical RPM setup for measure emissions from an area source, taken from U.S. EPA (2011).

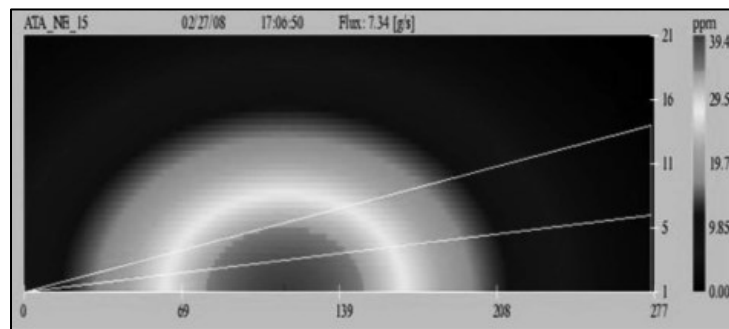


Figure 1.5 Example of a vertical RPM concentration gradient map. The x-axis represents the cross wind distance (TDL to tower in meters). Note that the concentration decreases with height. Sensor located on lower left. Taken from Goldsmith et al. (2012).

1.2.3.2 Horizontal plume mapping

For the horizontal RPM approach, the surveyed area is divided into a Cartesian grid, and a mirror is placed in each cell, usually close to ground level. The ORS instrument is located in one corner, alternately scanning the mirrors. Rather than estimating emission flux, this method provides information on the location of emission hotspots within the surveyed area.

1.2.4 Differential absorption LiDAR

LiDAR (light detection and ranging) systems emit short pulses of laser light and measure the light that is backscattered from objects towards the unit. LiDAR is used for a variety of purposes, such as high-resolution mapping, and measuring clouds, aerosols, and atmospheric gases. Depending on application, LiDAR units may be stationary, or fitted to aircraft, satellites, or vehicles. The wavelength of the laser is chosen based on the absorption spectrum of the compound of interest.

In differential absorption LiDAR (DIAL), light of two wavelengths (usually with a TDL) is emitted: one on-resonance wavelength and one off-resonance wavelength for a target species, such as CH₄. The on-resonance wavelength will be more strongly absorbed by the target species, and the difference in backscatter between the two wavelengths is proportional to the density of the target species (NIST, 2014). Similar to vertical RPM, DIAL can be used to make detailed measurements of plumes downwind from the source as well as create 3D emission maps. Existing DIAL systems can measure CH₄ at a distance of up to 800 meters (NPL, 2014) and therefore require no direct site access or traversing roads downwind (see methods discussed below). They are also well suited to take measurements from diffuse and complex sources and have been used in multiple studies on landfill CH₄ emissions (Babilotte et al., 2010; Goldsmith et al., 2012). The application of DIAL systems is primarily limited by the large size, cost, and complexity of the equipment involved. For example, the National Physics Laboratory's mobile DIAL facility is housed in a 20 t truck and requires specialist operators, limiting wide deployment (Babilotte et al., 2010).

1.2.5 Tracer release

The tracer release method is based on the release of a tracer gas from the site of the CH₄ release at a known rate. Both CH₄ and the tracer gas are measured along a traverse downwind of the site and perpendicular to the wind direction (Figure 1.6). Based on the assumption that the tracer is dispersed in the atmosphere the same way as CH₄, the ratio between tracer and CH₄ can be used to calculate the emission rate according to the equation:

$$E_{methane} = Q_{tracer} \times \frac{C_{methane} - C_{methane\ background}}{C_{tracer} - C_{tracer\ background}}$$

Where $E_{methane}$ is the CH₄ emission rate, Q_{tracer} is the tracer release rate, and $C_{methane}$ and C_{tracer} are the downwind CH₄ and tracer concentrations, respectively (Mønster et al., 2014).

Provided that CH₄ and tracer are perfectly mixed, emissions could be calculated from a single measurement point. In practice, cross plume transects are used to assure adequate mixing (Allen et al., 2013; Mønster et al., 2014). Methane concentrations along the traverse are expected to follow a Gaussian distribution (see insert Figure 1.6). Either the ratios of the integrated peak areas, the peak heights, or the slope of a regression of the concentration of the two gasses are used to calculate the emission rate (Mønster et al., 2014).

Measurements can be performed either by collecting gas samples in a series of evacuated gas containers along the traverse, or by driving a vehicle fitted with a mobile gas analyser along the traverse. The later method is preferred, as it gives a much higher number of measurements and therefore likely more accurate results (Babilotte et al., 2010). Different chemicals have been used as tracers, including acetylene, nitrous oxide, carbon monoxide, and sulphur hexafluoride (Babilotte et al., 2010; Mønster et al., 2014).

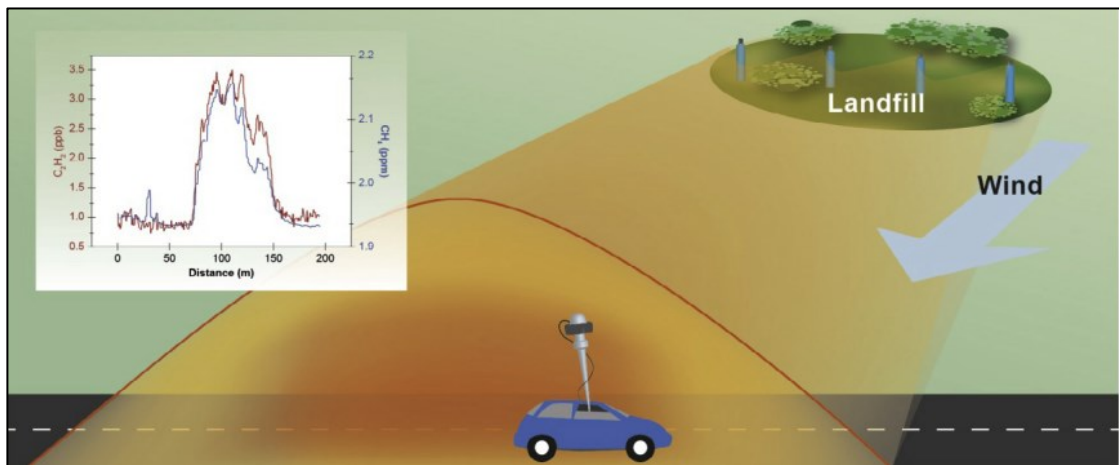


Figure 1.6 Schematic overview of tracer release method. Taken from Mønster et al. (2014).

1.2.6 Inverse Gaussian plume models

The Gaussian plume model is an air pollution model predicting the downwind concentration of an air pollutant from a point source. The model assumes that the pollutant dispersion follows a Gaussian distribution. By inverting the model, the emission rate of the source can be calculated from a downwind concentration measurement (Figueroa et al., 2009). The model typically has the form:

$$C(x, y, c) = \frac{Q}{2\pi V \sigma_y \sigma_z} e^{\frac{-y^2}{2\sigma_y(x)^2}} \left(e^{\frac{-(z-H)^2}{2\sigma_z(x)^2}} + e^{\frac{-(z+H)^2}{2\sigma_z(x)^2}} \right)$$

where C is the CH_4 concentration at any given point (x, y, z) in the plume, Q is the emission rate, V is the wind speed, σ_y and σ_z are the dispersion coefficients and H is the emission height above ground level (Mønster et al., 2014). The emission rate can thus be calculated from any point in the plume. In practise, CH_4 concentration is measured along a traverse perpendicular to the plume from a vehicle equipped with a gas analyser, similar to the tracer release method (Figure 1.6). By using the CH_4 concentration at the centre of the plume, where $y = 0$, the equation simplifies and only the wind speed, dispersion coefficients, emission height, measurement height (height of gas sensor air inlet), and the distance to the source need to be known. The dispersion coefficients are chosen based on wind speed, insolation and cloud cover (Mohan and Siddiqui, 1997).

Both Babilotte et al. (2010) and Mønster et al. (2014) have compared Gaussian plume modelling and the tracer release method using controlled CH_4 release experiments. Babilotte et al. (2010) have found that both methods overestimated CH_4 emissions by a factor of ~ 3 . The authors attributed this to a low emission rate combined with low wind speeds. Mønster et al. (2014) found that both methods yielded similarly accurate results when measurements were taken at a distance of 370 m from the source, but that Gaussian plume models progressively overestimated emissions at increasing distances as CH_4 concentrations approached background values.

Both tracer release and plume modelling methods have a number of limitations: Access to downwind roads at a suitable distance is required. The tracer release method also requires site access. While plume modelling has the advantage of being one of the few methods that does not require site access, assumptions have to be made about the dispersion of the analyte gas. Both methods require a flat topography and are susceptible to biases from the occurrence of emission sources located between the source of interest and the measurement road, as well as to variations in background concentrations. Also, they are not suitable for continuous measurements, and provide only an estimate of momentary emission rates.

1.2.7 Plume scanning

A different mathematical approach for the measurement of emission rates from plumes is used by the Picarro “Plume Scanner” technology (Picarro Inc., Santa Clara, CA, USA). Measurements are taken in a car equipped with a cavity ring-down spectroscopy (CRDS) gas analyser, an anemometer and a GPS device. The system measures CH₄ concentrations from four air inlets, ranging in height from 0.43 to 2.44 m (Jackson et al., 2014). To increase the sensitivity of the analysis, sample gas from the air inlets is recorded in an AirCore system (Karion et al., 2010) during plume measurements and then replayed at a slower speed for improved accuracy. Concentrations can be plotted as plume images (Figure 1.7), which indicate if the plume is adequately captured and provide a measure of data quality. The emission rate $E(t)$ is calculated by integrating over the y -axis (path of the vehicle) and the z -axis (height):

$$E(t) = \iint (C(y, z, t) - C_0) \times u(x, y, z) dy dz$$

where C is the measured concentration, C_0 is the background concentration, and u is the wind speed (Jackson et al., 2014). Unlike for Gaussian models, no assumptions about plume geometry are made. Also, as the emission rate is calculated only from a plume’s cross-sectional CH₄ concentration and the wind vector, the exact distance and location of the source do not need to be known.

Similar to tracer release and plume modelling, the technique is sensitive to emissions from unknown sources and is only suitable for temporary measurements. The accuracy of the method may be improved by including isotope analysis, particularly in situations where plumes from multiple sources with distinct isotopic signatures overlap.

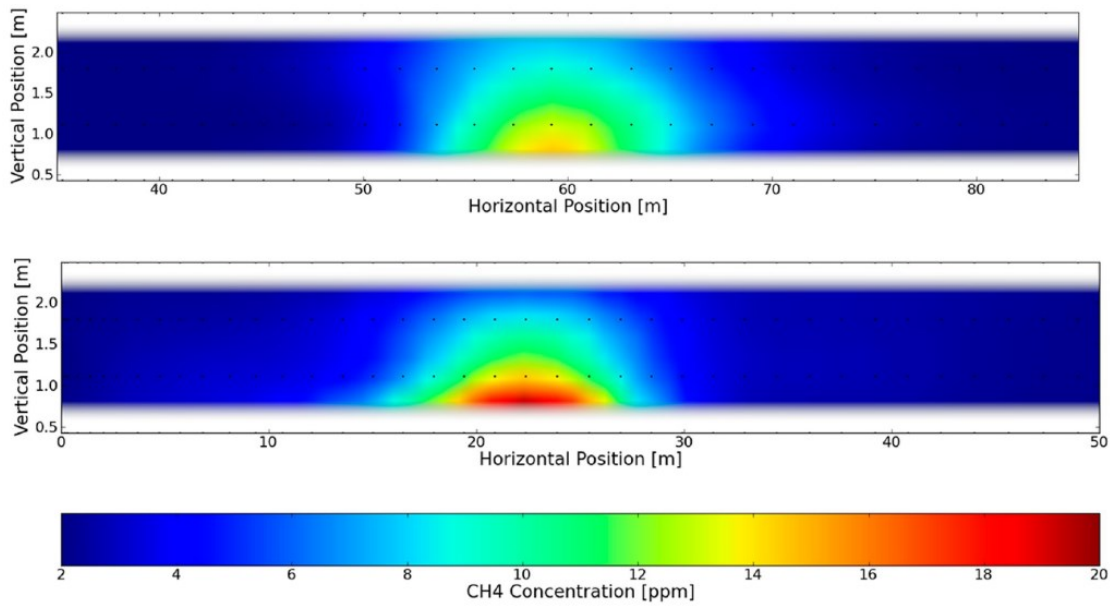


Figure 1.7 CH₄ concentration from gas pipe leaks in Washington, DC. The four sampling heights are represented by the vertical boundaries of the image and the two dashed lines. Taken from Jackson et al. (2014).

1.3 Source identification at local to regional scales

By analysing the isotopic or hydrocarbon ratios in air samples that integrate multiple sources in a region, the relative contribution of individual sources can be inferred. Such information can be used to independently verify emission inventory estimates, such as the UK National Atmospheric Emission Inventory (NAEI) or the Emission Database for Global Atmospheric Research (EDGAR), which aim to account for all emissions in a geographical area, as well as to monitor seasonal and long-term changes in the strength of different emission sources. At local to regional scales, there are multiple approaches based on the collection of atmospheric samples to attribute CH₄ emissions: Atmospheric samples can be taken at locations that are downwind of the area of interest, typically at an elevated location to ensure air is well-mixed and not influenced by emissions in the immediate surroundings (Lowry et al., 2001; Townsend-Small et al., 2012). Other authors have collected samples from multiple representative locations within the area of interest (Górka et al., 2014), or collected samples from aircraft (Peischl et al., 2013).

Methods that aim to quantify emissions at the source are typically time- and labour-intensive, often require detailed planning and setup, as well as site access, or the permanent installation of expensive equipment at a single site. They provide important data on total emissions and estimates from individual sources are used to derive emission factors. These

form the basis for building emission inventories that account for all source categories in a region or country. However, they are less suited to identify potential targets for investigation, and measurement locations are typically selected based on previous knowledge or assumptions. Particularly stochastic sources, such as leaks in natural and landfill gas infrastructure, including distribution pipelines, require efficient methods to survey, detect, and attribute emissions.

The development of portable, fast-responding spectroscopic gas analysers, such as described in sections 1.2.5 to 1.2.7, have led to mobile, vehicle-based surveying of CH₄ emissions at the landscape level. This approach combines a high spatial resolution of measurement with large spatial coverage. Allocation of detected CH₄ emissions to specific sources is typically performed based on location, wind direction measured on the vehicle, and potentially isotopic analysis. Through systematic surveys of regions, it is possible to both characterise isotopic signatures of emissions, and detect previously unknown emission sources (Zazzeri et al., 2015). By incorporating isotopic measurements, mobile surveys have been used to identify the contributions of different sources to total emissions on the landscape level (Lopez et al., 2017; Rella et al., 2015), while surveys of urban areas have often revealed considerable emissions from gas distribution pipelines (Fischer et al., 2017; Jackson et al., 2014; Phillips et al., 2013).

1.4 Thesis overview

1.4.1 Thesis aims

As I review in this chapter, atmospheric CH₄ is a potent greenhouse gas that is produced by a variety of both natural and anthropogenic sources. Due to the heterogeneity and variability of CH₄ emissions, there is considerable uncertainty surrounding the contribution of individual sources. This is of particular concern due to the large contribution of anthropogenic sources to total emissions. Stable isotope analysis is the primary tool for attributing emissions, but it relies on a comprehensive and accurate understanding of the different emission source categories.

The overarching aim of my thesis was the development and application of stable isotope-based approaches for detection, characterisation, and source attribution of CH₄ emissions in the landscape, using both mobile and stationary measurements. To this end, I here present three data chapters that address the following objectives:

Chapter 2

To assess how the specifications of gas analysers used in mobile measurement setups will affect the performance, suitability for different applications, optimization of sampling regimes, and the reproducibility of measurements.

Chapter 3

To 1) determine isotopic signatures of the major CH₄ source categories, as well as background isotopic signatures in the Fylde and Morecambe Bay area in North West England; 2) identify and attribute CH₄ emission sources in the region and identify emission and stable isotope patterns related to land use using mobile measurements prior to the start of shale gas exploration.

Chapter 4

To combine CH₄ emission and dual-isotope measurements in a wetland ecosystem to investigate seasonal variations in wetland emission signatures, and develop a better understanding of underlying microbial processes, such as methane production and oxidation, in response to environmental drivers.

1.4.2 Study approach and summary of findings

Chapter 2

I tested the effects of instrument speed on mobile CH₄ concentration measurements by outfitting a vehicle with two gas analysers with different response times and recorded concentration measurements over a total driving distance of 560 km. I found slower instrument response times lead to a greater underestimation of atmospheric concentrations, both while driving and during static measurements. However, the integral of concentration with respect to distance during mobile measurements is constant, regardless of instrument speed. This provides a means to compare data from different surveys and instruments. I further programmed a simple physical model that predicts the isotopic precision achievable under different measurement conditions and instrument specifications. I found that for a given instrument precision and speed, the precision of isotopic measurements primarily depends on the range of atmospheric concentrations measured and the duration of measurement. These results have important implications for the comparability of measurements between different instrumental setups and provide a framework for optimising sampling strategies under given objectives, conditions, and instrument capabilities.

Chapter 3

I performed dual isotope ($\delta^{13}\text{C}$, $\delta^2\text{H}$) analysis of CH_4 emission sources, background air, as well as mobile ^{13}C measurements in North-West England, in an area with potentially exploitable shale gas deposits before the start of drilling operations. Dual isotope analysis was performed for enteric fermentation, animal waste, landfill gas, wetland emissions, and natural gas from regional sources. I found that background air coming from the Irish sea was enriched in ^{13}C by 2.55 ‰, relative to the Atlantic background, and depleted in ^2H relative atmospheric CH_4 , potentially indicating an offshore emission source. Isotopic analysis of agricultural, landfill, and wetland emissions revealed that they overlapped in their $\delta^{13}\text{C}$ signatures. However, ^2H analysis may be able to distinguish between agricultural and landfill emissions. Mobile measurements detected emissions from two out of four surveyed managed landfills in the region. Multiple gas leaks were detected, which may confound emissions from other thermogenic sources with similar isotopic signature. When separating the surveyed area by land-use into agricultural and urban land, I found that background levels of CH_4 were more depleted by 1 ‰ in areas with agricultural land use compared to urban areas, but emissions from gas leaks and landfills are present in both categories. My findings demonstrate that the complex existing landscape of CH_4 emissions needs to be taken into account when evaluating the potential impacts of natural gas extraction in the region.

Chapter 4

To investigate the effects of seasonal variations in environmental conditions on peatland CH_4 emissions and their isotopic signatures I performed a 2.5-year monitoring study in an ombrotrophic peatbog in Northern England. I used a spectroscopic greenhouse gas analyser to perform dynamic flux chamber measurements as well as isotope ratio mass spectrometry to determine dual stable isotope ($\delta^{13}\text{C}$, $\delta^2\text{H}$) signatures. I found large seasonal and interannual variations in CH_4 fluxes, with uncharacteristically high emissions of over $100 \text{ mg CH}_4 \text{ m}^{-2} \text{ h}^{-1}$ in the summer of 2016, contrasting with median fluxes across the sampling period of $0.14\text{-}1.5 \text{ mg CH}_4 \text{ m}^{-2} \text{ h}^{-1}$. Fluxes showed strong relationships with abiotic conditions, increasing exponentially with soil temperature, and responding negatively to both high and low water table levels. Despite the large variations in fluxes, stable isotope signatures remained constant throughout the study period indicating that methanogenic pathways and the proportion of CH_4 oxidised in the peat remained stable throughout the study despite changes in abiotic conditions. Values of $\delta^{13}\text{C} = -83.99 \pm 0.04$ ‰ and $\delta^2\text{H} = -310.69 \pm 1.21$ ‰ indicate a relatively high contribution of hydrogenotrophic

methanogenesis at the study site, which contrasts with previous studies in peatlands. My results show that stable isotope signatures can be decoupled from flux rates and environmental conditions in peatlands.

1.4.3 Thesis structure

This thesis is written in the alternative format, with experimental Chapters 2–4 presented as manuscripts intended for submission to peer-reviewed journals. In Chapter 5, I synthesise the key findings of Chapters 2–4 and draw general conclusions as well as highlight future research directions. Bibliographies, as well as supplementary tables, figures, and code are presented at the end of each chapter.

1.5 References

- Allen, D.T., 2014. Methane emissions from natural gas production and use: Reconciling bottom-up and top-down measurements. *Curr. Opin. Chem. Eng.* 5, 78–83. <https://doi.org/10.1016/j.coche.2014.05.004>
- Allen, D.T., Torres, V.M., Thomas, J., Sullivan, D.W., Harrison, M., Hendler, A., Herndon, S.C., Kolb, C.E., Fraser, M.P., Hill, A.D., Lamb, B.K., Miskimins, J., Sawyer, R.F., Seinfeld, J.H., 2013. Measurements of methane emissions at natural gas production sites in the United States. *Proc. Natl. Acad. Sci.* 110, 17768–17773. <https://doi.org/10.1073/pnas.1304880110>
- Andreae, M.O., Merlet, P., 2001. Emission of trace gases and aerosols from biomass burning. *Global Biogeochem. Cycles* 15, 955–966. <https://doi.org/10.1029/2000GB001382>
- Babilotte, A., 2011. Field comparison of methods for assessment of methane fugitive emissions from landfills.
- Babilotte, A., Lagier, T., Fiani, E., Taramini, V., 2010. Fugitive Methane Emissions from Landfills: Field Comparison of Five Methods on a French Landfill. *J. Environ. Eng.* 136, 777–784. [https://doi.org/10.1061/\(ASCE\)EE.1943-7870.0000260](https://doi.org/10.1061/(ASCE)EE.1943-7870.0000260)
- Balcombe, P., Anderson, K., Speirs, J., Brandon, N., Hawkes, A., 2017. The Natural Gas Supply Chain: The Importance of Methane and Carbon Dioxide Emissions. *ACS Sustain. Chem. Eng.* 5, 3–20. <https://doi.org/10.1021/acssuschemeng.6b00144>
- Bergamaschi, P., Houweling, S., Segers, A., Krol, M., Frankenberg, C., Scheepmaker, R. A., Dlugokencky, E., Wofsy, S.C., Kort, E. A., Sweeney, C., Schuck, T., Brenninkmeijer, C., Chen, H., Beck, V., Gerbig, C., 2013. Atmospheric CH₄ in the first decade of the 21st century: Inverse modeling analysis using SCIAMACHY satellite retrievals and NOAA surface measurements. *J. Geophys. Res. Atmos.* 118, 7350–7369. <https://doi.org/10.1002/jgrd.50480>
- Bergamaschi, P., Lubina, C., Königstedt, R., Fischer, H., Veltkamp, A.C., Zwaagstra, O., 1998. Stable isotopic signatures ($\delta^{13}\text{C}$, δD) of methane from European landfill sites. *J. Geophys. Res. Atmos.* 103, 8251–8265. <https://doi.org/10.1029/98JD00105>
- Brandt, A.R., Heath, G.A., Kort, E.A., O’Sullivan, F., Petron, G., Jordaan, S.M., Tans, P., Wilcox, J., Gopstein, A.M., Arent, D., Wofsy, S., Brown, N.J., Bradley, R., Stucky, G.D., Eardley, D., Harriss, R., 2014. Methane Leaks from North American Natural Gas Systems. *Science* (80-.). 343, 733–735. <https://doi.org/10.1126/science.1247045>
- Chanton, J., Liptay, K., 2000. Seasonal variation in methane oxidation in a landfill cover soil as determined by an in situ stable isotope technique. *Global Biogeochem. Cycles* 14, 51–60. <https://doi.org/10.1029/1999GB900087>

- Christen, A., 2014. Atmospheric measurement techniques to quantify greenhouse gas emissions from cities. *Urban Clim.* 10, 241–260.
<https://doi.org/10.1016/j.uclim.2014.04.006>
- Christiansen, J.R., Korhonen, J.F.J., Juszczak, R., Giebels, M., Pihlatie, M., 2011. Assessing the effects of chamber placement, manual sampling and headspace mixing on CH₄ fluxes in a laboratory experiment. *Plant Soil* 343, 171–185.
<https://doi.org/10.1007/s11104-010-0701-y>
- Ciais, P., Sabine, C., Bala, G., Bopp, L., Brovkin, V., Canadell, J., Chhabra, A., DeFries, R., Galloway, J., Heimann, M., Jones, C., Quéré, C. Le, Myneni, R.B., Piao, S., Thornton, P., 2013. Carbon and Other Biogeochemical Cycles, in: Intergovernmental Panel on Climate Change (Ed.), *Climate Change 2013 - The Physical Science Basis. Contribution of Working Group I to the Fifth Assessment Report of the Intergovernmental Panel on Climate Change*. Cambridge University Press, Cambridge, pp. 465–570. <https://doi.org/10.1017/CBO9781107415324.015>
- Cicerone, R.J., Oremland, R.S., 1988. Biogeochemical aspects of atmospheric methane. *Global Biogeochem. Cycles* 2, 299–327.
<https://doi.org/10.1029/GB002i004p00299>
- Daelman, M.R.J., van Voorthuizen, E.M., van Dongen, U.G.J.M., Volcke, E.I.P., van Loosdrecht, M.C.M., 2012. Methane emission during municipal wastewater treatment. *Water Res.* 46, 3657–70. <https://doi.org/10.1016/j.watres.2012.04.024>
- Dean, J.F., Middelburg, J.J., Röckmann, T., Aerts, R., Blauw, L.G., Egger, M., Jetten, M.S.M., de Jong, A.E.E., Meisel, O.H., Rasigraf, O., Slomp, C.P., in't Zandt, M.H., Dolman, A.J., 2018. Methane Feedbacks to the Global Climate System in a Warmer World. *Rev. Geophys.* 56, 207–250. <https://doi.org/10.1002/2017RG000559>
- Desjardins, R.L., Lemon, E.R., 1974. Limitations of an eddy-correlation technique for the determination of the carbon dioxide and sensible heat fluxes. *Boundary-Layer Meteorol.* 5, 475–488. <https://doi.org/10.1007/BF00123493>
- Detweiler, A.M., Bebout, B.M., Frisbee, A.E., Kelley, C. a, Chanton, J.P., Prufert-Bebout, L.E., 2014. Characterization of methane flux from photosynthetic oxidation ponds in a wastewater treatment plant. *Water Sci. Technol.* 70, 980–9.
<https://doi.org/10.2166/wst.2014.317>
- Dlugokencky, E.J., 2018. Recent Global CH₄ [WWW Document]. NOAA/ESRL. URL www.esrl.noaa.gov/gmd/ccgg/trends_ch4/ (accessed 9.14.18).
- Dlugokencky, E.J., Nisbet, E.G., Fisher, R., Lowry, D., 2011. Global atmospheric methane: budget, changes and dangers. *Philos. Trans. R. Soc. A Math. Phys. Eng. Sci.* 369, 2058–2072. <https://doi.org/10.1098/rsta.2010.0341>
- EIA, 2018. U.S. Energy Information Administration [WWW Document]. U.S. Energy Inf.

- Administration. URL <https://www.eia.gov/> (accessed 9.24.18).
- Etioppe, G., Sherwood Lollar, B., 2013. Abiotic methane on earth. *Rev. Geophys.* 51, 276–299. <https://doi.org/10.1002/rog.20011>
- Etminan, M., Myhre, G., Highwood, E.J., Shine, K.P., 2016. Radiative forcing of carbon dioxide, methane, and nitrous oxide: A significant revision of the methane radiative forcing. *Geophys. Res. Lett.* 43, 12,614–12,623. <https://doi.org/10.1002/2016GL071930>
- Fan, S.M., Wofsy, S.C., Bakwin, P.S., Jacob, D.J., Anderson, S.M., Keabian, P.L., McManus, J.B., Kolb, C.E., Fitzjarrald, D.R., 1992. Micrometeorological measurements of CH₄ and CO₂ exchange between the atmosphere and subarctic tundra. *J. Geophys. Res.* 97, 16627. <https://doi.org/10.1029/91JD02531>
- Figueroa, V.K., Mackie, K.R., Guarriello, N., Cooper, C.D., 2009. A Robust Method for Estimating Landfill Methane Emissions. *J. Air Waste Manage. Assoc.* 59, 925–935. <https://doi.org/10.3155/1047-3289.59.8.925>
- Fischer, J.C. von, Cooley, D., Chamberlain, S., Gaylord, A., Griebenow, C.J., Hamburg, S.P., Salo, J., Schumacher, R., Theobald, D., Ham, J., 2017. Rapid, Vehicle-Based Identification of Location and Magnitude of Urban Natural Gas Pipeline Leaks. *Environ. Sci. Technol.* 51, 4091–4099. <https://doi.org/10.1021/acs.est.6b06095>
- Fisher, R.E., France, J.L., Lowry, D., Lanoisellé, M., Brownlow, R., Pyle, J.A., Cain, M., Warwick, N., Skiba, U.M., Drewer, J., Dinsmore, K.J., Leeson, S.R., Bauguitte, S.J., Wellpott, A., Shea, S.J.O., Allen, G., Gallagher, M.W., Pitt, J., Percival, C.J., Bower, K., George, C., Hayman, G.D., Aalto, T., Lohila, A., Aurela, M., Laurila, T., Crill, P.M., McCalley, C.K., Nisbet, E.G., 2017. Measurement of the ¹³C isotopic signature of methane emissions from northern European wetlands. *Global Biogeochem. Cycles* 31, 605–623. <https://doi.org/10.1002/2016GB005504>
- Flanagan, L.B., Ehleringer, J.R., Pataki, D.E., Chanton, J., Chaser, L., Glasser, P., Siegel, D., 2005. Carbon and Hydrogen Isotopic Effects on Microbial Methane from Terrestrial Environments, in: *Stable Isotopes and Biosphere Atmosphere Interactions*. Elsevier, pp. 85–105. <https://doi.org/10.1016/B978-012088447-6/50006-4>
- Franco, B., Mahieu, E., Emmons, L.K., Tzompa-Sosa, Z.A., Fischer, E. V, Sudo, K., Bovy, B., Conway, S., Griffin, D., Hannigan, J.W., Strong, K., Walker, K.A., 2016b. Evaluating ethane and methane emissions associated with the development of oil and natural gas extraction in North America. *Environ. Res. Lett.* 11, 044010. <https://doi.org/10.1088/1748-9326/11/4/044010>
- Giri, C., Zhu, Z., Reed, B., 2005. A comparative analysis of the Global Land Cover 2000 and MODIS land cover data sets. *Remote Sens. Environ.* 94, 123–132. <https://doi.org/10.1016/j.rse.2004.09.005>

- Goldsmith, C.D., Chanton, J., Abichou, T., Swan, N., Green, R., Hater, G., 2012. Methane emissions from 20 landfills across the United States using vertical radial plume mapping. *J. Air Waste Manage. Assoc.* 62, 183–197. <https://doi.org/10.1080/10473289.2011.639480>
- Górka, M., Lewicka-Szczebak, D., Fuß, R., Jakubiak, M., Jędrysek, M.O., 2014. Dynamics and origin of atmospheric CH₄ in a Polish metropolitan area characterized by wetlands. *Appl. Geochemistry* 45, 72–81. <https://doi.org/10.1016/j.apgeochem.2014.03.007>
- Hakala, J.A., 2014. Use of stable isotopes to identify sources of methane in Appalachian Basin shallow groundwaters: a review. *Environ. Sci. Process. Impacts* 16, 2080–6. <https://doi.org/10.1039/c4em00140k>
- Heinemeyer, A., McNamara, N.P., 2011. Comparing the closed static versus the closed dynamic chamber flux methodology: Implications for soil respiration studies. *Plant Soil* 346, 145–151. <https://doi.org/10.1007/s11104-011-0804-0>
- Hornibrook, E.R.C., Bowes, H.L., 2007. Trophic status impacts both the magnitude and stable carbon isotope composition of methane flux from peatlands. *Geophys. Res. Lett.* 34, 2–6. <https://doi.org/10.1029/2007GL031231>
- Howarth, R.W., 2014. A bridge to nowhere: methane emissions and the greenhouse gas footprint of natural gas. *Energy Sci. Eng.* 2, 47–60. <https://doi.org/10.1002/ese3.35>
- Hsu, Y.-K., VanCuren, T., Park, S., Jakober, C., Herner, J., FitzGibbon, M., Blake, D.R., Parrish, D.D., 2010. Methane emissions inventory verification in southern California. *Atmos. Environ.* 44, 1–7. <https://doi.org/10.1016/j.atmosenv.2009.10.002>
- Jackson, R.B., Down, A., Phillips, N.G., Ackley, R.C., Cook, C.W., Plata, D.L., Zhao, K., Phillips, N.G., Ackley, R.C., Cook, C.W., Plata, D.L., Zhao, K., 2014. Natural gas pipeline leaks across Washington, DC. *Environ. Sci. Technol.* 48, 2051–8. <https://doi.org/10.1021/es404474x>
- Jackson, R.B., Vengosh, A., Darrah, T.H., Warner, N.R., Down, A., Poreda, R.J., Osborn, S.G., Zhao, K., Karr, J.D., 2013. Increased stray gas abundance in a subset of drinking water wells near Marcellus shale gas extraction. *Proc. Natl. Acad. Sci.* 110, 11250–11255. <https://doi.org/10.1073/pnas.1221635110>
- Janssens-Maenhout, G., Crippa, M., Guizzardi, D., Muntean, M., Schaaf, E., Dentener, F., Bergamaschi, P., Pagliari, V., Olivier, J.G.J., Peters, J.A.H.W., van Aardenne, J.A., Monni, S., Doering, U., Petrescu, A.M.R., 2017. EDGAR v4.3.2 Global Atlas of the three major Greenhouse Gas Emissions for the period 1970 - 2012. *Earth Syst. Sci. Data Discuss.* 1–55. <https://doi.org/10.5194/essd-2017-79>

- Jay Katz, B., 2011. Microbial Processes and Natural Gas Accumulations. *Open Geol. J.* 5, 75–83. <https://doi.org/10.2174/1874262901105010075>
- Joos, F., Roth, R., Fuglestvedt, J.S., Peters, G.P., Enting, I.G., Von Bloh, W., Brovkin, V., Burke, E.J., Eby, M., Edwards, N.R., Friedrich, T., Frölicher, T.L., Halloran, P.R., Holden, P.B., Jones, C., Kleinen, T., Mackenzie, F.T., Matsumoto, K., Meinshausen, M., Plattner, G.K., Reisinger, A., Segschneider, J., Shaffer, G., Steinacher, M., Strassmann, K., Tanaka, K., Timmermann, A., Weaver, A.J., 2013. Carbon dioxide and climate impulse response functions for the computation of greenhouse gas metrics: A multi-model analysis. *Atmos. Chem. Phys.* 13, 2793–2825. <https://doi.org/10.5194/acp-13-2793-2013>
- Judd, M.J., Kellier, F.M., Ulyatt, M.J., Lassey, K.R., Tate, K.R., Shelton, I.D., Harvey, M.J., Walker, C.F., 1999. Net methane emissions from grazing sheep. *Glob. Chang. Biol.* 5, 647–657. <https://doi.org/10.1046/j.1365-2486.1999.00264.x>
- Karion, A., Sweeney, C., Tans, P., Newberger, T., 2010. AirCore: An Innovative Atmospheric Sampling System. *J. Atmos. Ocean. Technol.* 27, 1839–1853. <https://doi.org/10.1175/2010JTECHA1448.1>
- Keeling, C.D., 1979. The Suess effect: ¹³Carbon-¹⁴Carbon interrelations. *Environ. Int.* 2, 229–300. [https://doi.org/10.1016/0160-4120\(79\)90005-9](https://doi.org/10.1016/0160-4120(79)90005-9)
- Killops, S., Killops, V., 2013. Long-Term Fate of Organic Matter in the Geosphere, in: *Introduction to Organic Geochemistry*. Blackwell Publishing Ltd., Malden, MA USA, pp. 117–165. <https://doi.org/10.1002/9781118697214.ch4>
- Kirschke, S., Bousquet, P., Ciais, P., Saunoy, M., Canadell, J.G., Dlugokencky, E.J., Bergamaschi, P., Bergmann, D., Blake, D.R., Bruhwiler, L., Cameron-Smith, P., Castaldi, S., Chevallier, F., Feng, L., Fraser, A., Heimann, M., Hodson, E.L., Houweling, S., Josse, B., Fraser, P.J., Krummel, P.B., Lamarque, J.-F., Langenfelds, R.L., Le Quéré, C., Naik, V., O’Doherty, S., Palmer, P.I., Pison, I., Plummer, D., Poulter, B., Prinn, R.G., Rigby, M., Ringeval, B., Santini, M., Schmidt, M., Shindell, D.T., Simpson, I.J., Spahni, R., Steele, L.P., Strode, S. A., Sudo, K., Szopa, S., van der Werf, G.R., Voulgarakis, A., van Weele, M., Weiss, R.F., Williams, J.E., Zeng, G., 2013. Three decades of global methane sources and sinks. *Nat. Geosci.* 6, 813–823. <https://doi.org/10.1038/ngeo1955>
- Klevenhusen, F., Bernasconi, S.M., Hofstetter, T.B., Bolotin, J., Kunz, C., Soliva, C.R., 2009. Efficiency of monolaurin in mitigating ruminal methanogenesis and modifying C-isotope fractionation when incubating diets composed of either C3 or C4 plants in a rumen simulation technique (Rusitec) system. *Br. J. Nutr.* 102, 1308–17. <https://doi.org/10.1017/S0007114509990262>
- Kormann, R., Müller, H., Werle, P., 2001. Eddy flux measurements of methane over the fen “Murnauer Moos”, 11°11'E, 47°39'N, using a fast tunable diode laser spectrometer. *Atmos. Environ.* 35, 2533–2544. <https://doi.org/10.1016/S1352->

2310(00)00424-6

- Kvenvolden, K.A., Rogers, B.W., 2005. Gaia's breath - Global methane exhalations. *Mar. Pet. Geol.* 22, 579–590. <https://doi.org/10.1016/j.marpetgeo.2004.08.004>
- Lai, D.Y.F., 2009. Methane Dynamics in Northern Peatlands : A Review. *Pedosphere* 19, 409–421. [https://doi.org/10.1016/S1002-0160\(09\)00003-4](https://doi.org/10.1016/S1002-0160(09)00003-4)
- Lassey, K. R., Etheridge, D.M., Lowe, D.C., Smith, A. M., Ferretti, D.F., 2007a. Centennial evolution of the atmospheric methane budget: what do the carbon isotopes tell us? *Atmos. Chem. Phys.* 7, 2119–2139. <https://doi.org/10.5194/acp-7-2119-2007>
- Lassey, K. R., Lowe, D.C., Smith, A.M., 2007b. The atmospheric cycling of radiomethane and the “fossil fraction” of the methane source. *Atmos. Chem. Phys.* 7, 2141–2149. <https://doi.org/10.5194/acp-7-2141-2007>
- Laubach, J., Kelliher, F.M., 2004. Measuring methane emission rates of a dairy cow herd by two micrometeorological techniques. *Agric. For. Meteorol.* 125, 279–303. <https://doi.org/10.1016/j.agrformet.2004.04.003>
- Le Quéré, C., Andrew, R.M., Friedlingstein, P., Sitch, S., Pongratz, J., Manning, A.C., Korsbakken, J.I., Peters, G.P., Canadell, J.G., Jackson, R.B., Boden, T.A., Tans, P.P., Andrews, O.D., Arora, V.K., Bakker, D.C.E., Barbero, L., Becker, M., Betts, R.A., Bopp, L., Chevallier, F., Chini, L.P., Ciais, P., Cosca, C.E., Cross, J., Currie, K., Gasser, T., Harris, I., Hauck, J., Haverd, V., Houghton, R.A., Hunt, C.W., Hurtt, G., Ilyina, T., Jain, A.K., Kato, E., Kautz, M., Keeling, R.F., Klein Goldewijk, K., Körtzinger, A., Landschützer, P., Lefèvre, N., Lenton, A., Lienert, S., Lima, I., Lombardozzi, D., Metzl, N., Millero, F., Monteiro, P.M.S., Munro, D.R., Nabel, J.E.M.S., Nakaoka, S.-I., Nojiri, Y., Padin, X.A., Pregon, A., Pfeil, B., Pierrot, D., Poulter, B., Rehder, G., Reimer, J., Rödenbeck, C., Schwinger, J., Séférian, R., Skjelvan, I., Stocker, B.D., Tian, H., Tilbrook, B., Tubiello, F.N., Van Der Laan-Luijkx, I.T., Van Der Werf, G.R., Van Heuven, S., Viovy, N., Vuichard, N., Walker, A.P., Watson, A.J., Wiltshire, A.J., Zaehle, S., Zhu, D., 2018. Global Carbon Budget 2017. *Earth Syst. Sci. Data* 10, 405–448. <https://doi.org/10.5194/essd-10-405-2018>
- Lessard, R., Rochette, P., Topp, E., Pattey, E., Desjardins, R.L., Beaumont, G., 1994. Methane and carbon dioxide fluxes from poorly drained adjacent cultivated and forest sites. *Can. J. Soil Sci.* 74, 139–146. <https://doi.org/10.4141/cjss94-021>
- Levin, I., Glatzel-Mattheier, H., Marik, T., Cuntz, M., Schmidt, M., Worthy, D.E., 1999. Verification of German methane emission inventories and their recent changes based on atmospheric observations. *J. Geophys. Res. Atmos.* 104, 3447–3456. <https://doi.org/10.1029/1998JD100064>
- Liebetrau, J., Reinelt, T., Clemens, J., Hafermann, C., Friehe, J., Weiland, P., 2013. Analysis of greenhouse gas emissions from 10 biogas plants within the agricultural

- sector. *Water Sci. Technol.* 67, 1370–9. <https://doi.org/10.2166/wst.2013.005>
- Limpens, J., Berendse, F., Blodau, C., Canadell, J.G., Freeman, C., Holden, J., Roulet, N., Rydin, H., Schaepman-Strub, G., 2008. Peatlands and the carbon cycle: from local processes to global implications - a synthesis. *Biogeosciences* 5, 1475–1491. <https://doi.org/10.5194/bgd-5-1379-2008>
- Liptay, K., Chanton, J., Czepiel, P., Mosher, B., 1998. Use of stable isotopes to determine methane oxidation in landfill cover soils. *J. Geophys. Res. Atmos.* 103, 8243–8250. <https://doi.org/10.1029/97JD02630>
- Lopez, M., Sherwood, O.A., Dlugokencky, E.J., Kessler, R., Giroux, L., Worthy, D.E.J., 2017. Isotopic signatures of anthropogenic CH₄ sources in Alberta, Canada. *Atmos. Environ.* 164, 280–288. <https://doi.org/10.1016/j.atmosenv.2017.06.021>
- Lowry, D., Holmes, C.W., Rata, N.D., O'Brien, P., Nisbet, E.G., 2001. London methane emissions: Use of diurnal changes in concentration and $\delta^{13}\text{C}$ to identify urban sources and verify inventories. *J. Geophys. Res. Atmos.* 106, 7427–7448. <https://doi.org/10.1029/2000JD900601>
- Martini, A.M., Budai, J.M., Walter, L.M., Schoell, M., 1996. Microbial generation of economic accumulations of methane within a shallow organic-rich shale. *Nature* 383, 155–158. <https://doi.org/10.1038/383155a0>
- McCalley, C.K., Woodcroft, B.J., Hodgkins, S.B., Wehr, R. A., Kim, E.-H., Mondav, R., Crill, P.M., Chanton, J.P., Rich, V.I., Tyson, G.W., Saleska, S.R., 2014. Methane dynamics regulated by microbial community response to permafrost thaw. *Nature* 514, 478–481. <https://doi.org/10.1038/nature13798>
- McEwing, K.R., Fisher, J.P., Zona, D., 2015. Environmental and vegetation controls on the spatial variability of CH₄ emission from wet-sedge and tussock tundra ecosystems in the Arctic. *Plant Soil* 388, 37–52. <https://doi.org/10.1007/s11104-014-2377-1>
- McKain, K., Down, A., Raciti, S.M., Budney, J., Hutyra, L.R., Floerchinger, C., Herndon, S.C., Nehrkorn, T., Zahniser, M.S., Jackson, R.B., Phillips, N., Wofsy, S.C., 2015. Methane emissions from natural gas infrastructure and use in the urban region of Boston, Massachusetts. *Proc. Natl. Acad. Sci.* 112, 1941–1946. <https://doi.org/10.1073/pnas.1416261112>
- Miller, S.M., Wofsy, S.C., Michalak, A.M., Kort, E.A., Andrews, A.E., Biraud, S.C., Dlugokencky, E.J., Eluszkiewicz, J., Fischer, M.L., Janssens-maenhout, G., Miller, B.R., Miller, J.B., Montzka, S.A., Nehrkorn, T., Sweeney, C., 2013. Anthropogenic emissions of methane in the United States. *Proc. Natl. Acad. Sci. U. S. A.* <https://doi.org/10.1073/pnas.1314392110>
- Mohan, M., Siddiqui, T.A., 1997. An Evaluation of Dispersion Coefficients for use in Air

- Quality Models. *Boundary-Layer Meteorol.* 84, 177–205.
<https://doi.org/10.1023/A:1000317704452>
- Monks, P.S., Archibald, A.T., Colette, A., Cooper, O., Coyle, M., Derwent, R., Fowler, D., Granier, C., Law, K.S., Mills, G.E., Stevenson, D.S., Tarasova, O., Thouret, V., Von Schneidmesser, E., Sommariva, R., Wild, O., Williams, M.L., 2015. Tropospheric ozone and its precursors from the urban to the global scale from air quality to short-lived climate forcer. *Atmos. Chem. Phys.* 15, 8889–8973.
<https://doi.org/10.5194/acp-15-8889-2015>
- Mønster, J.G., Samuelsson, J., Kjeldsen, P., Rella, C.W., Scheutz, C., 2014. Quantifying methane emission from fugitive sources by combining tracer release and downwind measurements - a sensitivity analysis based on multiple field surveys. *Waste Manag.* 34, 1416–28. <https://doi.org/10.1016/j.wasman.2014.03.025>
- Myhre, G., Shindell, D.T., Bréon, F.-M., Collins, W., Fuglestedt, J., Huang, J., Koch, D., Lamarque, J.-F., Lee, D., Mendoza, B., Nakajima, T., Robock, A., Stephens, G., Takemura, T., Zhang, H., 2013. Anthropogenic and Natural Radiative Forcing. *Clim. Chang. 2013 Phys. Sci. Basis. Contrib. Work. Gr. I to Fifth Assess. Rep. Intergov. Panel Clim. Chang.* 659–740. <https://doi.org/10.1017/CBO9781107415324.018>
- Nisbet, E.G., Dlugokencky, E.J., Manning, M.R., Lowry, D., Fisher, R.E., France, J.L., Michel, S.E., Miller, J.B., White, J.W.C., Vaughn, B., Bousquet, P., Pyle, J.A., Warwick, N.J., Cain, M., Brownlow, R., Zazzeri, G., Lanoisellé, M., Manning, A.C., Gloor, E., Worthy, D.E.J., Brunke, E.-G., Labuschagne, C., Wolff, E.W., Ganesan, A.L., 2016. Rising atmospheric methane: 2007-2014 growth and isotopic shift. *Global Biogeochem. Cycles* 30, 1356–1370.
<https://doi.org/10.1002/2016GB005406>
- NIST, 2014. Differential absorption LIDAR for the detection and quantification of greenhouse gases [WWW Document]. *Natl. Inst. Stand. Technol.* URL <http://www.nist.gov/pml/div686/molec-biophotonics/other-activities.cfm> (accessed 12.1.14).
- NPL, 2014. Remote Emissions Surveys - DIAL [WWW Document]. *Natl. Phys. Lab.* URL <http://www.npl.co.uk/measurement-services/environmental-monitoring/remote-emissions-surveys-dial> (accessed 12.1.14).
- Ono, S., Wang, D.T., Gruen, D.S., Sherwood Lollar, B., Zahniser, M.S., McManus, B.J., Nelson, D.D., 2014. Measurement of a Doubly Substituted Methane Isotopologue, 13CH3D, by Tunable Infrared Laser Direct Absorption Spectroscopy. *Anal. Chem.* 86, 6487–6494. <https://doi.org/10.1021/ac5010579>
- Oshita, K., Okumura, T., Takaoka, M., Fujimori, T., Appels, L., Dewil, R., 2014. Methane and nitrous oxide emissions following anaerobic digestion of sludge in Japanese sewage treatment facilities. *Bioresour. Technol.* 171, 175–81.

<https://doi.org/10.1016/j.biortech.2014.08.081>

- Papa, F., Prigent, C., Aires, F., Jimenez, C., Rossow, W.B., Matthews, E., 2010. Interannual variability of surface water extent at the global scale, 1993–2004. *J. Geophys. Res.* 115, D12111. <https://doi.org/10.1029/2009JD012674>
- Peischl, J., Ryerson, T.B., Brioude, J., Aikin, K.C., Andrews, A. E., Atlas, E., Blake, D., Daube, B.C., de Gouw, J. A., Dlugokencky, E., Frost, G.J., Gentner, D.R., Gilman, J.B., Goldstein, A. H., Harley, R. A., Holloway, J.S., Kofler, J., Kuster, W.C., Lang, P.M., Novelli, P.C., Santoni, G.W., Trainer, M., Wofsy, S.C., Parrish, D.D., 2013. Quantifying sources of methane using light alkanes in the Los Angeles basin, California. *J. Geophys. Res. Atmos.* 118, 4974–4990. <https://doi.org/10.1002/jgrd.50413>
- Phillips, N.G., Ackley, R., Crosson, E.R., Down, A., Hutyra, L.R., Brondfield, M., Karr, J.D., Zhao, K., Jackson, R.B., 2013. Mapping urban pipeline leaks: Methane leaks across Boston. *Environ. Pollut.* 173, 1–4. <https://doi.org/10.1016/j.envpol.2012.11.003>
- Poulter, B., Bousquet, P., Canadell, J.G., Ciais, P., Peregón, A., Saunio, M., Arora, V.K., Beerling, D.J., Brovkin, V., Jones, C.D., Joos, F., Gedney, N., Ito, A., Kleinen, T., Koven, C.D., McDonald, K., Melton, J.R., Peng, C., Peng, S., Prigent, C., Schroeder, R., Riley, W.J., Saito, M., Spahni, R., Tian, H., Taylor, L., Viovy, N., Wilton, D., Wiltshire, A., Xu, X., Zhang, B., Zhang, Z., Zhu, Q., 2017. Global wetland contribution to 2000–2012 atmospheric methane growth rate dynamics. *Environ. Res. Lett.* 12, 094013. <https://doi.org/10.1088/1748-9326/aa8391>
- Povinec, P., Chudý, M., Šivo, A., 1986. Anthropogenic Radiocarbon: Past, Present, and Future. *Radiocarbon* 28, 668–672. <https://doi.org/10.1017/S0033822200007876>
- Prinzhofer, A., Pernaton, É., 1997. Isotopically light methane in natural gas: Bacterial imprint or diffusive fractionation? *Chem. Geol.* 142, 193–200. [https://doi.org/10.1016/S0009-2541\(97\)00082-X](https://doi.org/10.1016/S0009-2541(97)00082-X)
- Quay, P., Stutsman, J., Wilbur, D., Snover, A., Dlugokencky, E., Brown, T., 1999. The isotopic composition of atmospheric methane. *Global Biogeochem. Cycles* 13, 445–461. <https://doi.org/10.1029/1998GB900006>
- Rella, C.W., Hoffnagle, J., He, Y., Tajima, S., 2015. Local- and regional-scale measurements of CH₄, δ¹³CH₄, and C₂H₆ in the Uintah Basin using a mobile stable isotope analyzer. *Atmos. Meas. Tech.* 8, 4539–4559. <https://doi.org/10.5194/amt-8-4539-2015>
- Santoni, G.W., Lee, B.H., Goodrich, J.P., Varner, R.K., Crill, P.M., McManus, J.B., Nelson, D.D., Zahniser, M.S., Wofsy, S.C., 2012. Mass fluxes and isofluxes of methane (CH₄) at a New Hampshire fen measured by a continuous wave quantum cascade laser spectrometer. *J. Geophys. Res.* 117, D10301.

<https://doi.org/10.1029/2011JD016960>

- Saunio, M., Bousquet, P., Poulter, B., Peregon, A., Ciais, P., Canadell, J.G., Dlugokencky, E.J., Etiope, G., Bastviken, D., Houweling, S., Janssens-Maenhout, G., Tubiello, F.N., Castaldi, S., Jackson, R.B., Alexe, M., Arora, V.K., Beerling, D.J., Bergamaschi, P., Blake, D.R., Brailsford, G., Brovkin, V., Bruhwiler, L., Crevoisier, C., Crill, P., Covey, K., Curry, C., Frankenberg, C., Gedney, N., Höglund-Isaksson, L., Ishizawa, M., Ito, A., Joos, F., Kim, H.S., Kleinen, T., Krummel, P., Lamarque, J.F., Langenfelds, R., Locatelli, R., Machida, T., Maksyutov, S., McDonald, K.C., Marshall, J., Melton, J.R., Morino, I., Naik, V., O'Doherty, S., Parmentier, F.J.W., Patra, P.K., Peng, C., Peng, S., Peters, G.P., Pison, I., Prigent, C., Prinn, R., Ramonet, M., Riley, W.J., Saito, M., Santini, M., Schroeder, R., Simpson, I.J., Spahni, R., Steele, P., Takizawa, A., Thornton, B.F., Tian, H., Tohjima, Y., Viovy, N., Voulgarakis, A., Van Weele, M., Van Der Werf, G.R., Weiss, R., Wiedinmyer, C., Wilton, D.J., Wiltshire, A., Worthy, D., Wunch, D., Xu, X., Yoshida, Y., Zhang, B., Zhang, Z., Zhu, Q., 2016a. The global methane budget 2000-2012. *Earth Syst. Sci. Data* 8, 697–751. <https://doi.org/10.5194/essd-8-697-2016>
- Saunio, M., Bousquet, P., Poulter, B., Peregon, A., Ciais, P., Canadell, J.G., Dlugokencky, E.J., Etiope, G., Bastviken, D., Houweling, S., Janssens-Maenhout, G., Tubiello, F.N., Castaldi, S., Jackson, R.B., Alexe, M., Arora, V.K., Beerling, D.J., Bergamaschi, P., Blake, D.R., Brailsford, G., Brovkin, V., Bruhwiler, L., Crevoisier, C., Crill, P., Covey, K., Curry, C., Frankenberg, C., Gedney, N., Höglund-Isaksson, L., Ishizawa, M., Ito, A., Joos, F., Kim, H.S., Kleinen, T., Krummel, P., Lamarque, J.F., Langenfelds, R., Locatelli, R., Machida, T., Maksyutov, S., McDonald, K.C., Marshall, J., Melton, J.R., Morino, I., Naik, V., O'Doherty, S., Parmentier, F.J.W., Patra, P.K., Peng, C., Peng, S., Peters, G.P., Pison, I., Prigent, C., Prinn, R., Ramonet, M., Riley, W.J., Saito, M., Santini, M., Schroeder, R., Simpson, I.J., Spahni, R., Steele, P., Takizawa, A., Thornton, B.F., Tian, H., Tohjima, Y., Viovy, N., Voulgarakis, A., Van Weele, M., Van Der Werf, G.R., Weiss, R., Wiedinmyer, C., Wilton, D.J., Wiltshire, A., Worthy, D., Wunch, D., Xu, X., Yoshida, Y., Zhang, B., Zhang, Z., Zhu, Q., 2016b. The Global Methane Budget 2000-2012 [WWW Document]. URL www.globalcarbonproject.org/methanebudget (accessed 1.18.19).
- Schaefer, H., Fletcher, S.E.M., Veidt, C., Lassey, K.R., Brailsford, G.W., Bromley, T.M., Dlugokencky, E.J., Michel, S.E., Miller, J.B., Levin, I., Lowe, D.C., Martin, R.J., Vaughn, B.H., White, J.W.C., 2016. A 21st-century shift from fossil-fuel to biogenic methane emissions indicated by $^{13}\text{CH}_4$. *Science* (80-). 352, 80–84. <https://doi.org/10.1126/science.aad2705>
- Schwietzke, S., Griffin, W.M., Matthews, H.S., Bruhwiler, L.M.P., 2014a. Natural gas fugitive emissions rates constrained by global atmospheric methane and ethane. *Environ. Sci. Technol.* 48, 7714–22. <https://doi.org/10.1021/es501204c>
- Schwietzke, S., Griffin, W.M., Matthews, H.S., Bruhwiler, L.M.P., 2014b. Global Bottom-Up Fossil Fuel Fugitive Methane and Ethane Emissions Inventory for Atmospheric

- Modeling. *ACS Sustain. Chem. Eng.* 2, 1992–2001.
<https://doi.org/10.1021/sc500163h>
- Sherwood, O.A., Schwietzke, S., Arling, V.A., Etiope, G., 2017. Global inventory of gas geochemistry data from fossil fuel, microbial and burning sources, version 2017. *Earth Syst. Sci. Data* 9, 639–656. <https://doi.org/10.5194/essd-9-639-2017>
- Shindell, D.T., Kuylenstierna, J.C.I., Vignati, E., van Dingenen, R., Amann, M., Klimont, Z., Anenberg, S.C., Muller, N., Janssens-Maenhout, G., Raes, F., Schwartz, J., Faluvegi, G., Pozzoli, L., Kupiainen, K., Hoglund-Isaksson, L., Emberson, L., Streets, D., Ramanathan, V., Hicks, K., Oanh, N.T.K., Milly, G., Williams, M., Demkine, V., Fowler, D., 2012. Simultaneously Mitigating Near-Term Climate Change and Improving Human Health and Food Security. *Science* (80-.). 335, 183–189. <https://doi.org/10.1126/science.1210026>
- Simpson, I.J., Sulbaek Andersen, M.P., Meinardi, S., Bruhwiler, L., Blake, N.J., Helmig, D., Rowland, F.S., Blake, D.R., 2012. Long-term decline of global atmospheric ethane concentrations and implications for methane. *Nature* 488, 490–4. <https://doi.org/10.1038/nature11342>
- Slater, C., Preston, T., Weaver, L.T., 2001. Stable isotopes and the international system of units. *Rapid Commun. mass Spectrom.* 15, 1270–3. <https://doi.org/10.1002/rcm.328>
- Stocker, T.F., Qin, D., Plattner, G.-K., Tignor, M.M.B., Allen, S.K., Boschung, J., Nauels, A., Xia, Y., Bex, V., Midgley, P.M., (eds.), 2013. *Climate Change 2013: The Physical Science Basis. Contribution of Working Group I to the Fifth Assessment Report of the Intergovernmental Panel on Climate Change.* Cambridge, United Kingdom and New York, NY, USA.
- Stolper, D.A., Lawson, M., Davis, C., Ferreira, A., Santos Neto, E., Ellis, G., Lewan, M., Martini, A., Tang, Y., Schoell, M., Sessions, A.L., Eiler, J., 2014a. Formation temperatures of thermogenic and biogenic methane. *Science* (80-.). 344, 1500–3. <https://doi.org/10.1126/science.1254509>
- Stolper, D.A., Sessions, A.L., Ferreira, A.A., Santos Neto, E.V., Schimmelmann, A., Shusta, S.S., Valentine, D.L., Eiler, J.M., 2014b. Combined ^{13}C – D and D – D clumping in methane: Methods and preliminary results. *Geochim. Cosmochim. Acta* 126, 169–191. <https://doi.org/10.1016/j.gca.2013.10.045>
- Stolper, D.A., DA, Martini, A.M.A., Clog, M., Douglas, P.M., Shusta, S.S., Valentine, D.L., Sessions, A.L., Eiler, J.J.M.J.M., Eiler, J.J.M.J.M., 2015. Distinguishing and understanding thermogenic and biogenic sources of methane using multiply substituted isotopologues. *Geochim. Cosmochim. Acta* 161, 219–247. <https://doi.org/10.1016/j.gca.2015.04.015>
- Thoma, E.D., Green, R.B., Hater, G.R., Goldsmith, C.D., Swan, N.D., Chase, M.J.,

- Hashmonay, R.A., 2010. Development of EPA OTM 10 for Landfill Applications. *J. Environ. Eng.* 136, 769–776. [https://doi.org/10.1061/\(ASCE\)EE.1943-7870.0000157](https://doi.org/10.1061/(ASCE)EE.1943-7870.0000157)
- Townsend-Small, A., Tyler, S.C., Pataki, D.E., Xu, X., Christensen, L.E., 2012. Isotopic measurements of atmospheric methane in Los Angeles, California, USA: Influence of “fugitive” fossil fuel emissions. *J. Geophys. Res. Atmos.* 117, n/a-n/a. <https://doi.org/10.1029/2011JD016826>
- Treat, C.C., Bloom, A.A., Marushchak, M.E., 2018. Nongrowing season methane emissions—a significant component of annual emissions across northern ecosystems. *Glob. Chang. Biol.* 24, 3331–3343. <https://doi.org/10.1111/gcb.14137>
- Turetsky, M.R., Kotowska, A., Bubier, J., Dise, N.B., Crill, P., Hornibrook, E.R.C., Minkinen, K., Moore, T.R., Myers-Smith, I.H., Nykänen, H., Olefeldt, D., Rinne, J., Saarnio, S., Shurpali, N., Tuittila, E.-S., Waddington, J.M., White, J.R., Wickland, K.P., Wilmking, M., 2014. A synthesis of methane emissions from 71 northern, temperate, and subtropical wetlands. *Glob. Chang. Biol.* 20, 2183–97. <https://doi.org/10.1111/gcb.12580>
- Turner, A.J., Frankenberg, C., Wennberg, P.O., Jacob, D.J., 2017. Ambiguity in the causes for decadal trends in atmospheric methane and hydroxyl. *Proc. Natl. Acad. Sci.* 114, 5367–5372. <https://doi.org/10.1073/pnas.1616020114>
- U.S. EPA, 2011. EPA Handbook: Optical Remote Sensing for Measurement and Monitoring of Emission Flux. U.S. Environmental Protection Agency.
- U.S. EPA, 2007. Evaluation of Fugitive Emissions Using Ground-Based Optical Remote Sensing Technology Evaluation of Fugitive Emissions Using Ground-Based Optical Remote Sensing Technology.
- US EPA, 2017. Lanfill Gas Energy Project Development Handbook.
- Velasco, E., Roth, M., 2010. Cities as Net Sources of CO₂: Review of Atmospheric CO₂ Exchange in Urban Environments Measured by Eddy Covariance Technique. *Geogr. Compass* 4, 1238–1259. <https://doi.org/10.1111/j.1749-8198.2010.00384.x>
- Wang, J., Zhang, J., Xie, H., Qi, P., Ren, Y., Hu, Z., 2011. Methane emissions from a full-scale A/A/O wastewater treatment plant. *Bioresour. Technol.* 102, 5479–85. <https://doi.org/10.1016/j.biortech.2010.10.090>
- Wang, Z., Schauble, E. A., Eiler, J.M., 2004. Equilibrium thermodynamics of multiply substituted isotopologues of molecular gases. *Geochim. Cosmochim. Acta* 68, 4779–4797. <https://doi.org/10.1016/j.gca.2004.05.039>
- West, J.J., Fiore, A.M., Horowitz, L.W., Mauzerall, D.L., 2006. Global health benefits of mitigating ozone pollution with methane emission controls. *Proc. Natl. Acad. Sci.*

103, 3988–3993. <https://doi.org/10.1073/pnas.0600201103>

- Whalen, S.C., 2005. Biogeochemistry of methane exchange between natural wetlands and the atmosphere. *Environ. Eng. Sci.* 22. <https://doi.org/10.1089/ees.2005.22.73>.
- Whiticar, M.J., 1999. Carbon and hydrogen isotope systematics of bacterial formation and oxidation of methane. *Chem. Geol.* 161, 291–314. [https://doi.org/10.1016/S0009-2541\(99\)00092-3](https://doi.org/10.1016/S0009-2541(99)00092-3)
- Worden, J.R., Bloom, A.A., Pandey, S., Jiang, Z., Worden, H.M., Walker, T.W., Houweling, S., Röckmann, T., 2017. Reduced biomass burning emissions reconcile conflicting estimates of the post-2006 atmospheric methane budget. *Nat. Commun.* 8, 1–11. <https://doi.org/10.1038/s41467-017-02246-0>
- Wright, A.-D.G., Klieve, A. V., 2011. Does the complexity of the rumen microbial ecology preclude methane mitigation? *Anim. Feed Sci. Technol.* 166–167, 248–253. <https://doi.org/10.1016/j.anifeedsci.2011.04.015>
- Yoshida, H., Mønster, J.G., Scheutz, C., 2014. Plant-integrated measurement of greenhouse gas emissions from a municipal wastewater treatment plant. *Water Res.* 61, 108–18. <https://doi.org/10.1016/j.watres.2014.05.014>
- Zavala-Araiza, D., Lyon, D., Alvarez, R.A., Palacios, V., Harriss, R., Lan, X., Talbot, R., Hamburg, S.P., 2015. Toward a Functional Definition of Methane Super-Emitters: Application to Natural Gas Production Sites. *Environ. Sci. Technol.* 49, 8167–8174. <https://doi.org/10.1021/acs.est.5b00133>
- Zazzeri, G., Lowry, D., Fisher, R.E., France, J.L., Lanoisellé, M., Grimmond, C.S.B., Nisbet, E.G., 2017. Evaluating methane inventories by isotopic analysis in the London region. *Sci. Rep.* 7, 4854. <https://doi.org/10.1038/s41598-017-04802-6>
- Zazzeri, G., Lowry, D., Fisher, R.E., France, J.L., Lanoisellé, M., Nisbet, E.G., 2015. Plume mapping and isotopic characterisation of anthropogenic methane sources. *Atmos. Environ.* 110, 151–162. <https://doi.org/10.1016/j.atmosenv.2015.03.029>

2

Mobile methane measurements: Effects of instrument specifications on data interpretation, reproducibility, and isotopic precision

Takriti, M., Wynn P., Elias, D., Ward, S., McNamara, N.

2.1 Abstract

Mobile vehicle-based measurements are an emerging tool in identifying emissions of methane (CH₄) as well as air pollutants. This technology has significant potential for applications in research, industry and regulatory compliance while the number of instrumental setups is increasing. It is thus important to consider how the specifications of instruments used in such applications impact the results obtained, and their interpretation. Beyond simple concentration measurements, tracers such as isotope ratios associated with different emission sources are increasingly used in mobile measurements to attribute emissions. However, instrument precision and data analysis differ from traditional laboratory analysis, e.g. using IRMS systems, and the precision of mobile isotopic measurements depends heavily on sampling conditions. We thus tested the effects of instrument speed on CH₄ concentration measurements by outfitting a vehicle with two gas analysers with respective rise times (T_{90}) of 38 s and 14 s and recorded concentration measurements over a total distance of 560 km. We further programmed a simple physical model that predicts the precision achievable under different measurement conditions and instrument specifications. We found slower instrument response times lead to a greater

underestimation of atmospheric concentrations, both while driving and during static measurements, however, there is a perfect agreement between peak areas. This has important implications for the comparability of measurements between surveys with different instrumental setups, particularly when absolute values are important. We further found that for a given instrument precision and speed, the precision of isotopic measurements primarily depends on the range of atmospheric concentrations measured and the duration of measurement. These results provide a framework for optimising sampling strategies under given objectives, conditions, and instrument capabilities.

2.2 Introduction

Atmospheric concentrations of methane (CH_4), a greenhouse gas with 32 times the global warming potential of carbon dioxide (CO_2), continue to rise (Etminan et al., 2016). There has thus been increasing focus on reducing CH_4 emissions from anthropogenic sources, such as natural gas infrastructure, agriculture, and waste treatment. However, efforts to reduce emissions are still hampered by uncertainty around the location and contribution of fugitive emission sources, and there is considerable disagreement between inventory estimates and atmospheric measurements (e.g. Turner et al., 2016).

Mobile measurement systems, which use gas analysers based on infrared absorption spectroscopy, were used as early as the 1990s to detect CH_4 emissions (Czepiel et al., 1996), but more recent advancements in spectroscopic gas analysers have led to the increasing use of mobile, vehicle mounted systems to map CH_4 concentrations, detect fugitive emission sources, and quantify emission rates (e.g. Fischer et al., 2017; Jackson et al., 2014). The origin of emissions can be ambiguous, particularly if there are multiple emission sources in an area or the source is unknown. Analysers that measure both CH_4 concentration and a tracer, such as $^{13}\text{CH}_4$ and/or C_2H_6 , can distinguish between emission sources. In particular, it becomes possible to distinguish between microbial sources, such as landfills or agricultural emissions, which are typically depleted in $^{13}\text{CH}_4$ and do not emit C_2H_6 , and thermogenic sources, such as natural gas extraction and distribution, which are typically enriched in $^{13}\text{CH}_4$ and co-emit C_2H_6 .

Real-time mobile CH_4 measurements offer several advantages compared to static measurements or lab analysis of field samples: 1) High spatial resolution as CH_4 concentration can be mapped at a scale of meters; 2) Good spatial coverage, as depending on road access and desired density of measurements, tens to hundreds of square kilometres

can be covered within days; 3) Immediate detection of elevated concentrations enabling rapid investigation and response to gas leaks; 4) Potential sources can be surveyed from nearby roads in situations where direct access may be difficult. This approach therefore offers wide applications within academic research, industry monitoring and maintenance, as well as regulatory oversight and compliance monitoring.

Instrument manufacturers have been developing systems that integrate sampling, gas analysis, navigation, and data processing, marketed primarily as turn-key solutions for leak detection in the natural gas industry. Both ready-made and custom-built set-ups have been used variously for applications such as detecting fugitive emissions from waste water treatment plants (Yoshida et al., 2014), landfills (Mønster et al., 2014), fossil fuel production (e.g. Eapi et al., 2014; Rella et al., 2015), urban gas pipe lines (Fischer et al., 2017; Jackson et al., 2014), and geological fault lines (Boothroyd et al., 2016).

Mobile survey systems may therefore see more use in the future as spectroscopic gas analysers become more widely available, and new applications, such as operation on unmanned aerial vehicles, are explored. However, the published literature on mobile CH₄ measurements has mainly focussed on the dissemination of results, and while instrument setup and performance have been described in detail elsewhere (e.g. Rella et al., 2015a), the effects of instrument specifications on results obtained and their interpretation have rarely been considered.

Current mobile spectroscopic gas analysers measure concentrations with precisions in the ppb range. While this level of precision is generally sufficient for the requirements of mobile surveys, measured concentrations are not necessarily equal to atmospheric concentrations, due to a lag in instrument response. Gas in the optical cavity of a spectroscopic gas analyser is replaced continuously over the course of multiple measurement cycles, described by the rise time of the instrument. When a step change in concentration occurs, the final concentration is only measured if it is sampled for the duration of the rise (or corresponding fall) time (Brunner and Westenskow, 1988). This can lead to underestimation of atmospheric concentrations in mobile measurements and impede comparability of results obtained with different instrumental setups.

The use of isotopic analysers to attribute and characterise emissions holds great potential to improve understanding of CH₄ emission sources and to improve emission estimates. However, current mobile spectroscopic gas analysers measure ¹³CH₄/¹²CH₄ ratios with two

orders of magnitude lower precision than isotope ratio mass spectrometry (IRMS) systems (Zazzeri et al., 2015). Moreover, instrument precision is generally specified for averages of continuous measurements of a sample over a period of time, while mobile measurements are variable and typically use regression analysis, such as Keeling plots, to derive source isotope signature estimates (e.g. Lopez et al., 2017; Rella et al., 2015a). The effective precision during mobile measurements thus depends on a variety of factors, including both instrument and emission characteristics.

The range of instrumental setups, particularly the gas analysers used, is increasing, and applications are moving beyond isolated surveys. It is therefore essential to consider how the specifications of the hardware used in mobile laboratories will affect the performance, suitability for different applications, optimization of sampling regimes, and particularly the reproducibility of measurements.

To address this need, we here compare data produced by two different instruments using a custom-built mobile system built around both an isotopic ($^{13}\text{C}/^{12}\text{C}$) gas analyser, and a concentration-only gas analyser, and evaluate the effects of instrument speed on different measures of CH_4 emissions and their comparability between instruments. Additionally, we aimed to further investigate generalizable patterns in isotopic uncertainty in mobile measurements, independent of both instrumentation and environmental conditions. To accomplish this, we used Monte Carlo simulations of a simple physical model to evaluate the effects of instrument precision, speed, and emission characteristics on estimated precision of isotopic measurements. The model results were validated by comparing our empirical estimates of source signature precision with outputs of model simulations.

2.3 Materials and methods

2.3.1 Methane measurements

To evaluate the effect of instrument characteristics on CH_4 measurements in the field, a vehicle (Mitsubishi L200) was equipped with two gas analysers, a Picarro G2201-*i* isotopic gas analyser (henceforth G2201-*i*, Picarro Inc. Santa Clara, USA) and a Los Gatos Research Ultraportable Greenhouse Gas Analyzer (henceforth UGGA, Los Gatos Research Inc., San Jose, USA). The G2201-*i* and the UGGA have rise times (T_{90}) of 38 s and 14 s, flow rates of 25 mL min^{-1} and 650 mL min^{-1} , and a measurement frequency of 0.26 Hz and 1.2 Hz, respectively. Both instruments measure CO_2 , CH_4 , and H_2O in air. The difference in

specification between the two instruments is largely because they are optimized for different tasks and capabilities: the G2201-*i*'s lower flow rate enables more precise isotope measurements, whereas the UGGA is designed for rapid flux measurements.

The air inlet was mounted on the roof of the vehicle and connected to the air inlet of the UGGA via a 310-cm nylon tube with an outer/inner diameter of 6 mm/3 mm. A PTFE air filter (Vacushield, Pall Life Sciences, MI, USA) was mounted on the inlet and airflow could be redirected via a solenoid valve to a drying column inside the vehicle during instrument shutdown or to protect the instrument from moisture intake. The two gas analysers were connected in series with the G2201-*i* air inlet connected to the UGGA air outlet (Figure 2.1). Excess air flow was vented via an open split. The output of each analyser, as well as the anemometer (see below), was broadcast via Wi-Fi to two tablet devices mounted in front of the passenger seat to monitor measurements in real time. The G2201-*i* was powered by five 72 Ah deep cycle batteries connected in parallel to a pure sine wave power inverter, other components used DC power from a single battery (Figure 2.1). The batteries provided enough charge to operate the system for over 10 h of continuous measurements. For electrical safety, fuses were installed between the batteries and the power inverter, as well as in the DC circuit, and the AC system was grounded to the chassis of the vehicle.

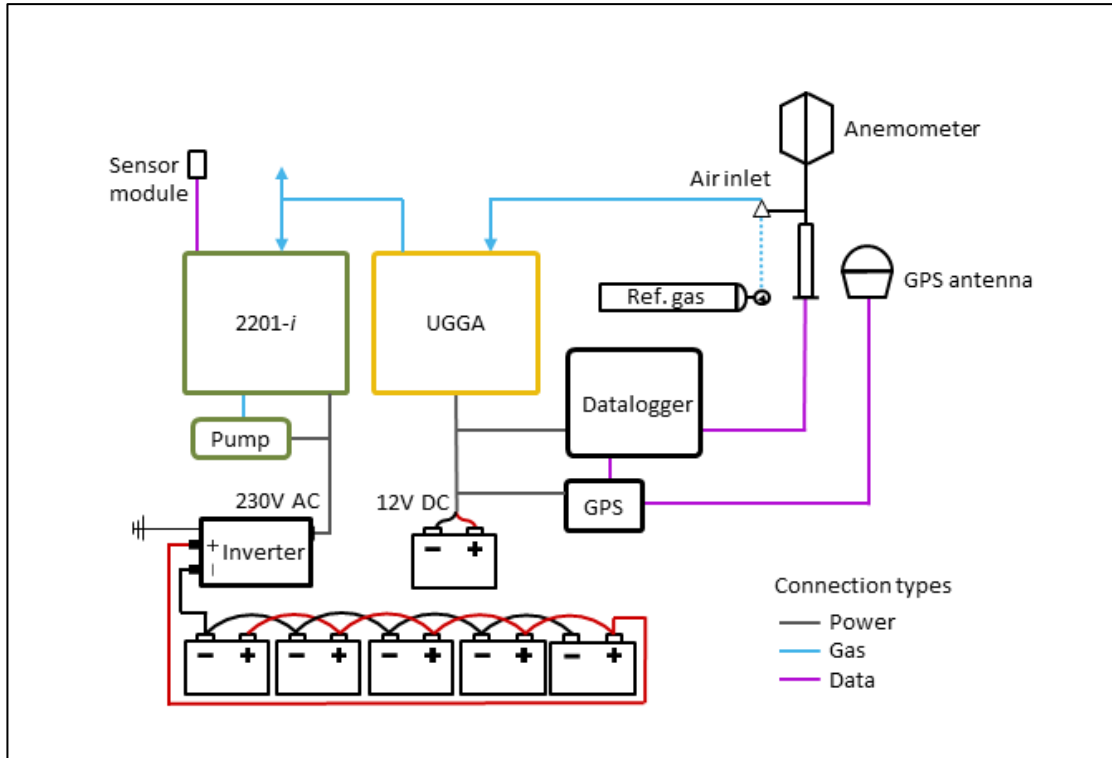


Figure 2.1 Schematic of mobile system. Dotted line shows a temporary connection between the reference gas cylinder and the air inlet only used during drift checks.

2.3.2 Coordinates and wind data

Location and speed were measured by a R330 GNSS Receiver with a Hemisphere A21 Antenna (Hemisphere GNSS Inc., Arizona, USA) mounted on the vehicle roof providing location data with a nominal accuracy of ≤ 0.5 m. Wind speed and direction were measured using a roof mounted WindMaster PRO 3-Axis Ultrasonic Anemometer (Gill Instruments Ltd. Hampshire, UK). Data from both instruments was recorded to a datalogger (Campbell Scientific, Loughborough, UK) at 10 Hz and calculations were made in post processing. The driving direction was calculated as the bearing (forward Azimuth) between successive coordinates using the formula:

$$\theta = \text{atan2}(\sin \Delta\lambda \cdot \cos \varphi_2, \cos \varphi_1 \cdot \sin \varphi_2 - \sin \varphi_1 \cdot \cos \varphi_2 \cdot \cos \Delta\lambda)$$

where φ_1 and φ_2 are the latitude of the first and second coordinate, and $\Delta\lambda$ is the difference in longitude between the two coordinates (Williams, 2011).

An Arduino-based sensor module with an accelerometer (10-DOF IMU Breakout, Adafruit, New York, USA), was mounted on the vehicle roof to measure angle of the vehicle relative to the vertical when used on slopes or uneven ground. The anemometer

measures wind direction relative to the heading and horizontal plane of the vehicle. To get the true wind direction, the wind vector was corrected for the vehicle heading.

2.3.3 Laboratory testing

The transit time between the air inlet and the gas analysers was measured by connecting two reference gases to the air inlet via a three-way valve and measuring the delay in the change in concentration when switching from one reference gas to another. Gas passing through an instrument's cavity may be mixed and therefore affect subsequent measurements at the outlet. To test if setting up the two gas analysers in series would affect measurements made by the G2201-*i*, standards with 3.03 ppm CH₄ and 10.1 ppm CH₄ were run through either just the G2201-*i* or both instruments, connected in series for 10, 30, 60, and 120 seconds. No significant differences in peak height, peak width, and peak area were found (paired t-test, $n = 3$ p-values > 0.3).

2.3.4 Standard calibration and drift check

Before surveys, the gas analysers were calibrated for concentration using certified standards with a nominal range of 1 to 100 ppm CH₄ (BOC Ltd., Guildford, UK) introduced through the system's air inlet. The G2201-*i* was calibrated for $\delta^{13}\text{CH}_4$ using isotopic standards with -23.9 ‰, -54.5 ‰, and -66.5 ‰ (Isometric Instruments, Victoria, Canada), covering the range of expected isotope ratios in the study area. Calibration standards were measured for 10 minutes each. To check for instrument drift, a reference gas cylinder was mounted in the vehicle and gas was run through the sampling system immediately before, during, and after sampling campaigns for 10 minutes each. For individual sampling days, the standard deviations for mean CH₄ concentration measurements were 4 ppb for the UGGA and 0.9 ppb for the G2201-*i*, on average. Mean precision of $\delta^{13}\text{CH}_4$ measurements for individual sampling days was 0.73 ‰. Across all sampling days, those values were 0.014 ppm, 0.013 ppm, and 0.74 ‰, respectively.

2.3.5 Field data collection

Field data were collected between November 2016 and March 2017 in the Fylde and Morecambe Bay areas in Lancashire and Cumbria, North West England, UK (54°00'N., 2°48'W). The area includes farmland, landfills, coastal wetlands, and natural gas processing and distribution infrastructure, and therefore a range of biogenic as well as thermogenic emission sources. A total of 560 km were driven at a mean speed of 41 km h⁻¹. When

encountering notable emissions, the vehicle was stopped downwind for ~ 10 minutes, traffic conditions permitting, to improve precision of isotopic measurements.

2.3.6 Data analysis

2.3.6.1 Methane concentration analysis

The interpretation of mobile survey data is dependent upon what is defined as an elevated concentration or peak. The simplest approach is to use a fixed threshold and to define measurements above the threshold as peaks. However, background concentrations can vary between different areas and measurement times. Moving averages can therefore be more suitable unless a very conservative threshold is used. E.g. Fischer et al. (2017) used a 2-minute rolling mean as a local background, and defined concentrations 0.0086 ppm above that as elevated or peaks. Since our survey approach involved slowing down or stopping the vehicle for several minutes when encountering elevated concentrations, a rolling mean would have been influenced by prolonged measurements of higher concentrations. We therefore instead chose to use a symmetric rolling 1st ventile (lowest 5%) over a 15-minute time window calculated separately for both gas analysers. This assumes that the lowest values at any given location will correspond to the background. To test the effect of threshold selection on results obtained we tested three different thresholds: 0.02 ppm (corresponding to $10 \times$ and $52 \times$ the standard deviations of instrument precision above the local background for the UGGA and G2201-*i* analysers, respectively), 0.1 ppm, and 0.3 ppm.

2.3.6.2 Isotope analysis

To determine the $\delta^{13}\text{CH}_4$ isotopic source signatures of emissions, a Miller-Tans plot was created for each peak. In this method, the isotope source signature is given as the slope of a regression of $\delta^{13}\text{C} \times [\text{CH}_4]$ and $[\text{CH}_4]$ (Miller and Tans, 2003). To determine the best fit line for the regression, we used York's method of regression for data with errors in both variables (York, 1969). This method was chosen over more conventional simple linear regression as it has been shown to provide a more accurate unbiased estimate of the slope (Wehr and Saleska, 2017). The standard error (SE) of the slope was used to evaluate the precision of isotopic measurements. Given that the precision for a single measurement of the G2201-*i* is 3.01 ‰ (1σ), numerous measurements at different concentrations are needed to obtain an accurate estimate of $\delta^{13}\text{CH}_4$ and so the source signature of smaller peaks cannot be accurately estimated. For this study, we therefore excluded all peaks with

a standard error for the regression slope $> 5 \%$. This threshold was chosen as it allows distinguishing microbial sources of CH_4 ($\sim -62 \%$) and fossil sources of CH_4 ($\sim -43 \%$, Schwietzke et al., 2016) with reasonable confidence.

2.3.7 Isotope precision model

2.3.7.1 Model design

To evaluate the effects of instrument specifications and plume characteristics on the precision of isotope measurements, we programmed a simple physical model to simulate gas measurements in the cavity of a spectroscopic gas analyser. The model generates a normally distributed gas peak with a given peak height (maximum concentration above background), isotope signature, and peak length (n_p), which represents the duration for which the peak is measured and therefore determines the number of measurements made (Figure 2.2). Assuming a measurement frequency of 1 Hz, a peak with $n_p = 60$ corresponds to passing a peak in 1 min, however, for the sake of general applicability, we defined parameters relative to dimensionless measurement cycles rather than units of volume or time. To account for the dilution of the peak with background air in the cavity, an exchange rate (r) is specified which gives the number of measurement cycles over which the gas in the cavity is completely replaced. For an instrument measuring at 1 Hz, this would correspond to the rise time (T_{100}). This is modelled as a trailing moving average of length r and simulates the measurement of the air mixture in the cavity at any given time point. The total number of measurements per peak, n_t , is thus given as $n_t = n_p + r$. The gas peak is mixed with background air (1.9 ppm CH_4 at -47% $\delta^{13}\text{C}$) by calculating the true CH_4 concentration and $\delta^{13}\text{C}$ using a two-pool mixing model for each measurement point. Normal random noise is independently added to the CH_4 concentration and $\delta^{13}\text{C}$ with a mean of 0 and a standard deviation representing the instrument precision. Precision is assumed to be concentration independent. These are simplifying assumptions as random noise in concentration and $\delta^{13}\text{C}$ of spectroscopic measurements may be correlated (Wehr and Saleska, 2017) and concentration dependent (Rella et al., 2015a).

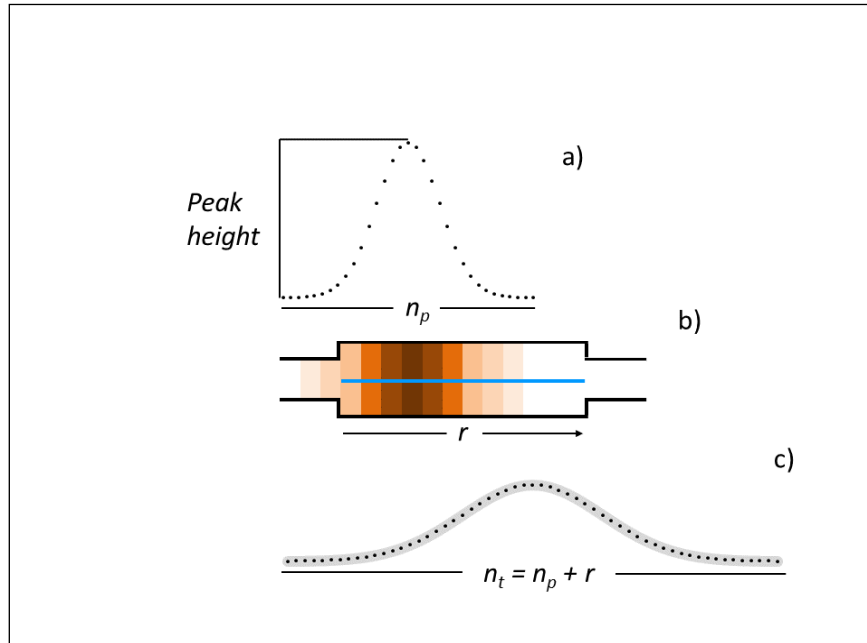


Figure 2.2 Graphical representation of isotope precision model, showing a) initial peak with true peak height (maximum concentration above background) and given peak length n_p relative to the number of measurement cycles (represented by points); b) representation of the instrument optical cavity and the gas concentration in it (blue line represents instrument laser and therefore the length over which concentration is measured); and c) broadened peak as measured by the instrument with random noise added (grey overlay).

A York regression is applied to the set of measurements of each peak and the SE of the slope recorded as output. Monte Carlo simulations are performed for sets of input parameters (see Table 2.2), performing 1,000 simulations for each combination of instrument precision, peak height, measurement duration (n_p), and instrument exchange rate (r).

The model, data processing, and analysis were coded in R (R Core Team, 2017) version 3.4.3, with the use of the IsoplotR (Vermeesch, 2018) and MonteCarlo (Leschinski, 2017) packages. For isotope precision model code, see supplementary information.

2.3.7.2 Model validation

To validate the isotope precision model, we compared model output with SE estimates gathered from the mobile surveys with an SE < 10 %. The model was run with instrument precision set to that of our G2201-*i*, and peak height and n_p parameters set to those of observed peaks. The r parameter was set to 1 as the measured peaks had already been

mixed in the cavity. There was very good agreement between simulated and empirical values with slope = 0.91, $R^2 = 0.96$ (Figure S2.1). The model slightly underestimated SE, likely due to factors such as peak shape or other stochastic processes not considered by the model. For the empirical measurements, SE was proportional to $n^{-0.8}$ (Figure S 2.4).

2.4 Results and discussion

2.4.1 Dual instrument measurements

2.4.1.1 Instrument response time

When taking real time mobile measurements, the response time of the gas analysers used will affect both measured values and sampling approach. Response time consists of two components: the transit time and the rise time (Figure 2.3). As introduced previously, transit time is the time required for a volume of air to move from the air inlet to the analyser cavity. This can easily be corrected for when matching concentration and location data, and does not affect the measured concentration as such, although diffusive mixing of air in the sampling system will increase with increasing tube volume and decreasing flow rate. The rise time is the time between an initial step change in concentration and the final concentration measured and reflects the change in gas composition in the analyser cavity. Typically, the rise time is given as T_{90} , the time it takes for the measured concentration to reach 90% of the final concentration (Brunner and Westenskow, 1988). The rise time depends on the cavity volume and the flow rate of the gas analyser. When an analyser is taking in a sample for less than the rise time (or correspondingly the fall time) the final concentration will not be reached. This is shown in Figure 2.3, where a 3 ppm CH_4 standard was run through the two instruments in series for either 10 s or 120 s, demonstrating the difference in transit time, rise time, and peak height. As air in the instrument cavity is continuously replaced, the measured concentration represents a mixture of incoming and present gas, such that the gas peak is broadened inversely proportional to the rate at which the gas is replaced. Hence, both instruments underestimate true concentration at 10 s, but the faster analyser reaches a higher concentration in that timespan. However, the area under the curve of concentration over time is the same for both instruments.

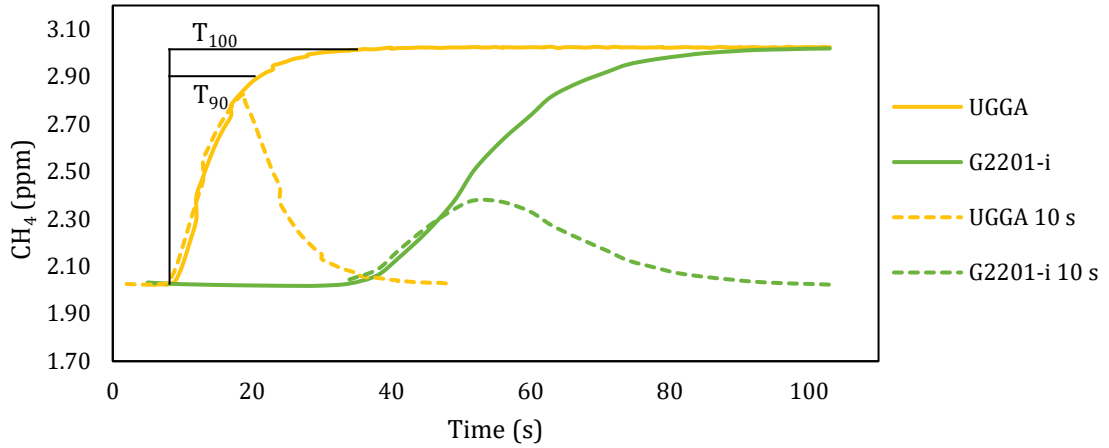


Figure 2.3 Concentration of a 3.03 ppm CH₄ standard gas as measured on a G2201-i isotopic gas analyser and an Ultraportable Greenhouse Gas Analyzer connected in series. Solid lines show measurements where the standard gas was connected for 120 s and both instruments reached stable readings. Dashed lines show measurements where the standard gas was connected for 10 s. Horizontal lines indicate rise times at which 90% (T_{90}) or 100% (T_{100}) of the final concentration have been reached for the UGGA.

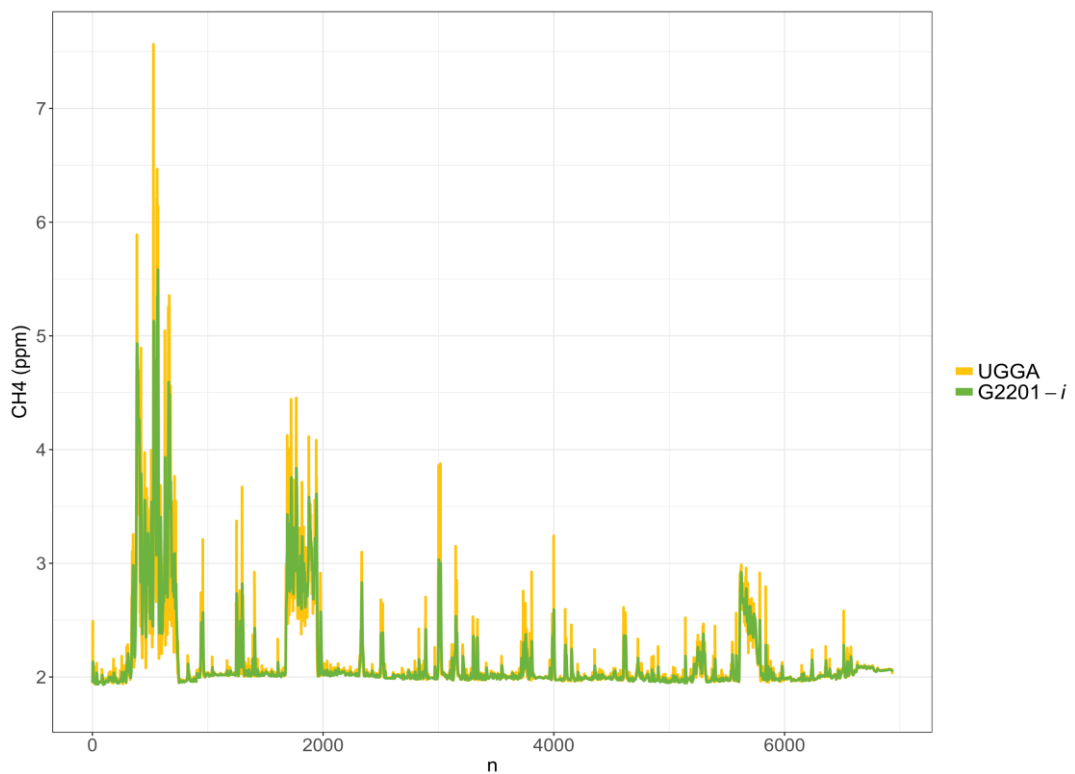


Figure 2.4 Mobile CH₄ measurements made simultaneously by a G2201-i isotopic gas analyser and a UGGA greenhouse gas analyser connected in series. Only data points above background concentration for at least one of the analysers are shown.

2.4.1.2 Methane concentrations

To assess the effect of differing rise times under real world conditions, we compared CH₄ concentration measurements of the UGGA and G2201-*i* gas analysers from four sampling days. There is a consistent discrepancy in measured concentration between the two gas analysers, with the G2201-*i* reporting lower concentrations (Figure 2.4). This effect is even observed during stationary measurements, as demonstrated by Figure S 2.1, which shows concentration data collected over a ten-minute period in a parking lot close to a gas leak. Due to micrometeorological variation, atmospheric CH₄ concentrations are not constant, and instruments may not reach stable measurements. Such dependence of concentration measurements on rise time may lead to underestimating emissions during mobile surveys, and limits the comparability of results, particularly when comparing data between instruments with significantly different rise times. However, the magnitude of underestimation is predictable by the instruments rise time. We plotted maximum peak concentrations measured by the two instruments against each other and found values from the G2201-*i* to be 40 % lower compared to the UGGA (Figure 2.5).

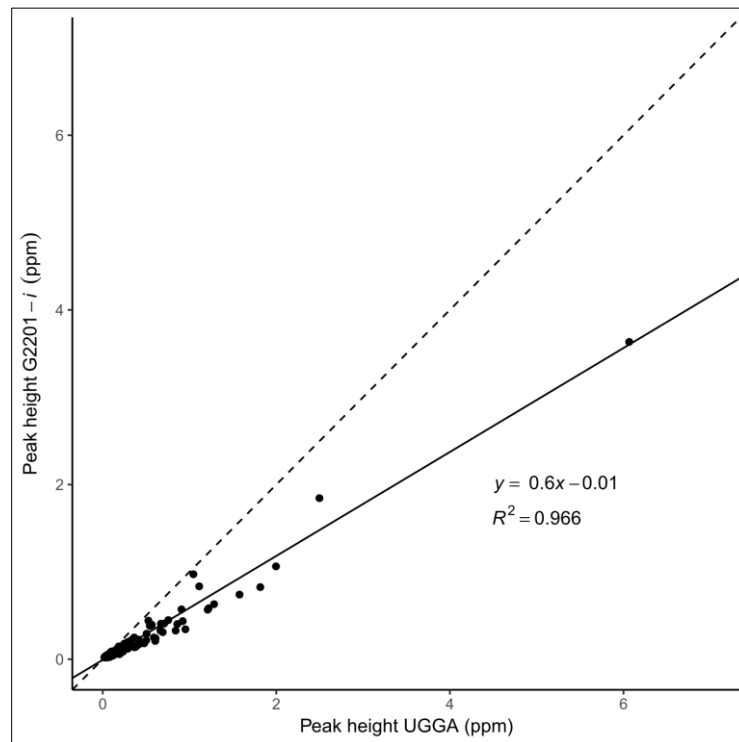


Figure 2.5 Maximum peak concentration above background for CH₄ peaks measured either by a G2201-*i* or a UGGA (n = 230). Peaks recorded by both analysers were matched

if they overlapped temporally. In case of multiple overlapping peaks, the highest peak was selected. Dashed line shows slope = 1.

2.4.1.3 Peak count

Another way for quantifying emissions is to count the number of peaks, i.e. concentrations that exceed some threshold (Boothroyd et al., 2016). However, this measure is also dependent on instrument response time, as any given threshold will be reached more quickly and therefore frequently on a faster instrument. Table 2.1 shows the number of CH₄ peaks above background levels for both instruments at three different thresholds, across four separate surveys. Depending on the selected threshold, around 60 % fewer peaks were detected on the G2201-*i* compared to the UGGA, due to the difference in response time. While selecting a higher threshold will mainly remove small and locally constrained emission plumes from the analysis, it does not eliminate the dependence on instrument response time. Interestingly, higher thresholds also eliminated peaks whose isotopic signature could be determined with sufficient precision, thus potentially eliminating useful data. Such data, while useful for specific questions, can therefore also be difficult to compare between instruments and studies.

Table 2.1 Number of CH₄ peaks counted during mobile surveys at different thresholds with two gas analysers and the number of peaks whose $\delta^{13}\text{CH}_4$ signature could be estimated with a precision of < 5 ‰.

Threshold (ppm)	G2201- <i>i</i>	UGGA	Ratio	SE < 5 ‰
0.02	236	726	0.33	6
0.1	67	157	0.43	4
0.3	32	80	0.40	3

2.4.1.4 Peak area

While peaks measured by a slower instrument are broadened relative to those measured by faster instruments, the peak area remains the same (Figure 2.3). We thus compared peak areas for both instruments. To account for the fact the UGGA occasionally measured several distinct peaks for every one peak of the G2201-*i*, temporally overlapping peak areas were added together. This results in a perfect relationship between the instruments, indicating that peak areas provide a robust means of comparing data between instruments

(Figure 2.6). Peak areas will be sensitive to driving speeds as the measurement duration and therefore area increases with decreasing speed. However, since driving speed is known and peak area decreases linearly with speed, this can be corrected for (Figure S 2.2). Also, depending on the research question, peak areas may provide additional insight. For example, Fischer et al. (2017) found that peak areas are correlated with emission rate for urban gas pipeline leaks. Such relationships may exist for other sources and peak areas may thus aid quantification of emission rates.

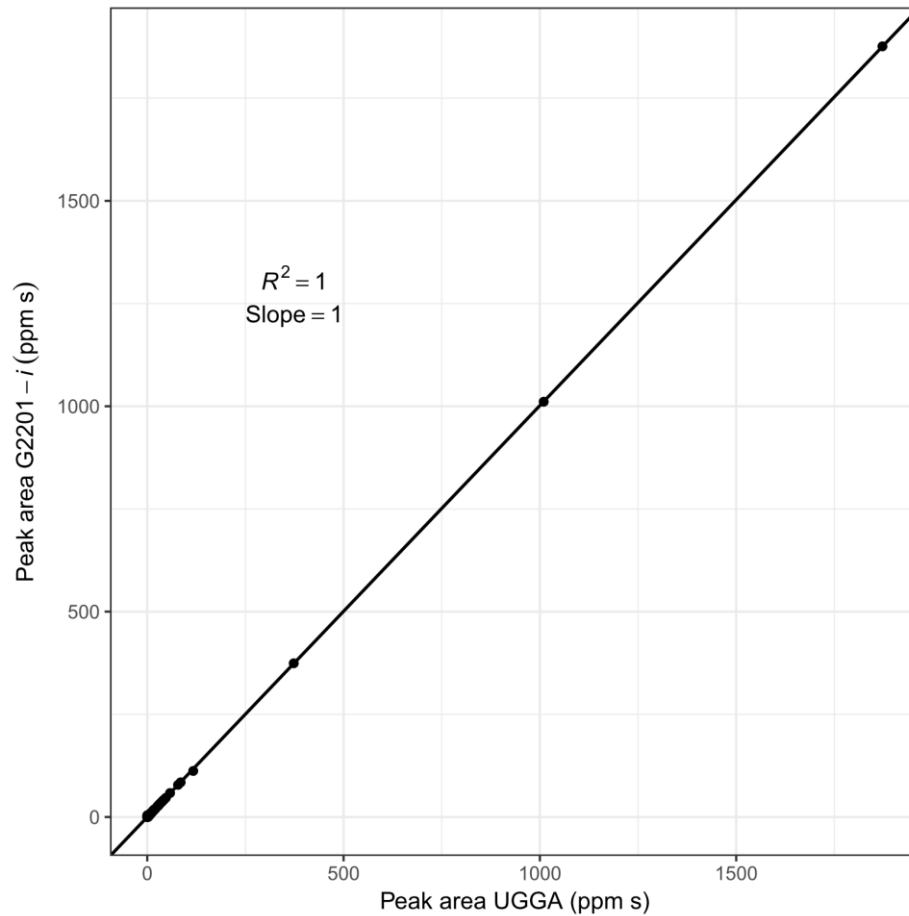


Figure 2.6 Scatter plot of peak CH₄ areas (n = 230) measured across four mobile surveys as measured by a G2201-i isotopic gas analyser and a UGGA greenhouse gas analyser connected in series.

2.4.2 Isotope precision model

For mobile isotopic measurements, where the isotopic signature is determined through regression analysis, the effective precision of the measurements depends not only on the precision of the instrument and measurement duration, but also on factors such as the range of concentrations measured and the instrument response time. As exploring the

relative importance of these effects experimentally is technically challenging, we programmed a physical model simulating gas flow through a spectroscopic analyser and used a Monte Carlo simulation to generate random noise in the measurements.

We ran the model with all possible combinations of parameters, namely instrument precision, peak height above background, measurement duration (n_p), and instrument exchange rate (r). For isotopic precision, we used settings approximating the performance of our G2201-*i*, as well as settings of hypothetical instruments with improved performance. For the CH₄ plume parameters, we used a range of values representative of data collected during our surveys or reported in the literature.

As would be expected, the precision of plume measurements increases linearly with the isotopic precision of the analyser (Table 2.2). Both isotopic and concentration measurement precision influence the precision estimate of plume isotope measurements. However, since the precision of concentration measurements of current spectroscopic CH₄ analysers is around four orders of magnitude higher than the precision of isotopic measurements, improving concentration precision has negligible effects (data not shown), and was therefore kept constant for all model iterations.

Peak height, i.e. the maximum concentration of the plume above background, also had a strong effect on isotopic precision as it extends the range of both variables in the Miller-Tans regression model. Because isotopic precision of gas analysers may increase with concentration, our model may slightly underestimate the improvement in precision. Increasing n_p (i.e. increasing measurement duration) also decreases SE, but not at the same rate as increasing the concentration. For practical applications, it may therefore not be possible to compensate for low plume concentrations by increasing the measurement time, e.g. by taking stationary downwind measurements. Increasing r , i.e. the rise time of the instrument, linearly reduces precision at lower n_p , but becomes negligible at $n = 500$. While increasing rise time increases n_s , it also increases response time and effectively reduces the measured maximum concentration which, as outlined above, has a stronger effect on SE than n_p . Such trade-offs occur e.g. when using AirCore technology where sampled gas is captured in a narrow tube during mobile surveys, and then “replayed” at a slower speed to increase the precision of the isotopic measurements (Karion et al., 2010; Rella et al., 2015b). The relationship between SE and peak height and SE and n_p are both described by power functions (Figure S 2.5, Figure S 2.6), meaning that for the practical domains, initial

improvements in these parameters will lead to large improvements in isotopic precision, however, approaching the asymptote any further will only result in marginal improvements.

Overall, our model demonstrates that for a given set of instrument parameters, achieved isotopic precision will heavily depend on both measurement duration and plume concentration. E.g., for increasing concentration from 1 ppm CH₄ to 2.5 ppm CH₄ above background while increasing n_p from 100 to 250 (corresponding to an increase from ~6.5 min to ~16 min at 0.26 Hz) reduces uncertainty more than threefold (Table 2.2).

Table 2.2 Results of Monte Carlo simulations of the effects of instrument and plume parameters on the precision of simulated $\delta^{13}\text{CH}_4$ plume measurements. Parameters are: precision = instrument precision given as 1σ for a single isotopic measurement, r = number of measurement cycles over which gas in the instrument cavity is replaced, n_p = measurement cycles, peak height = max peak concentration above background. Simulations of plume measurements for each parameter combination were repeated 1000 times. Precision of $\delta^{13}\text{CH}_4$ measurements is calculated as mean standard error for the slope of a Miller-Tans plot using York regression.

Precision (%)	r	n_p	Peak height (ppm)							
			0.5	1	2.5	5	7.5	10	15	20
3.0	20	100	3.81	2.13	1.13	0.78	0.66	0.60	0.53	0.50
		250	2.35	1.33	0.71	0.50	0.42	0.39	0.35	0.32
		500	1.66	0.94	0.50	0.35	0.30	0.27	0.25	0.23
		1000	1.18	0.67	0.36	0.25	0.21	0.19	0.17	0.16
	40	100	4.26	2.33	1.17	0.78	0.65	0.58	0.51	0.47
		250	2.37	1.33	0.71	0.49	0.42	0.38	0.34	0.32
		500	1.66	0.94	0.50	0.35	0.30	0.27	0.24	0.23
		1000	1.18	0.66	0.36	0.25	0.21	0.19	0.17	0.16
	60	100	4.91	2.62	1.25	0.80	0.64	0.56	0.49	0.44
		250	2.44	1.36	0.71	0.49	0.42	0.38	0.33	0.31
		500	1.66	0.94	0.50	0.35	0.30	0.27	0.24	0.23
		1000	1.17	0.66	0.35	0.25	0.21	0.19	0.17	0.16
1.5	20	100	1.90	1.06	0.56	0.39	0.33	0.30	0.27	0.25
		250	1.17	0.66	0.35	0.25	0.21	0.19	0.17	0.16
		500	0.83	0.47	0.25	0.18	0.15	0.14	0.12	0.11
		1000	0.59	0.33	0.18	0.13	0.11	0.10	0.09	0.08
	40	100	2.12	1.16	0.58	0.39	0.32	0.29	0.25	0.23
		250	1.18	0.67	0.35	0.25	0.21	0.19	0.17	0.16
		500	0.83	0.47	0.25	0.18	0.15	0.14	0.12	0.11
		1000	0.59	0.33	0.18	0.12	0.11	0.10	0.09	0.08
	60	100	2.45	1.31	0.63	0.40	0.32	0.28	0.24	0.22
		250	1.22	0.68	0.36	0.25	0.21	0.19	0.17	0.16
		500	0.83	0.47	0.25	0.17	0.15	0.14	0.12	0.11
		1000	0.58	0.33	0.18	0.12	0.11	0.10	0.09	0.08
0.5	20	100	0.63	0.35	0.19	0.13	0.11	0.10	0.09	0.08
		250	0.39	0.22	0.12	0.08	0.07	0.06	0.06	0.05
		500	0.27	0.15	0.08	0.06	0.05	0.05	0.04	0.04
		1000	0.19	0.11	0.06	0.04	0.04	0.03	0.03	0.03
	40	100	0.70	0.38	0.19	0.13	0.11	0.10	0.08	0.08
		250	0.39	0.22	0.12	0.08	0.07	0.06	0.06	0.05
		500	0.27	0.15	0.08	0.06	0.05	0.05	0.04	0.04
		1000	0.19	0.11	0.06	0.04	0.04	0.03	0.03	0.03
	60	100	0.81	0.43	0.21	0.13	0.11	0.09	0.08	0.07
		250	0.40	0.22	0.12	0.08	0.07	0.06	0.06	0.05
		500	0.27	0.15	0.08	0.06	0.05	0.04	0.04	0.04
		1000	0.19	0.11	0.06	0.04	0.04	0.03	0.03	0.03

2.5 Conclusions

It is important to appreciate the influence of instrument specifications and sampling method on both concentration measurements and isotopic precision. As we show, instrument response time affects measured concentrations during mobile surveys. This should be taken into consideration when comparing results across different setups, or when thresholds are important, such as for regulatory compliance. Therefore, instrument rise time should be reported consistently for mobile applications. Peak areas of emission plumes are independent of instrument response times, however, and as such may provide a more robust means for comparing data obtained across different instrument setups. Isotopic precision of mobile measurements determined with regression methods is not just a function of instrument precision, but also instrument configuration and sampling conditions. The model we developed can be used to predict isotopic precision for any given setup and application. It can therefore inform choices on equipment used, as well as sampling strategies, and estimate expected uncertainty. As the underlying principles are independent of chemical species, it could easily be adapted to purposes beyond CH₄ measurements, such as other forms of mobile air pollution measurements (Apte et al., 2017), allowing for a wide range of potential future applications.

2.6 References

- Apte, J.S., Messier, K.P., Gani, S., Brauer, M., Kirchstetter, T.W., Lunden, M.M., Marshall, J.D., Portier, C.J., Vermeulen, R.C.H., Hamburg, S.P., 2017. High-Resolution Air Pollution Mapping with Google Street View Cars: Exploiting Big Data. *Environ. Sci. Technol.* 51, 6999–7008. <https://doi.org/10.1021/acs.est.7b00891>
- Boothroyd, I.M., Almond, S., Worrall, F., Davies, R.J., 2016. Assessing the fugitive emission of CH₄ via migration along fault zones – Comparing potential shale gas basins to non-shale basins in the UK. *Sci. Total Environ.* <https://doi.org/10.1016/j.scitotenv.2016.09.052>
- Brunner, J.X., Westenskow, D.R., 1988. How the rise time of carbon dioxide analysers influences the accuracy of carbon dioxide measurements. *Br. J. Anaesth.* 61, 628–638. <https://doi.org/10.1093/bja/61.5.628>
- Czepiel, P.M., Mosher, B., Harriss, R.C., Shorter, J.H., McManus, J.B., Kolb, C.E., Allwine, E., Lamb, B.K., 1996. Landfill methane emissions measured by enclosure and atmospheric tracer methods. *J. Geophys. Res.* 101, 16711. <https://doi.org/10.1029/96JD00864>
- Eapi, G.R., Sabnis, M.S., Sattler, M.L., 2014. Mobile measurement of methane and hydrogen sulfide at natural gas production site fence lines in the Texas Barnett Shale. *J. Air Waste Manage. Assoc.* 64, 927–944. <https://doi.org/10.1080/10962247.2014.907098>
- Etminan, M., Myhre, G., Highwood, E.J., Shine, K.P., 2016. Radiative forcing of carbon dioxide, methane, and nitrous oxide: A significant revision of the methane radiative forcing. *Geophys. Res. Lett.* 43, 12,614–12,623. <https://doi.org/10.1002/2016GL071930>
- Fischer, J.C. von, Cooley, D., Chamberlain, S., Gaylord, A., Griebenow, C.J., Hamburg, S.P., Salo, J., Schumacher, R., Theobald, D., Ham, J., 2017. Rapid, Vehicle-Based Identification of Location and Magnitude of Urban Natural Gas Pipeline Leaks. *Environ. Sci. Technol.* 51, 4091–4099. <https://doi.org/10.1021/acs.est.6b06095>
- Jackson, R.B., Down, A., Phillips, N.G., Ackley, R.C., Cook, C.W., Plata, D.L., Zhao, K., Phillips, N.G., Ackley, R.C., Cook, C.W., Plata, D.L., Zhao, K., 2014. Natural gas pipeline leaks across Washington, DC. *Environ. Sci. Technol.* 48, 2051–8. <https://doi.org/10.1021/es404474x>
- Karion, A., Sweeney, C., Tans, P., Newberger, T., 2010. AirCore: An Innovative Atmospheric Sampling System. *J. Atmos. Ocean. Technol.* 27, 1839–1853. <https://doi.org/10.1175/2010JTECHA1448.1>
- Leschinski, C.H., 2017. MonteCarlo: Automatic Parallelized Monte Carlo Simulations.

- Lopez, M., Sherwood, O.A., Dlugokencky, E.J., Kessler, R., Giroux, L., Worthy, D.E.J., 2017. Isotopic signatures of anthropogenic CH₄ sources in Alberta, Canada. *Atmos. Environ.* 164, 280–288. <https://doi.org/10.1016/j.atmosenv.2017.06.021>
- Miller, J.B., Tans, P.P., 2003. Calculating isotopic fractionation from atmospheric measurements at various scales. *Tellus, Ser. B Chem. Phys. Meteorol.* 55, 207–214. <https://doi.org/10.1034/j.1600-0889.2003.00020.x>
- Mønster, J.G., Samuelsson, J., Kjeldsen, P., Rella, C.W., Scheutz, C., 2014. Quantifying methane emission from fugitive sources by combining tracer release and downwind measurements - a sensitivity analysis based on multiple field surveys. *Waste Manag.* 34, 1416–28. <https://doi.org/10.1016/j.wasman.2014.03.025>
- R Core Team, 2017. *R: A Language and Environment for Statistical Computing.*
- Rella, C.W., Hoffnagle, J., He, Y., Tajima, S., 2015a. Local- and regional-scale measurements of CH₄, δ¹³CH₄, and C₂H₆ in the Uintah Basin using a mobile stable isotope analyzer. *Atmos. Meas. Tech.* 8, 4539–4559. <https://doi.org/10.5194/amt-8-4539-2015>
- Rella, C.W., Hoffnagle, J., He, Y., Tajima, S., 2015b. Local- and regional-scale measurements of CH₄, Δ¹³CH₄, and C₂H₆ in the Uintah Basin using a mobile stable isotope analyzer. *Atmos. Meas. Tech.* 8, 4539–4559. <https://doi.org/10.5194/amt-8-4539-2015>
- Schwietzke, S., Sherwood, O.A., Bruhwiler, L.M.P., Miller, J.B., Etiope, G., Dlugokencky, E.J., Michel, S.E., Arling, V.A., Vaughn, B.H., White, J.W.C., Tans, P.P., 2016. Upward revision of global fossil fuel methane emissions based on isotope database. *Nature* 538, 88–91. <https://doi.org/10.1038/nature19797>
- Turner, A.J., Jacob, D.J., Benmergui, J., Wofsy, S.C., Maasakkers, J.D., Butz, A., Hasekamp, O., Biraud, S.C., 2016. A large increase in U.S. methane emissions over the past decade inferred from satellite data and surface observations. *Geophys. Res. Lett.* 43, 2218–2224. <https://doi.org/10.1002/2016GL067987>
- Vermeesch, P., 2018. IsoplotR: A free and open toolbox for geochronology. *Geosci. Front.* <https://doi.org/10.1016/j.gsf.2018.04.001>
- Wehr, R., Saleska, S.R., 2017. The long-solved problem of the best-fit straight line: application to isotopic mixing lines. *Biogeosciences* 14, 17–29. <https://doi.org/10.5194/bg-14-17-2017>
- Williams, E., 2011. Aviation Formulary v1.46 [WWW Document]. URL <http://www.edwilliams.org/avform.htm> (accessed 5.11.18).
- York, D., 1969. Least squares fitting of a straight line with correlated errors. *Earth Planet. Sci. Lett.* 5, 320–324. [https://doi.org/10.1016/S0012-821X\(68\)80059-7](https://doi.org/10.1016/S0012-821X(68)80059-7)

- Yoshida, H., Mønster, J.G., Scheutz, C., 2014. Plant-integrated measurement of greenhouse gas emissions from a municipal wastewater treatment plant. *Water Res.* 61, 108–18. <https://doi.org/10.1016/j.watres.2014.05.014>
- Zazzeri, G., Lowry, D., Fisher, R.E., France, J.L., Lanoisellé, M., Nisbet, E.G., 2015. Plume mapping and isotopic characterisation of anthropogenic methane sources. *Atmos. Environ.* 110, 151–162. <https://doi.org/10.1016/j.atmosenv.2015.03.029>

2.7 Supplementary material

2.7.1 Supplementary figures

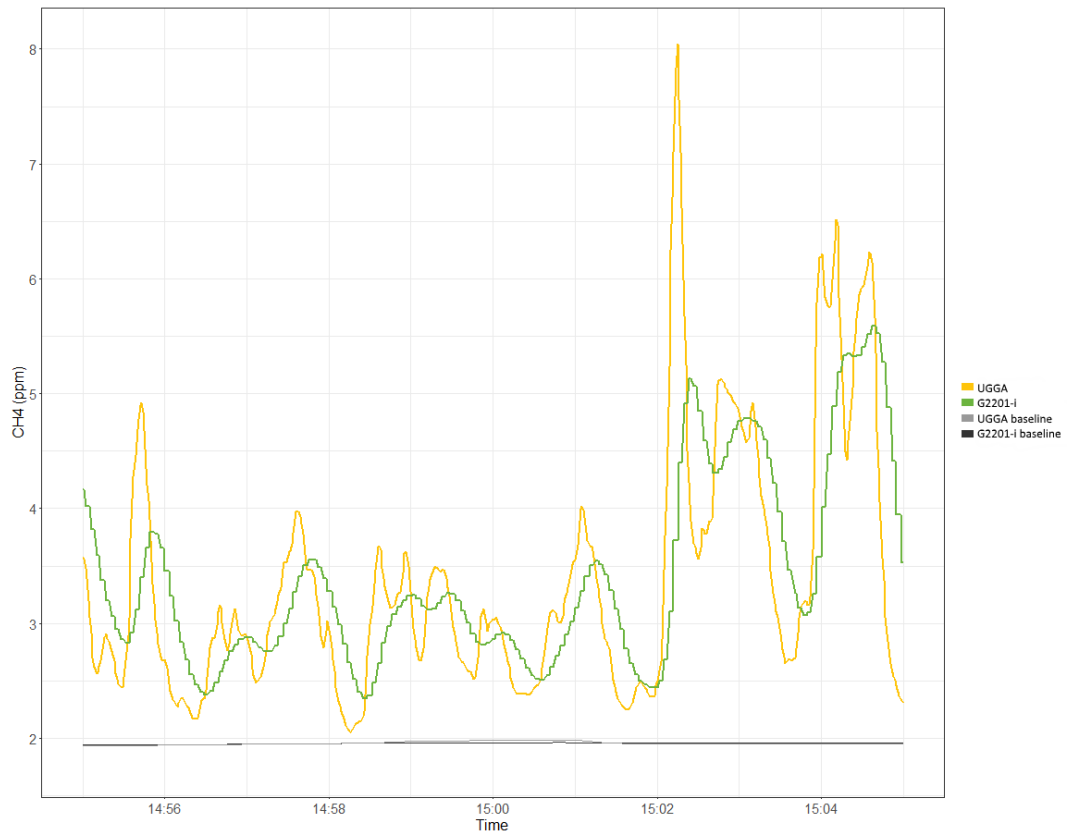


Figure S 2.1 CH₄ concentrations as measured by a G2201-i and a UGGA over a ten-minute stationary period in Lancaster city centre on November 24, 2016.

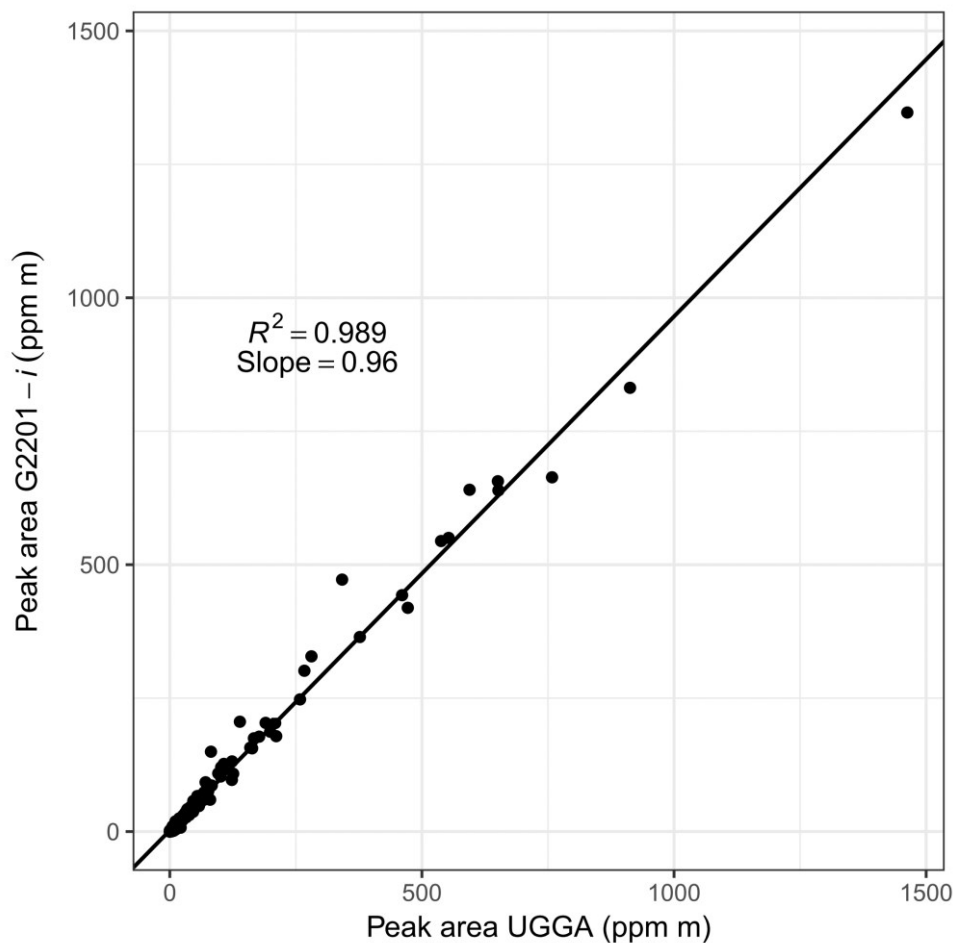


Figure S 2.2 Scatter plot of CH₄ peak areas corrected for driving speed by multiplying peak area in ppm s times speed in m s⁻¹ (n = 230) measured across four mobile surveys, as measured by a G2201-i isotopic gas analyser and a UGGA greenhouse gas analyser connected in series. The variation between the instruments is due to the difference in peak measurement time and changes in speed during that time.

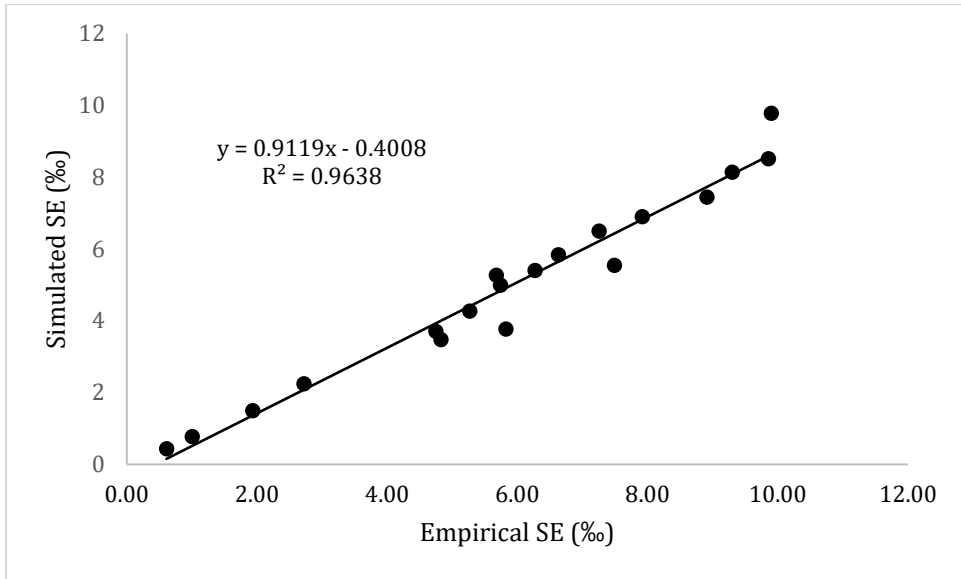


Figure S 2.3 Empirical vs simulated standard errors for peaks with an empirical SE < 10 ‰.

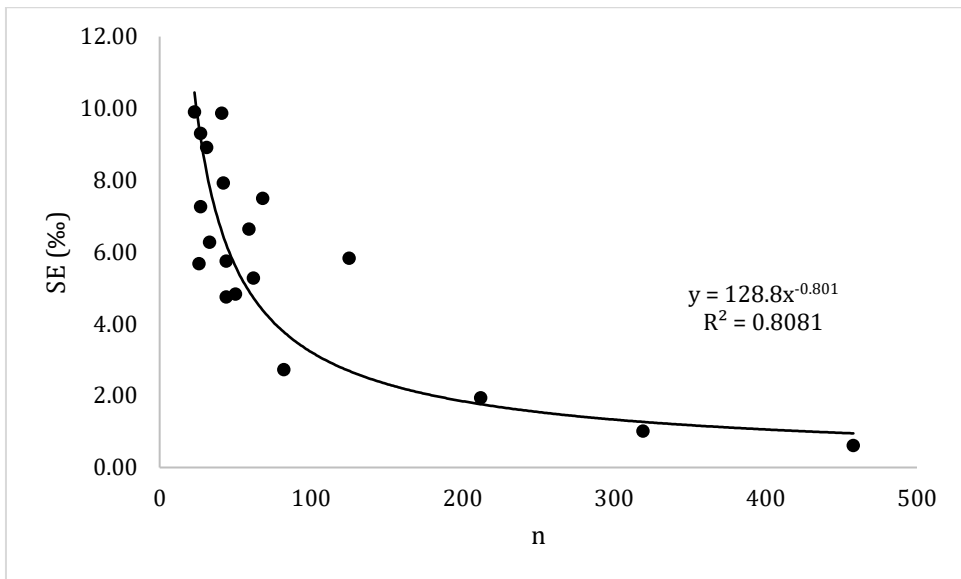


Figure S 2.4 Empirical standard error vs number of measurements.

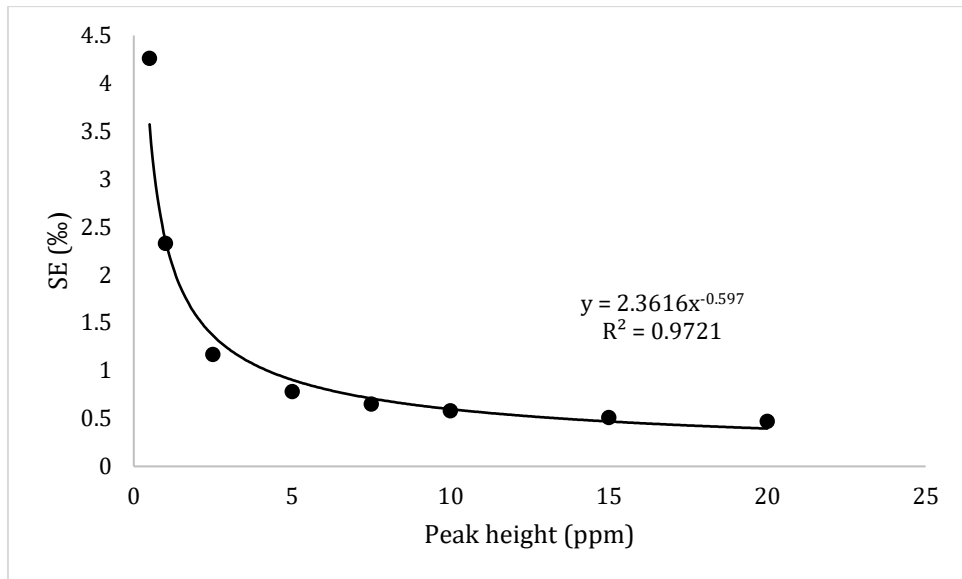


Figure S 2.5 Simulated standard error as a function of peak height at $r = 40$, precision = 3 %, $n_p = 100$.

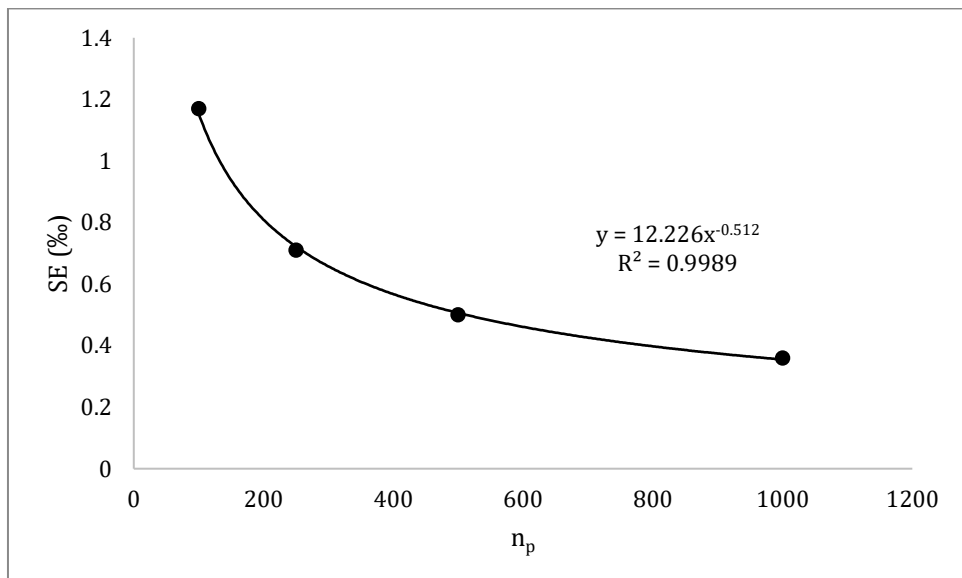


Figure S 2.6 Simulated standard error as a function of n_p at $r = 40$, precision = 3 %, peak height = 2.5 ppm.

2.7.2 Isotope precision model source code

```

library(IsoplotR)
library(MonteCarlo)

# Moving average function (credit: Matti Pastell,
# https://stackoverflow.com/questions/743812/calculating-moving-average)
ma <- function(x,n){filter(x,rep(1/n,n), sides=1)}

## Monte Carlo parameters ##

# Instrument precision
d_sd_grid <- c(3, 1.5, 0.5) # delta sd
# d_sd_grid <- 3 # delta sd
c_sd_grid <- 0.00039 # concentration sd of Picaroo
# c_sd_grid <- c(0.0020, 0.00039, 0.0001) # Concentration sd of LGR, G2201-
# i, and higher precision instrument

# Background air
d_bg_grid <- -47.56 # Based on 2015 mean Mace Head CH4 concentration
c_bg_grid <- 1.91 # Based on 2015 mean Mace Head CH4 concentration

# Source
# d_sc_grid <- c(-62.2, -44.0, -22.2) # Signatures of microbial, ff, and biomass
# burning from Schwietzke et al. 2016
d_sc_grid <- -44.0 # Estimate of fossil fuel from Schwietzke et al. 2016
# c_sc_grid <- c(0.5, 1, 2, 3.5, 6) # maximum peak height above background
# in ppm
c_sc_grid <- c(0.5, 1, 2, 3.5, 6, 9, 14, 20) # maximum peak height above
# background in ppm
sd_sc_grid <- 1 # Standard deviation/peak shape
# sd_sc_grid <- c(0.5 ,1, 2) # Standard deviation/peak shape

# Number of measurements per peak
n_grid <- c(90, 180, 360, 720)

# Exchange rate. How many units of time it takes to replace air in cavity
exch_rt_grid <- c(25, 50, 100)
# exch_rt_grid <- 90

# Parameter grid for MC simulation
param_grid <- list(d_sd = d_sd_grid, c_sd = c_sd_grid,
                  d_bg = d_bg_grid, c_bg = c_bg_grid,
                  d_sc = d_sc_grid, c_sc = c_sc_grid, sd_sc = sd_sc_grid,
                  exch_rt = exch_rt_grid,
                  n = n_grid)

## Model ##

```

```

cavity_sim <- function(d_sd, c_sd, d_bg, c_bg, d_sc, c_sc, sd_sc, exch_rt, n) {

  # Construct peak
  peak_length <- seq(0-4*sd_sc, 0+4*sd_sc, length = n) # Include values up to
  4 sigma from mean
  peak_conc <- dnorm(peak_length, mean = 0, sd = sd_sc)
  peak_conc <- peak_conc*c_sc/max(peak_conc)

  # Construct chamber
  cavity <- data.frame(timepoint = 1:(2 * length(peak_length) + exch_rt))
  cavity$peak_conc <- 0
  cavity$peak_conc[(exch_rt + 1):(length(peak_length) + exch_rt)] <-
  peak_conc
  cavity$CH4_true <- ma(cavity$peak_conc, exch_rt) + c_bg # Concentration
  above background at timepoint
  cavity[is.na(cavity)] <- c_bg

  # Source signature calculated with two-pool mixing model
  cavity$d13C_true <- (d_sc * (cavity$CH4_true - c_bg) + d_bg * c_bg) /
  cavity$CH4_true

  # Add random noise to concentration and isotope values
  cavity$c_sd <- c_sd
  cavity$c_noise <- rnorm(nrow(cavity), 0, c_sd)
  cavity$CH4_sim <- cavity$CH4_true + cavity$c_noise
  cavity$d_sd <- d_sd
  cavity$d_noise <- rnorm(nrow(cavity), 0, d_sd)
  cavity$d13C_sim <- cavity$d13C_true + cavity$d_noise

  # Set up data for York regression
  cavity <- cavity[cavity$CH4_true > c_bg, ]
  cavity$CH4_x_d13C <- cavity$CH4_sim * cavity$d13C_sim
  cavity$CH4_x_d13C_sd <- abs(
  cavity$CH4_x_d13C * sqrt(
  (cavity$c_sd / cavity$CH4_sim)^2 + (cavity$d_sd / cavity$d13C_sim)^2
  )) # Gaussian error propagation for CH4 * d13C

  cavity$cor <- cor(cavity$CH4_x_d13C, cavity$CH4_sim)
  cavity <- cavity[c("CH4_sim", "c_sd", "CH4_x_d13C", "CH4_x_d13C_sd", "cor")]

  # Run York regression
  result <- york(cavity)
  result <- as.numeric(result$b[2])
  return(list(se = result))

}

## Monte Carlo simulation ##
mc_results <- MonteCarlo(func = cavity_sim,

```

```
param_list = param_grid,  
time_n_test = T,  
nrep = 1000,  
save_res = T,  
ncpus = 2)
```

Make results table in LaTeX format. Note that package multirow is required.

```
rows <- c("sd_sc", "n", "exch_rt", "d_sd")  
cols <- c("c_sc")
```

```
MakeTable(output=mc_results,      rows=rows,      cols=cols,      digits=2,  
include_meta=FALSE)
```

3

Isotopic characterisation and mobile detection of methane emissions in North West England

Takriti, M., Ward, S., Wynn, P., McNamara, N.

3.1 Abstract

Understanding CH₄ sources at a regional level is important for reducing fugitive emissions as well as to better constrain atmospheric CH₄ budgets. The prospect of unconventional shale gas extraction in the UK has raised concerns about climate impacts of fugitive emissions from natural gas infrastructure. Such emissions need to be distinguished from those already present in the landscape, and stable isotope analysis is the most powerful method available for attributing emission sources. To this end, we performed dual isotope (¹³C, ²H) analysis of CH₄ emission sources, background air, as well as mobile ¹³C measurements in North-West England, in an area with potentially exploitable shale gas deposits. Dual isotope analysis was performed for enteric fermentation, animal waste, landfill gas, wetlands, and natural gas from the regional distribution network.

We found that background air coming from the Irish sea was enriched in ¹³C by an average of 2.55 ‰, relative to the Atlantic background, and depleted in ²H relative to atmospheric CH₄, potentially indicating an offshore emission source. Isotopic analysis of agricultural, landfill, and wetland emissions overlapped in their δ¹³C signatures, but ²H analysis may be able to distinguish between agricultural and landfill emissions. Mobile measurements detected emissions from two out of four surveyed managed landfills in the region. Multiple

gas leaks were detected, which may confound emissions from other thermogenic sources. When separating the surveyed area by land-use into agricultural and urban land, we found that background levels of CH₄ were more depleted by 1 ‰ in areas with agricultural land use compared to urban areas, but emissions from gas leaks and landfills are present in both categories, and the complex existing landscape of CH₄ emissions needs to be taken into account when evaluating the potential impacts of natural gas extraction in the region.

3.2 Introduction

Methane (CH₄) has a global warming potential 32 times that of CO₂ (Etminan et al., 2016), while atmospheric CH₄ concentrations have increased by over 160% since preindustrial times (Stocker et al., 2013). This has contributed to concerns about the achievability of limiting global temperature rise to below 2°C (Saunio et al., 2016c), as set out in the Paris Agreement. Increasing atmospheric concentrations of CH₄ are mainly attributed to increased emissions from agriculture, natural gas production, and wetlands, although the relative contribution from these sources is still debated (e.g. Allen, 2016; Saunio et al., 2016a; Turner et al., 2017). Over 50 % of total CH₄ emissions are anthropogenic (Saunio et al., 2016a), and due to the short lifetime of atmospheric CH₄ there is significant potential to reduce radiative forcing over decadal timescales by cutting emissions (Shindell et al., 2012).

Despite increasing availability of atmospheric measurements, including ground based, airborne and remote sensing, efforts to attribute and limit emissions are still hampered by uncertainty around spatially and temporally heterogeneous emissions at local and regional scales. The co-occurrence of different emission sources in the landscape makes top-down approaches to disentangle the importance of different sources challenging. At the same time, bottom up emission estimates are often not in agreement with top-down atmospheric measurements (Kirschke et al., 2013).

The main method for constraining emissions from different source categories to the atmosphere is stable isotope analysis (e.g. Allen, 2016; Feinberg et al., 2018; Kirschke et al., 2013; Schwietzke et al., 2016). Different emission categories have different isotopic signatures, in particular, microbial emissions from anaerobic respiration in ruminants, wetlands, and waste, are isotopically lighter, while natural gas from thermogenic sources is isotopically heavier (Whiticar, 1999). However, recent research has shown that there are considerable geographic variations in the isotopic signatures of CH₄ emissions, due to

differences in fossil fuel formation, latitudinal trends in wetland emissions signatures, use of C₃ vs C₄ plants in livestock fodder, climate differences and management practices in waste management (Chanton et al., 2008; Feinberg et al., 2018; Sherwood et al., 2017). Isotopic assessment of CH₄ emissions therefore requires an accurate knowledge of regional emission signatures, both for regional and global applications.

The main anthropogenic sources of microbial CH₄ emissions are enteric fermentation from ruminants, storage and application of animal waste, emissions from landfills, and fugitive emissions from natural gas infrastructure. The latter can occur during the extraction and processing stage as well as distribution through the pipeline network from storage facilities to end users and are estimated to account for 2 % of natural gas production (Schwietzke et al., 2016). The rapid expansion of natural gas production through hydraulic fracturing in the USA has meant that investigations into its environmental impacts, including fugitive emissions, have mostly started after commencing operations. Limited baseline measurements thereby add to the uncertainty surrounding the environmental impacts of shale gas exploration, particularly when co-located with other emission sources. At the same time, mobile measurements have shown that gas leaks from urban pipelines are common in at least some US cities, occasionally reaching hazardous levels (Fischer et al., 2017; Jackson et al., 2014; Phillips et al., 2013), while direct measurements from other regions are still sparse (e.g. Zazzeri et al., 2017).

Mobile measurements, enabled by recent advances in spectroscopic analyser technology, have led to new approaches to detecting and attributing CH₄ emissions at the landscape level, as they combine high spatial resolution with a comparatively large coverage. Combining mobile measurements with isotopic analysis can be used to identify the source of emissions with ambiguous origin, as well as infer contributions to total emission on a landscape level (Lopez et al., 2017; Rella et al., 2015a). Mobile measurements were successfully used for identifying emissions from different sources, including cattle farming, oil and gas production, landfills, and pipeline leaks (Fischer et al., 2017; Lopez et al., 2017; Phillips et al., 2013; Weller et al., 2018; Yoshida et al., 2014; Zazzeri et al., 2015).

Our research focussed on the Fylde peninsula and Morecambe Bay area in North West England, an area that on a small scale combines intensive agricultural use with urban environments and coastal wetlands. As such, this area has a range of different natural and anthropogenic methane sources, and it is also among the first regions outside the USA where hydraulic fracturing to extract shale gas has been approved. This area poses

particular challenges to attributing potential fugitive CH₄ emissions from shale gas exploration. The approved drill sites are mostly surrounded by dairy and cattle farmland and there are natural gas pipeline distribution networks and multiple landfills throughout the area. This means that there is potential for confounding pre-existing emission sources with emissions related to gas extraction, particularly when only relying on concentration measurements without the use of tracers such as CH₄ stable isotopes or other hydrocarbons co-emitted with CH₄.

Our aims for this study were to 1) determine isotopic signatures of the major CH₄ source categories 2) determine background and downwind isotopic signatures 3) identify and attribute CH₄ emission sources in the region 4) identify emission and stable isotope patterns related to land use.

We performed dual-isotope ($\delta^{13}\text{C}$ and $\delta^2\text{H}$) analysis of major CH₄ source types in the region as well as coastal and inland measurements of mixed air. We conducted mobile isotopic ($\delta^{13}\text{C}$) sampling campaigns to identify and attribute emission sources in the landscape and in relation to urban and agricultural land use. All sampling was carried out before the start of drilling operations for shale gas in the region.

3.3 Methods

3.3.1 Study area

The study was conducted on the Fylde peninsula (53°50'23"N, 2°52'16"W), south of the city of Lancaster (54° 2'44"N, 2°47'32"W) and Morecambe Bay area (54° 2'43"N, 2°55'40"W), along the coast of the Irish Sea (Figure 3.3). Under westerly winds, atmospheric composition is therefore dominated by local fluxes and/or well-mixed distant emissions. Land use in the Fylde area is dominated by dairy and cattle farming and the urban areas of Blackpool and Fleetwood along the coast. There are four actively managed landfills in the study area, which have gas extraction systems to capture produced CH₄, as well as numerous historic ones (Environment Agency, 2018). The Morecambe Bay area (Figure 3.4) north of Lancaster is again dominated by livestock farming with marshland along parts of the coast as well as a peatland. On the northern side of the Morecambe Bay is the Barrow Gas Terminal (54° 5'47"N, 3°10'50"W) which processes gas from oil and gas fields off the coast (Figure 3.5).

3.3.2 Background air sampling

To determine isotopic composition of air upwind and downwind of the Fylde area, gas samples were collected at two locations: A coastal site north of the Fylde area (54°1'30"N, 2°54'43.48"W, elevation 8 m), and an elevated inland site northeast of the Fylde (53°55'51"N, 2°44'14"W, elevation 200 m). Both sites were chosen for a lack of nearby industrial or agricultural CH₄ sources or wetlands. Samples were collected on three dates at each location: at the coastal site on 2 September 2016, 20 February and 27 July 2017, at the inland site on 8 September 2016, 21 February and 28 July 2017. Sampling dates were selected based on stable wind directions from the Southwest. During each sampling, continuous measurements were made with a Los Gatos Research Ultraportable Greenhouse Gas Analyzer (henceforth UGGA, Los Gatos Research Inc., San Jose, USA) analyser with the air inlet mounted around 1.5 m above ground. Atmospheric conditions, including wind speed and direction, were recorded throughout the sampling period at 20 s intervals using a Kestrel 4500 mobile weather station (Kestrel, Boothwyn, PA, USA). Air samples were collected at hourly intervals by connecting 10 l FlexFoil® PLUS sample bags (SKC Ltd., Dorset, UK) to the UGGA's air outlet for around 10 minutes. Sampling periods lasted for 5-7 hours during daytime. After return to the laboratory, samples for isotopic analysis were transferred, on the same day, to pre-evacuated 12 mL Exetainer® vials (Labco Ltd. Ceredigion, UK) for $\delta^{13}\text{C}$ analysis and 100 mL Wheaton® serum bottles for $\delta^2\text{H}$ analysis. Stable isotope analysis of CH₄ was performed at UC Davis stable isotope facility by gas chromatography-combustion/pyrolysis-isotope-ratio mass spectrometry as described in Yarnes (2013) with a precision (1 SD) of 0.2 ‰ for $\delta^{13}\text{CH}_4$ and 2 ‰ for $\delta^2\text{H}$ (UC Davis SIF, 2019). The UGGA was calibrated using certified standards (BOC Ltd., Guildford, UK), and the samples stored in the sampling bags were re-measured to improve accuracy.

3.3.3 Characterisation of emission sources

3.3.3.1 Wetland sites

Samples were collected at two wetland sites in the Morecambe Bay area: At Leighton Moss RSPB reserve, a coastal reed bed (54°10'7"N, 2°47'39"W), and at Roudsea Wood and Mosses National Nature Reserve, a lowland raised bog (54°14'5.70"N, 3°1'24.04"W), indicated on Figure 3.4). At Leighton Moss, samples were collected in June and September 2015. At each sampling, within the reed beds, a grass dominated, a moss dominated, and a

mostly bare location in the process of being colonised by young reeds, were selected. Due to conservation management practices at the site, it was not possible to sample the same locations at both times, but locations with similar vegetation structure were selected at both samplings. At Roudsea Wood, samples were collected in August 2015. Two dominant vegetation types, heather and moss, were selected.

For each vegetation type, three replicate samples were collected via flux chambers. A 30 cm diameter 10 cm high gas sampling chamber collar was installed for each replicate to a depth of around 5 cm. Flux measurements of CH₄ were conducted using the UGGA: Collars were sealed with opaque 19 L dome-shaped chambers and the CH₄ concentration in each chamber was measured for a minimum of five minutes. Flux rates were calculated from the rate of CH₄ concentration change as described in McEwing et al. (2015) and based on a minimum of 30 s of continuous measurements.

At the end of the flux measurements, chambers were left on the collars for a total of 15 to 40 minutes, depending on flux rates, to allow gas concentrations to build up to the necessary concentration for isotopic analysis. At the end, 20 mL samples of headspace gas were extracted with a syringe through septa in the chambers and filled into evacuated 12 mL Exetainer vials. Isotopic analysis was performed at UC Davis Stable Isotope Facility as described in section 3.3.2. A further 10 mL were filled into 3 mL Exetainers vials for CO₂ and CH₄ concentration analysis. Syringes were purged with ambient air between each sample. CH₄ concentrations were measured by gas chromatography using an Autosystem XL GC (Perkin Elmer, Waltham, MA, USA).

3.3.3.2 Landfill sites

Samples were collected at two managed landfill sites in the Fylde area, Clifton Marsh Landfill Site (53°45'2"N, 2°48'49"W) and Jameson Rd Landfill Site (53°54'14"N, 3°0'59"W). In both sites, the non-operational parts are capped and both sites have gas extraction systems and use landfill gas for energy generation. Gas samples were collected from manifolds of the gas extraction system by connecting 1 L Tedlar gas sampling bags to valves in the manifolds. Samples were transferred on the same day to 12 mL evacuated Exetainer valves via syringe and samples were analysed at UC Davis Stable Isotope Facility as described in section 3.3.2. Chamber flux measurements on capped sections of the landfills were performed as described in section 3.3.3.1, for a total of nine replicates at each site. No significant fluxes were detected during those measurements and atmospheric

concentrations of CH₄ on the sites were close to the atmospheric background at around 2 ppm throughout the measurement campaigns.

3.3.3.3 Agricultural sources

Samples of emissions from cow-breath, liquid manure, and solid manure were collected at Myerscough College's Lodge Farm (53°51'4"N, 2°46'36"W) in March and August 2015. Samples from eight beef and dairy cows on a C₃ diet were collected. To collect the breath samples, we used a vacuum sampling device to fill air into a Tedlar gas sampling bag: The Tedlar bag was placed into an airtight box connected to a hand pump. The valve of the bag was connected, through the box's lid, to a tube with a funnel attached to it. Air was pumped into the bag while holding the funnel in front of the cows' mouths. Emissions from liquid manure were sampled by using the vacuum sampling device to take air samples above a ventilation hole in a collection pit. Samples were transferred from Tedlar sampling bags to evacuated Exetainers and analysed as described in section 3.3.2. The solid manure emissions were sampled by placing a flux chamber on the solid manure and, after letting the gas build up for several minutes, collecting a sample through a septum with a syringe.

3.3.3.4 Natural gas

To obtain isotope signatures of natural gas that were representative for the local gas distribution network, we sampled gas from a laboratory gas outlet at Lancaster University. Samples were collected at multiple timepoints between 2015 and 2017 to capture changes in gas composition over time, and specifically at times of mobile or background air sampling campaigns. For each sampling, a Tedlar bag was attached to the outlet and filled with gas. Gas samples were transferred into Exetainer vials and analysed as described in section 3.3.2.

3.3.4 Mobile measurements

To conduct mobile isotopic measurements, a vehicle (Mitsubishi L200) was equipped with two gas analysers, a Picarro G2201-*i* isotopic gas analyser (henceforth G2201-*i*, Picarro Inc. Santa Clara, USA) and the UGGA. Both instruments measure CO₂, CH₄, and H₂O in air. The UGGA has a faster response to changes in ambient CH₄ concentrations with a rise time (T_{90}) of 14 s compared to 38 s for the G2201-*i*. This is largely because the two instruments are optimized for different tasks and capabilities: the G2201-*i*'s lower flow rate

and response enables more precise isotope measurements, whereas the UGGA is designed for rapid flux measurements.

The air inlet was mounted on the roof of the vehicle and connected to the air inlet of the UGGA via a 310-cm nylon tube with an outer/inner diameter of 6 mm/3 mm. A PTFE air filter was mounted on the inlet. The two gas analysers were connected in series with the G2201-*i* air inlet connected to the UGGA air outlet. Excess air flow was vented via an open split. The output of each analyser, as well as the anemometer (see below), was broadcast via Wi-Fi to two tablet devices mounted in front of the passenger seat to monitor measurements in real time. The G2201-*i* was powered by five 86 Ah deep cycle batteries connected in parallel to a pure sine wave power inverter, other components used DC power from a single battery. The batteries provided enough charge to operate the system for over 10 h of continuous measurements.

Location and speed were measured by a R330 GNSS Receiver with a Hemisphere A21 Antenna (Hemisphere GNSS Inc., Arizona, USA) mounted on the vehicle roof providing location data with a nominal accuracy of ≤ 0.5 m. Wind speed and direction were measured using a roof mounted WindMaster PRO 3-Axis Ultrasonic Anemometer (Gill Instruments Ltd. Hampshire, UK). Data from both instruments was recorded to a datalogger (Campbell, UK) at 10 Hz and calculations were made in post processing. The driving direction was calculated as the bearing (forward Azimuth) between successive coordinates according to Williams (2011). The anemometer measures wind direction relative to the heading and horizontal plane of the vehicle. To get the true wind direction, the wind vector was corrected for the vehicle heading.

Before surveys, the gas analysers were calibrated for concentration using certified BOC gas standards (see section 3.3.2) introduced through the system's air inlet. The G2201-*i* was calibrated for $\delta^{13}\text{CH}_4$ using isotopic standards with -23.9 ‰, -54.5 ‰, and -66.5 ‰ diluted to around 5 ppm (Isometric Instruments, Victoria, Canada), covering the range of expected isotope ratios in the study area. Calibration standards were measured for 10 minutes each. To correct for instrument drift, a reference gas cylinder was mounted in the vehicle and gas was run through the sampling system immediately before, during, and after sampling campaigns for 10 minutes each. For individual sampling days, the standard deviations for mean CH_4 concentration measurements were 4 ppb for the UGGA and 0.9 ppb for the G2201-*i*, on average. Mean precision of $\delta^{13}\text{CH}_4$ measurements for individual sampling days

was 0.73 ‰. Across all sampling days, those values were 0.014 ppm, 0.013 ppm, and 0.74 ‰, respectively.

Potential CH₄ emission sources in the study area were selected, including landfills, farms, waste water treatment plants, and the Barrow Gas Terminal. In addition, two proposed drill sites for shale gas exploration, Preston New Rd and Roseacre Wood (Figure 3.3), as well as randomly selected urban and coastal locations not nearby any known emission sources were chosen. Where road access permitted, we selected multiple points around each potential emission source to maximise the chance of downwind measurements under different wind conditions. A route connecting all points was planned using a genetic algorithm to optimise driving distance. Measurements were taken during the daytime on a total of four days in November 2016 and February and March 2017. When elevated CH₄ emissions were detected, the vehicle was stopped for around 10 minutes, traffic conditions permitting, to take more precise isotopic measurements. Measurements were collected over a total of 557 km at a mean speed of 41 km h⁻¹.

3.3.5 Data analysis

3.3.5.1 Mobile data analysis

Peaks in methane concentration were defined as two or more consecutive measurements 0.02 ppm above a moving background. While using such a relatively low threshold leads to the inclusion of many small peaks, 0.02 ppm is well above instrument precision and our sensitivity analysis demonstrated that more conservative thresholds could lead to the exclusion of useful data. The isotope signature of peaks was determined from Miller-Tans plots as the slope of a regression of the product of CH₄ concentration and δ -value against CH₄ concentration (Miller and Tans, 2003). For the regression we used York's method to obtain unbiased estimates of the regression parameters that allow for errors in both variables and produce an uncertainty estimate that is based on the empirical instrument precision (Wehr and Saleska, 2017; York, 1969). Most of the detected peaks were too small to confidently determine the isotopic signature. As a threshold, we used a standard error (SE) of the slope of 6 ‰, values above that were not considered for isotopic analysis. This level of precision allowed for distinguishing between CH₄ from microbial and thermogenic sources whose $\delta^{13}\text{C}$ signature differs by around 20 ‰ (Table 3.2).

Data analysis was performed in R version 3.4.4 (R Core Team, 2018), with the additional use of the IsoplotR (Vermeesch, 2018), fossil (Vavrek, 2011), and geosphere (Hijmans, 2017) packages.

3.3.5.2 Spatial analysis and land use

To investigate links between emissions and land use, we used the British Land Cover Map 2015 (Rowland et al., 2017) to assign each measurement to either urban or agricultural land use, two dominant forms of land use in the study area with contrasting emission sources. For this purpose, land classified as “improved grassland” (mainly used for grazing with potential manure application) and “arable and horticulture” (potential manure application) were grouped as agricultural land. Built up areas are classified as either “urban” or “suburban”. Since suburban land is often intermixed with other land cover and tends to form a buffer between densely populated urban and agricultural land, it was excluded from the analysis (Figure S 3.4). Together urban and agricultural land covers make up 69 % of the study area (Table S 3.1). Emission $\delta^{13}\text{C}$ signatures for the study area were determined using Miller-Tans plots excluding stationary data to avoid bias towards longer measurements for some sources.

This is a simplified categorisation as the agricultural land use group is heterogeneous, built-up areas are dispersed within agricultural land and mixing will occur between the two. However, our main aim was to distinguish broadly between more densely populated urban areas (4.0 % of land cover in the study area) where we expected upwind emissions to be more strongly dominated by leaks from natural gas pipelines and traffic emissions, and agricultural land (65% of land cover in the study area) where we expected upwind emissions to be more strongly dominated by enteric fermentation from cows and sheep as well as manure application. While the urban area as a percentage of the total study area was small, a disproportionate amount of sampling was performed in urban areas (Figure S 3.4, Table S 3.1).

Concentrations of CH_4 , $\delta^{13}\text{C}$ ratios, and wind speed and direction were mapped using QGIS v2.18. For major peaks, we aimed to identify the source based on location, isotope signature, and wind direction at the time of measurement.

3.4 Results

3.4.1 Background air sampling

We performed two-way ANOVA to assess the effects of location and sampling date on stable isotope ratios. Mean values for $\delta^{13}\text{C}$ were lower at the inland site compared to the coastal site on two out of three sampling dates (Table 3.1), as such there was a significant interaction between site and sampling date ($F(2,35) = 5.139$, $p = 0.011$). It must be noted that, due to changing wind conditions, there was a six-day gap between the two samplings in September 2016. This may have affected the comparison between coastal and inland measurements in that month, as atmospheric conditions and regional inputs may have changed over that period. Across all samplings, mean $\delta^{13}\text{C}$ values were -45.14 ± 0.08 ‰ for coastal, and -45.32 ± 0.06 ‰ for inland measurements, and varied significantly with location ($F(1,35) = 5.328$, $p = 0.027$) and sampling date ($F(2,35) = 12.843$, $p = 6.6 \times 10^{-5}$). Mean differences in $\delta^2\text{H}$ were marginal, with values of -119.48 ± 1.18 ‰ for coastal and, -119.65 ± 0.89 ‰ for inland measurements, particularly considering the lower precision of the IRMS measurements for $\delta^2\text{H}$. A significant effect was only found for sampling date ($F(2,31) = 5.118$, $p = 0.012$).

We compared our $\delta^{13}\text{C}$ data to 2016 data, the latest available at the time of writing, from the Mace Head Atmospheric Research Station in Galway, on the west coast of Ireland. The aim was to determine if the incoming air under westerly winds has a similar isotopic composition as the Atlantic background air. Mean 2016 Mace Head $\delta^{13}\text{C}$ values were -47.69 ‰, 2.55 ‰ more depleted than mean values at the coastal site. Mean yearly values may not be representative of the atmospheric conditions on any given sampling day, even though the predominant wind directions in Ireland are West and South (MET Éireann, 2018). Atmospheric isotope signatures are also subject to seasonal variations (Bréas et al., 2001). The upper quartile of $\delta^{13}\text{C}$ at Mace Head in 2016 was -47.47 ‰, 2.33 ‰ depleted compared to coastal values, and the maximum value was -46.89 ‰, 1.75 ‰ depleted compared to our coastal measurements.

Table 3.1 Stable isotope ratios of mixed air collected at a coastal and an inland site. Wind speed and direction show mean values during the sampling period.

Site	Date	$\delta^{13}\text{C} \pm \text{SE} (\text{‰})$	n	$\delta^2\text{H} \pm \text{SE} (\text{‰})$	n	$\text{CH}_4 \pm \text{SE}$ (ppm)	Wind sp. (m s^{-1})	Wind dir. ($^\circ$)
Coastal	02 Sep 2016	-45.61 ± 0.13	5	-120.60 ± 2.78	4	$2.13 \pm .001$	7.1	254
Inland	08 Sep 2016	-45.46 ± 0.10	7	-122.13 ± 0.79	6	$2.06 \pm .002$	7.5	233
Coastal	20 Feb 2017	-44.94 ± 0.07	7	-122.94 ± 1.72	5	$2.08 \pm .002$	8.2	250
Inland	21 Feb 2017	-45.37 ± 0.07	8	-119.58 ± 1.7	8	$2.13 \pm .010$	5.7	205
Coastal	27 Jul 2017	-45.02 ± 0.08	7	-116.36 ± 1.10	7	$2.08 \pm .001$	7.5	234
Inland	28 Jul 2017	-45.11 ± 0.10	7	-117.60 ± 1.41	7	$2.11 \pm .003$	6.6	227
Coastal	Mean	-45.15 ± 0.08	19	-119.48 ± 1.18	16	$2.09 \pm .007$	7.6	246
Inland	Mean	-45.32 ± 0.06	22	-119.65 ± 0.89	21	$2.10 \pm .007$	6.6	222

3.4.2 Fylde isotopic source characterisation

Our sampled sources in the Fylde area showed a clear distinction between microbial sources and natural gas (Table 3.2). The $\delta^{13}\text{C}$ signature for natural gas ranged from -43‰ to -33‰ while the range for microbial sources was -72‰ to -59‰ . Similarly, $\delta^2\text{H}$ in natural gas was more enriched with values between -195‰ and -174‰ , while microbial sources ranged from -282‰ to -339‰ . The sampled landfills and agricultural sources overlapped in their $\delta^{13}\text{C}$ signatures, with agricultural sources being more depleted, on average. A clearer distinction between agricultural sources and landfills was found in $\delta^2\text{H}$ values, as landfills were more depleted in $\delta^2\text{H}$ by around 35‰ .

Table 3.2 Stable isotope signatures of CH₄ emission source categories in the study area determined by IRMS. Landfill phases refer to individual cells of the landfill, n.a. indicates samples lost due to technical errors.

Category	Source	Date	$\delta^{13}\text{C} \pm \text{SE} (\text{‰})$	n	$\delta^2\text{H} \pm \text{SE} (\text{‰})$	n
Agriculture	Cow breath	March/August 2015	-66.75 ± 0.83	8	-339.37 ± 2.62	8
	Liquid manure	August 2015	-72.25 ± 0.22	3	-338.14 ± 0.84	3
	Solid manure	March/August 2015	-65.52 ± 0.44	4	-319.73 ± 19.61	4
	Agriculture mean		-67.52 ± 0.78	15	-333.88 ± 5.39	15
Landfill	Clifton Marsh - phase 1	July 2015	-59.23 ± 0.26	2	-311.91 ± 0.25	2
	Clifton Marsh - phase 2	July 2015	-61.35 ± 0.19	3	-299.99 ± 0.87	3
	Clifton Marsh - phase 3	August 2015	-60.12 ± 0.83	2	-303.68 ± 2.07	2
	Clifton Marsh - phase 4	June 2015	-62.86 ± 1.06	3	-286.97 ± 5.93	3
	Jameson Rd - phase 1	June 2015	-64.41	1	-294.9	1
	Jameson Rd - phase 2	June 2015	-65.17	1	-303.6	1
	Jameson Rd – restored phase	June 2015	-70.43	1	-282.4	1
	Landfills mean		-62.41 ± 0.87	13	-297.93 ± 2.93	13
Natural gas	Network gas	September 2015	-33.14	1	n.a.	
	Network gas	November 2015	-39.79	1	-190.3	1
	Network gas	August 2016	-43.45	1	-174.0	1
	Network gas	January 2017	-40.55	1	-178.3	1
	Network gas	February 2017	-39.67	1	-194.5	1
	Network gas	July 2017	-40.07	1	n.a.	
	Network gas mean		-39.45 ± 1.38	6	-184.28 ± 4.85	4

Table 3.3 Major CH₄ plumes identified in the study area with $\delta^{13}\text{C}$ signature SE < 6.0 ‰ determined using a G2201-*i* isotopic gas analyser.

Location	Date	Source	Coordinates	Max CH ₄ (ppm)	Peak height (ppm)	$\delta^{13}\text{C}_{\text{CH}_4} \pm \text{SE}$ (‰)	Peak area (ppm m) ^b
Midgeland Farm landfill, Blackpool	February 2017	Landfill	53° 46' 54" N, 3° 0' 0" W	2.82	0.83	-59.64 ± 4.83	831
Midgeland Farm landfill, Blackpool ^a	February 2017	Landfill	53° 46' 54" N, 2° 59' 60" W	2.74	0.74	-59.23 ± 5.68	419
Jameson Rd Landfill, Fleetwood	February 2017	Landfill	53° 54' 40" N, 3° 1' 21" W	2.83	0.83	-59.51 ± 4.75	640
Newton Dr, Blackpool	February 2017	Gas leak	53° 49' 32" N, 3° 0' 14" W	3.84	1.84	-35.34 ± 1.01	472
Cable St, Lancaster	November 2016	Gas leak	54° 3' 5" N, 2° 47' 51" W	5.59	3.63	-34.32 ± 0.61	301
Preston Lancaster New Rd, Garstang	February 2017	Gas leak	53° 53' 34" N, 2° 47' 6" W	3.03	1.06	-33.45 ± 2.72	1347
Preston Lancaster New Rd, Garstang ^a	February 2017	Gas leak	53° 52' 59" N, 2° 46' 50" W	2.57	0.58	-30.74 ± 5.74	664
Garstang Rd, Barton	February 2017	Gas leak	53° 50' 38" N, 2° 44' 33" W	2.53	0.57	-28.05 ± 5.27	656
Roose Rd, Barrow-in-Furness	March 2017	Gas leak	54° 6' 40" N, 3° 12' 22" W	2.38	0.44	-27.81 ± 5.82	127
Rampside Rd, Barrow-in-Furness	March 2017	Gas terminal	54° 6' 20" N, 3° 10' 32" W	2.92	0.97	-23.73 ± 1.93	328

^aSecond measurement from the same location as previous row.

^bPeak areas corrected for driving speed by multiplying peak area in ppm s times speed in m s⁻¹.

3.4.3 Wetland sites

Analysis of isotope data from the two wetland sites by constructing Miller-Tans plots revealed multiple distinct regression slopes. For $\delta^{13}\text{C}$ measurements at Leighton Moss, samples from vegetated locations (moss or grass) fell onto the same regression slope but differed between the two timepoints (Figure 3.1). Emissions in June had a $\delta^{13}\text{C}$ signature of -55.19‰ , while emissions in September were considerably more depleted at 67.12‰ , indicating either seasonal variations in emission signatures or differences between the sampling plots. For the bare plots with nascent vegetation, $\delta^{13}\text{C}$ was not affected by the sampling date and showed an identical signature to the June vegetated plots. The emissions from Roudsea Woods, from heather and moss dominated locations, were considerably more depleted with a $\delta^{13}\text{C}$ of -78.46‰ . The $\delta^2\text{H}$ values followed a different pattern. At Leighton Moss, there was no seasonal effect, but signatures differed by vegetation type, with grass dominated sites at -309.98‰ being more than 50‰ more depleted than moss dominated sites at 257.54‰ (Figure 3.2). Bare sites had a $\delta^2\text{H}$ value of -287.88‰ , while emissions from Roudsea Wood were the most depleted with a value of -335.42‰ .

Table 3.4 Flux rates measured for different vegetation types in a reed bed (Leighton Moss) and a lowland raised bog (Roudsea Wood).

Site	Date	Vegetation	Flux ($\text{mg CH}_4 \text{ m}^{-2} \text{ h}^{-1}$)	n
Leighton Moss	June 2015	Moss	6.39 ± 2.43	3
Leighton Moss	June 2015	Grass	32.78 ± 14.25	3
Leighton Moss	June 2015	Bare	19.02 ± 13.48	3
Leighton Moss	September 2015	Moss	1.03 ± 0.31	3
Leighton Moss	September 2015	Grass	3.8 ± 1.72	3
Leighton Moss	September 2015	Bare	1.34 ± 0.67	3
Roudsea Wood	August 2015	Heather	1.15 ± 0.22	3
Roudsea Wood	August 2015	Moss	10.62 ± 9.22	3

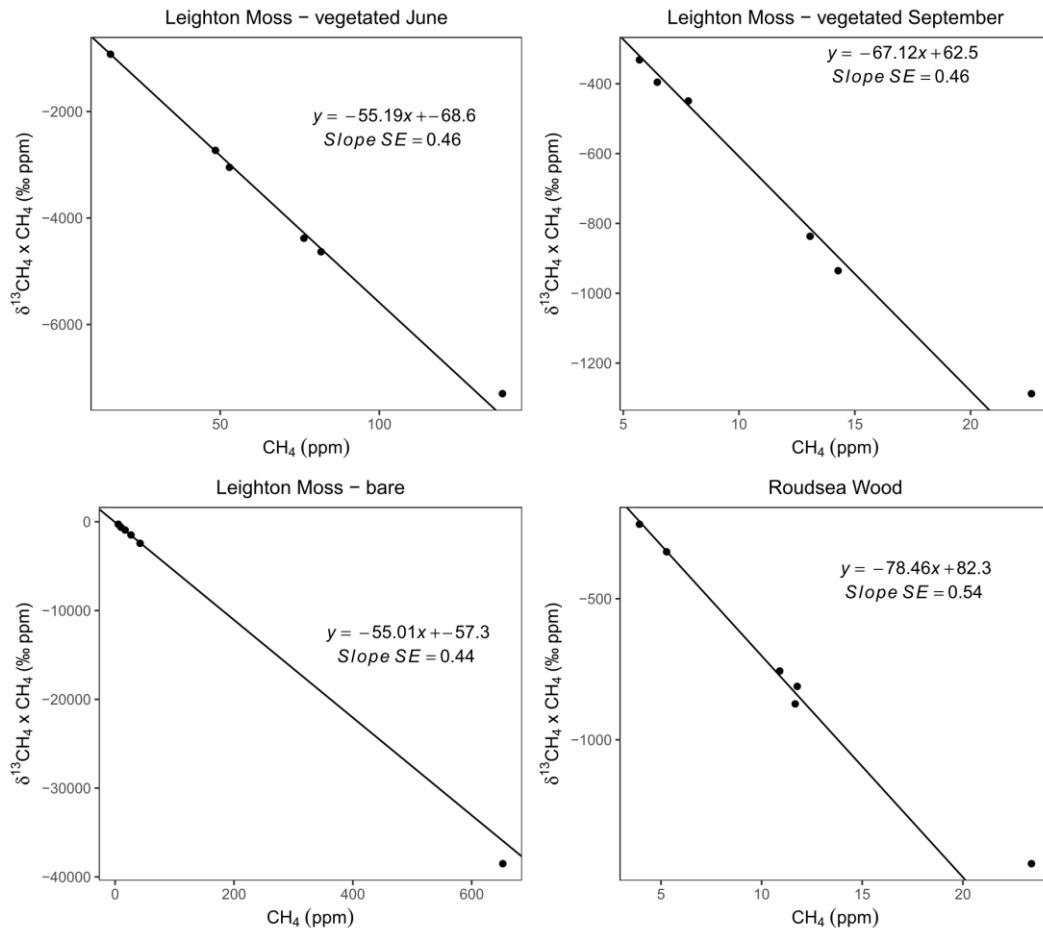


Figure 3.1 Miller-Tans plots of $\delta^{13}\text{C}$ signatures of vegetated plots, dominated by mosses or grasses, and plots with nascent vegetation at Leighton Moss reed bed and vegetated plots, dominated by heather or mosses, at Roudsea Wood lowland raised bog. Regressions calculated using York's method.

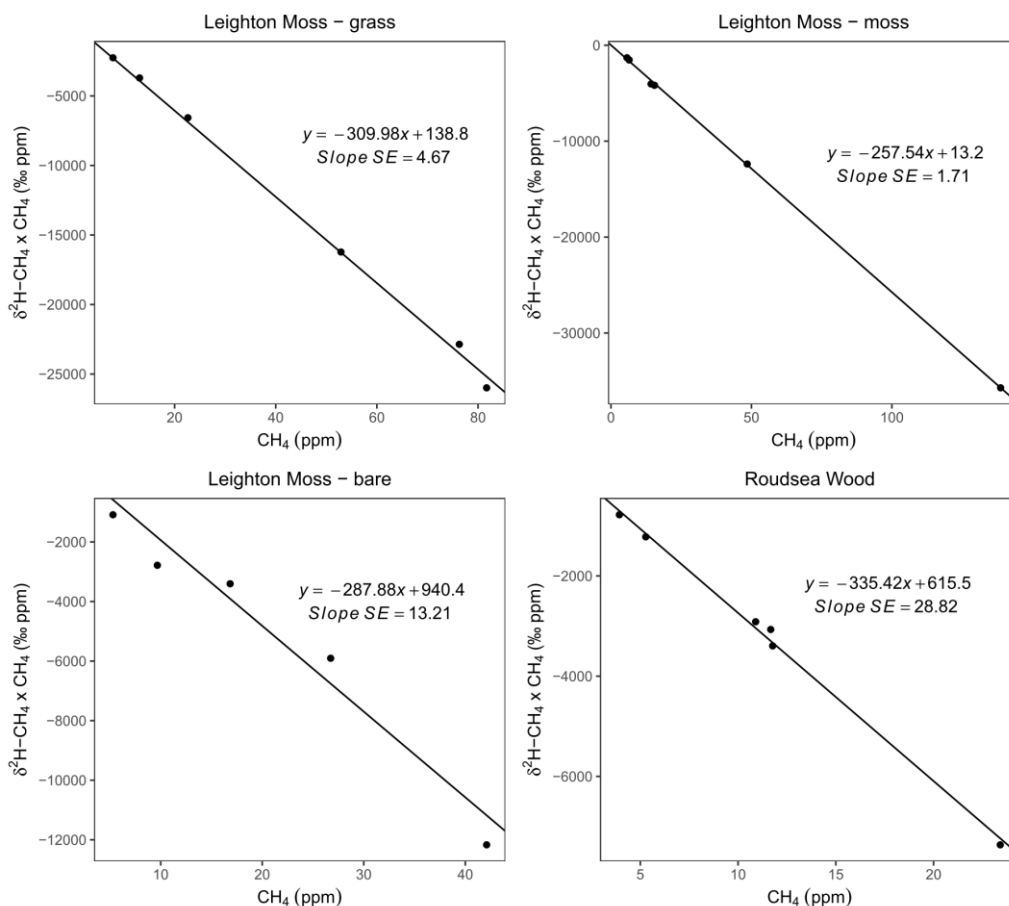


Figure 3.2 Miller-Tans plots of $\delta^2\text{H-CH}_4$ signatures of vegetated plots and plots with nascent vegetation at Leighton Moss reed bed and vegetated plots at Roudsea Wood lowland raised bog. Regressions calculated using York's method.

3.4.4 Mobile CH_4 source identification and land use

We surveyed a total of 557 km of road, with 72 km driven in urban and 238 km driven in agricultural areas. Background, i.e. non-peak, concentrations throughout the study area averaged 1.97 ppm CH_4 (Table S 3.2). Background $\delta^{13}\text{C}$ values were -44.99 ± 0.03 ‰ (mean \pm SE) for urban and -45.98 ± 0.03 ‰ for agricultural areas.

We measured a total of 232 peaks above background, as measured with the G2201-*i*, and a total of 707 peaks with the UGGA. Maximum concentrations measured were 5.6 ppm for the G2201-*I* and 8.0 ppm for the UGGA. This discrepancy is due to the difference in measurement speed between the two instruments. The median of the peak area, i.e. the integrated CH_4 concentration over the distance driven, as measured by the G2201-*i*, was 92.4 ppm m and 109.1 ppm m for urban and agricultural areas, respectively. Peak area was heavily right skewed with many small and a few large peaks (Figure S 3.1).

We detected notable emissions at eight locations where the isotopic signature could be determined within ± 6 ‰. In each case, isotope and wind data indicate an anthropogenic source (Table 3.3, Figure 3.3-5). We found emissions from two of the four landfill sites with gas extraction systems that were surveyed. Five plumes with $\delta^{13}\text{C} < 40$ ‰ are likely attributable to gas pipeline leaks, an average of one leak per 112 km driven. One plume with a heavily enriched, thermogenic ^{13}C signature was detected next to the Barrow Gas Terminal. While elevated concentrations of up to 0.56 ppm above background were observed near cow barns and near fields with active slurry spreading, isotopic signatures for these emissions could not be determined with sufficient accuracy.

The two landfill sites were the only emission sources in the study area whose isotopic signature could be identified as microbial with a combined $\delta^{13}\text{C}$ source signature of -58.33 ‰. The remaining elevated concentrations are dominated by isotopically enriched emissions with an overall $\delta^{13}\text{C}$ source signature of -36.57 ‰ (Figure 3.6).

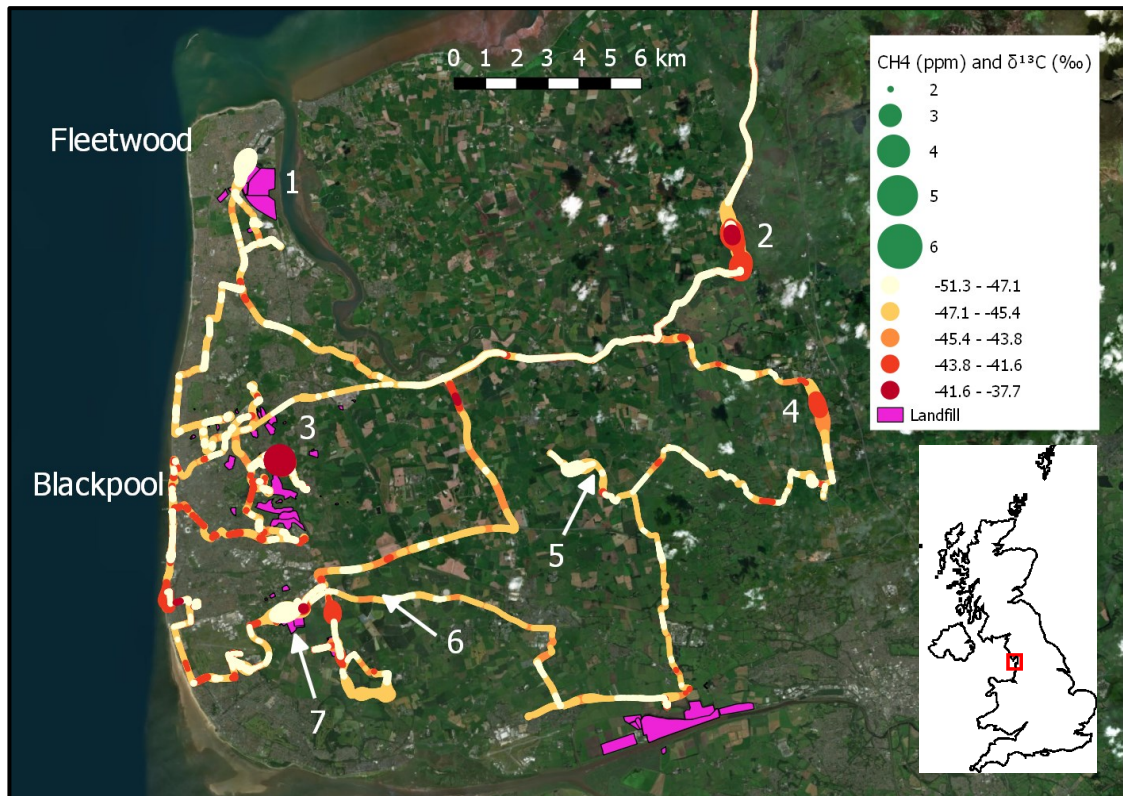


Figure 3.3 Map of mobile measurements in the Fylde area. Map insert highlights the study area within the UK. Symbol width indicates CH₄ concentration as measured by a Picarro G2201-*i* isotopic gas analyser. Colour indicates 30 s running mean measured δ¹³C values grouped by variance. Numbered locations refer to CH₄ emission plumes listed in Table 3.3 and drilling sites: 1 Jameson Rd landfill, 2 Preston Lancaster New Rd, 3 Newton Dr, 4 Garstang Rd, 5 Roseacre Wood drilling site, 6 Preston New Rd drilling site, 7 Midgeland Farm landfill.

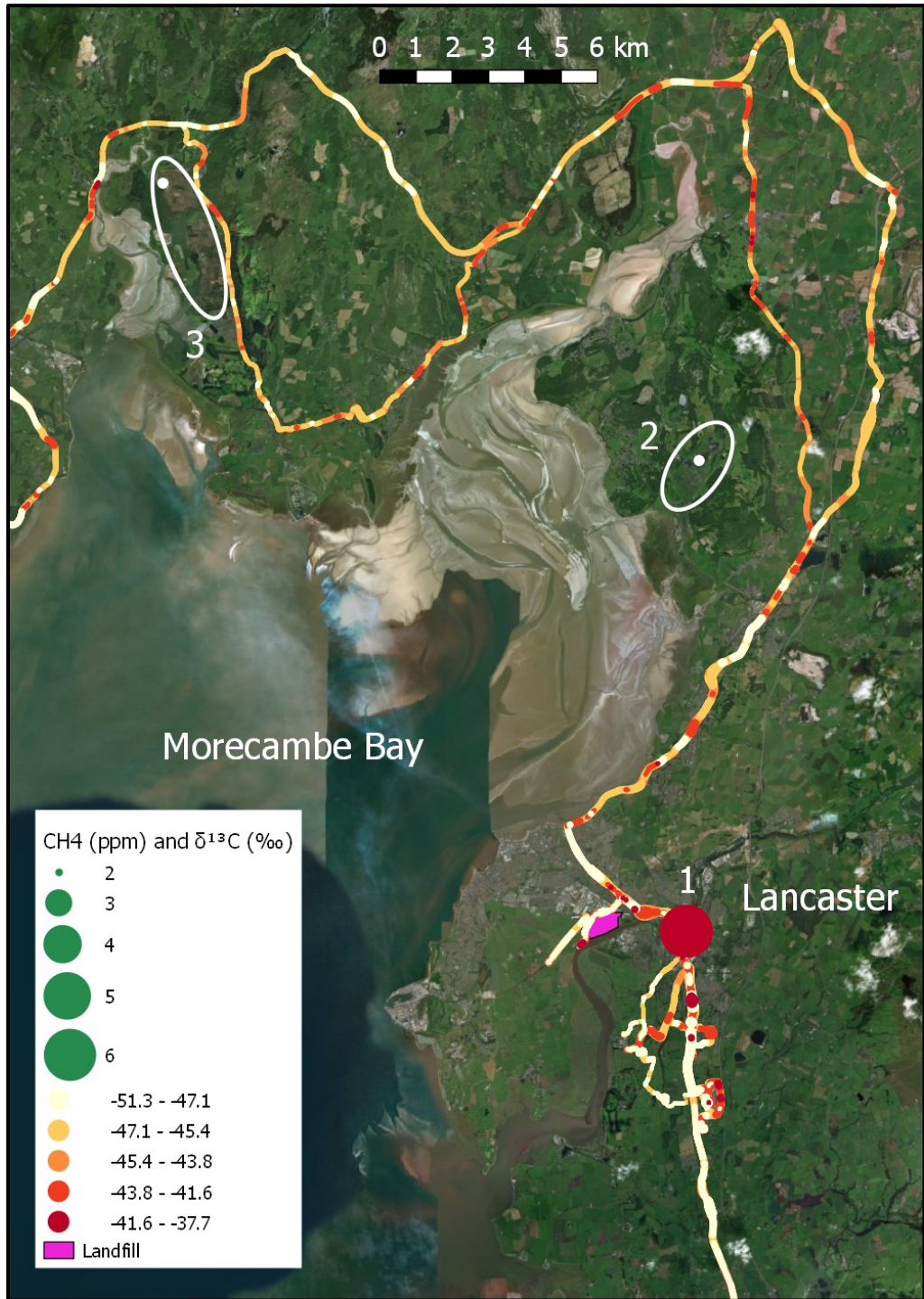


Figure 3.4 Map of mobile measurements around Lancaster and Morecambe Bay. Symbol width indicates CH₄ concentration as measured by a Picarro G2201-*i* isotopic gas analyser. Colour indicates 30 s running mean measured δ¹³C values, grouped by variance. Numbered locations: 1 high concentration measurement in Lancaster city centre is in Cable St, see Table 3.3, 2 Leighton Moss RSPB Nature Reserve, 3 Roudsea Wood Nature Reserve. Points mark wetland sites sampling locations.



Figure 3.5 Map of mobile measurements around Barrow-in-Furness. Symbol width indicates CH₄ concentration as measured by a Picarro G2201-*i* isotopic gas analyser. Colour indicates 30 s running mean measured δ¹³C values, grouped by variance. Numbered locations: 1 Roose Rd, 2 Rampside Gas Terminal with emissions measured to the East at Rampside Rd, see Table 3.3.

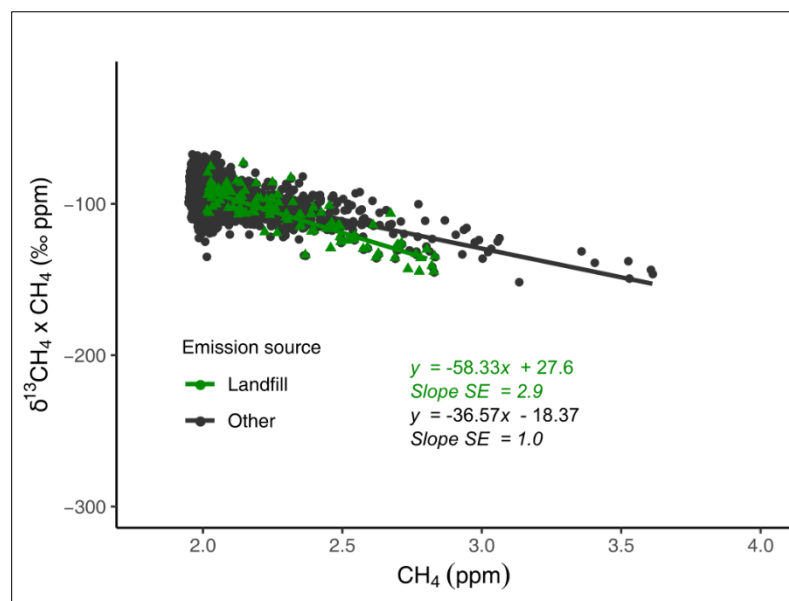


Figure 3.6 Miller-Tans plot for elevated CH₄ data across land use types, excluding stationary measurements (n = 4,189). A separate regression was calculated for known emissions from landfill sites (n = 120).

3.5 Discussion

3.5.1 Background air sampling

We measured isotopic ratios at a coastal and an inland location, north-west of the main study area, under comparable wind conditions to characterise the isotopic composition of well mixed air upwind and downwind of the Fylde area. The slight decrease in $\delta^{13}\text{C}$ signature between the coast and inland site on two sampling dates may be indicative of overall microbially dominated inputs over the Fylde area. Similarly, the relatively lower values of -45.6 ‰ measured in September 2016 at the coastal site may have been the result of local emissions from coastal littoral sediments exposed during low tide. The relative enrichment of $\delta^{13}\text{C}$ in the Fylde area of at least 1.75 ‰ under south-westerly winds compared to the 2016 values of the Atlantic background indicates that there is an enriched source between the west coast of Ireland and the west coast of England. Ireland's main source of CH₄ emissions is agriculture, with around 90% according to inventory estimates, followed by waste (Duffy et al., 2015), both microbial sources depleted in ^{13}C relative to the atmospheric background. There are, however, around 90 active oil and gas wells off the coast of the Fylde and Morecambe Bay area (Oil & Gas Authority, 2018), potentially releasing CH₄ enriched in ^{13}C . There is less data available on atmospheric ^2H values from Atlantic monitoring stations. Bergamaschi et al. (2000) measured $\delta^2\text{H}$ at Izaña, Tenerife,

between July 1996 and December 1998 and have found $\delta^2\text{H}$ values ranging from -85 ‰ in the winter to -76 ‰ in the summer. Our observations of $\delta^2\text{H}$ are more depleted by 35-45 ‰, again suggesting input from another source, though both microbial and thermogenic sources are depleted compared to the atmospheric background (Whiticar, 1999).

3.5.2 Fylde isotopic source characterisation

The emission signatures found in our sampling are within the range of values reported for thermogenic and microbial sources (Whiticar, 1999). They do differ, however, from global weighted averages as reported by Schwietzke et al. (2016), or even from mean UK emissions. Our local natural gas $\delta^{13}\text{C}$ values of -39.45 ± 1.38 ‰ are considerably more enriched than the national mean for oil and gas of -47.38 ± 1.76 ‰ as reported by Sherwood et al. (2017), but closer to the value of -36 ‰ reported in Zazzeri et al. (2017). While our data only include samples of network gas, these are likely the major contributor to fugitive natural gas emissions in the study area (see below). Our $\delta^2\text{H}$ values of -184.28 ± 4.85 ‰ are conversely more depleted than the national average for oil and gas of -165.8 ± 5.8 ‰. Our $\delta^{13}\text{C}$ values for cow breath of -66.75 ± 0.83 ‰ are within the range of values reported for cows fed on a C_3 diet (Sherwood et al., 2017) and in close agreement with the value of -66 ‰ from Zazzeri et al. (2017). Values for $\delta^2\text{H}$ are rarely reported and range from 295 ‰ (Levin et al., 1993) to 358 ‰ (Bilek et al., 2001), encompassing our results. We are only aware of one other study, Levin et al. (1993), that has reported CH_4 isotopes for animal waste. Compared to our data, that study reported similar values for liquid manure but more enriched $\delta^{13}\text{C}$ values for manure piles. Given that over 10 % of total livestock emissions are estimated to originate from manure management globally (Janssens-Maenhout et al., 2017), and around 16 % in the UK according the National Atmospheric Emissions Inventory (NAEI, 2018), more data on the effect of animal waste management practices on emission signatures is needed.

3.5.3 Wetland sites

The emission signatures at Leighton Moss and Roudsea Wood indicate temporal and spatial dynamics in the wetland emissions. The $\delta^{13}\text{C}$ values at Leighton Moss are in the range expected for acetoclastic methanogenesis, using acetate as a substrate (Whiticar, 1999). The relatively more depleted values at Roudsea Wood may indicate a higher proportion of hydrogenotrophic methanogenesis, using CO_2 and H_2 as a substrate. While

$\delta^{13}\text{C}$ values were consistent within vegetated plots, but varied between time and/or location, $\delta^2\text{H}$ varied between vegetation types, but was constant over time and/or location. This may indicate that the processes regulating CH_4 emission signatures, which are a composition of available substrate, metabolic pathway of CH_4 production, microbial oxidation, and transport to the surface (Deng et al., 2017) may be uncoupled for the two isotopes.

While the measurements represent the specific conditions at the sampling sites and are not necessarily representative of the entire system, they indicate that accounting for seasonal variability and wetland vegetation may be important for constructing local isotope based CH_4 budgets in areas where their contribution to total emissions is high.

3.5.4 Mobile CH_4 source identification

Our aim was to verify the existence of potential CH_4 emission sources, as well as to identify potential gas leaks, in comparison to background levels of CH_4 throughout the study area. As found in previous studies (e.g. Brandt et al., 2016; Fischer et al., 2017), emissions, as indicated by peak area, were highly right-skewed, indicating that a small fraction of sources are responsible for the majority of emissions (Figure S 3.1). Elevated concentrations of CH_4 were found throughout the region (Figure 3.3, Figure 3.4 & Figure 3.5), and we found multiple locations where the isotopic signature of significant sources could be determined. We detected CH_4 plumes from two out of the five landfills examined. On average, the $\delta^{13}\text{C}$ source signature of CH_4 plumes measured downwind of landfills was enriched by around 4 ‰ relative to samples collected directly from gas extraction systems (Table 3.2, Figure 3.6). This moderate difference indicates that fugitive emissions have undergone some level of microbial oxidation and fractionation in the cover soil. However, part of the CH_4 emissions may originate as direct emissions to the atmosphere via cracks or leakages or from the uncovered active site of the landfill at Jameson Rd where new waste is deposited (Bergamaschi et al., 1998). Chamber measurements from capped landfill sections found no emissions from the cover soil and emissions were not detected at all landfills, despite having surveyed one of them, Salt Ayre near Lancaster, on three separate occasions. In total, these findings suggest that the combination of landfill capping and gas extraction systems employed at these sites is largely effective at limiting emissions through the cover soil, while fugitive emissions may still occur from the active site of a landfill or from (preventable)

leaks in the landfill cover and/or gas extraction system. Routine mobile measurements thus potentially provide a means for identifying and reducing emissions from landfills.

Four point-sources of CH₄ could be identified as likely gas leaks based on their thermogenic $\delta^{13}\text{C}$ signature, while one, in Lancaster city centre, was confirmed as a known gas leak by the utility operator. The $\delta^{13}\text{C}$ values, including uncertainty estimates, of these gas leaks were within the range of values collected from a laboratory gas outlet, but notably more enriched on average (Table 3.2 & Table 3.3). It is important to note that the true number of gas pipeline leaks is likely considerably higher as most leaks will be too small to accurately determine their isotopic value. Ground surveys using hand-held gas analysers could be used to determine the source of smaller peaks identified in mobile surveys (Weller et al., 2018). Pipeline gas leaks are both a source of preventable CH₄ emissions and a potential safety hazard. While iron pipelines in the UK are gradually being replaced with less leak prone materials since 1977 (HSE, 2005) and the leaks observed in our study were not as severe as those found in mobile surveys in e.g. some US cities (Jackson et al., 2014; Phillips et al., 2013), identifying them so they can be monitored and repaired is still an important concern. The CH₄ detected downwind of the Barrow Gas Terminal was more enriched in ¹³C at -23.73 ± 1.93 ‰ than other sources, possibly indicative of the isotopic signature of natural gas from the Irish Sea.

Overall, there was reasonable agreement between the mobile measurements and samples collected directly from emission sources, given the precision of ± 6 ‰ of the mobile measurements in this study. Moreover, the combination of isotopic and wind measurements allows for source attribution in instances where concentration measurements alone might be ambiguous, such as close to landfill sites. Nonetheless, the origin of emissions can be ambiguous as isotope values for smaller or more diffuse sources, like agricultural emissions, could often not be determined with sufficient accuracy. Such limitations may be addressed with mobile sampling methods that either involve collection of discrete samples (Zazzeri et al., 2015) or systems to remeasure plumes at slower instrument speed and higher precision (Rella et al., 2015a). While a system to collect discrete samples was installed in the vehicle, it proved challenging to consistently stop the vehicle within plumes to collect samples due to traffic conditions.

3.5.5 Land use

Investigating emissions in a region that alternates mainly between agricultural and urban land use, we expected to find overall $\delta^{13}\text{C}_{\text{CH}_4}$ values dominated either by relatively ^{13}C depleted emissions from livestock and animal waste or relatively enriched urban gas distribution and traffic emissions (Nakagawa et al., 2005).

While background concentrations were similar for both land use categories, in urban areas, $\delta^{13}\text{C}$ signatures were indeed enriched by around 1 ‰ compared to agricultural areas. The overall background signature of -45.47 ‰ obtained during mobile surveys was in close agreement with the value of -45.32 ‰ obtained during inland background air sampling campaigns (Table 3.1 & Table S 3.2).

The overall source signature of emissions, i.e. elevated concentrations, detected during the mobile measurements, is dominated by ^{13}C enriched thermogenic sources due to the presence of gas leaks (Figure 3.6). The same pattern is apparent when analysing urban and agricultural areas separately as gas leaks are present in both land use types (Figure S 3.2). While this indicates that fugitive emissions from oil and gas distribution networks are an important source of CH_4 in the region, these results must be interpreted carefully as mobile, vehicle-based, measurements may not capture all sources equally in heterogeneous environments. Emissions from infrastructure, such as gas pipelines which follow the road network, can be measured close to the source, with little dispersion. Sources that are often at a distance from public roads and/or diffuse, such as pastures, barns, slurry pits, or wetlands, will be more dispersed. Depending on sampling regime and sources present in the environment, mobile measurements may disproportionately capture road-accessible sources of CH_4 emissions, influencing total landscape level estimates. This is supported by our coastal and inland measurements, which do not indicate an enrichment in CH_4 across the Fylde area.

3.5.6 Conclusion

Characterising CH_4 emissions in a heterogeneous environment poses challenges that typically require multiple approaches. Establishing an understanding of existing emission sources is important for future work aiming to assess the impact of potential additional sources such as shale gas production. Regional isotope data is rarely available, particularly for ^2H , while our data show that agricultural and landfill emissions differ in their $\delta^2\text{H}$ values and may therefore be distinguishable.

While land use affects emission signatures, the presence of gas leaks and landfills in both urban and agricultural areas and the close proximity of different land use types confounds these differences. Overall, the combination of mobile and stationary measurements indicates that both microbial emissions, mainly from landfills and agriculture, and thermogenic CH₄ from fugitive emissions in natural gas infrastructure, contribute to total emissions in the region. Such pre-existing thermogenic emissions, which can occur randomly throughout the gas distribution network, are detectable using mobile measurements. They may show similar isotopic signatures as shale gas, and therefore need to be taken into consideration when assessing the impact of gas production operations.

3.6 References

- Allen, D., 2016. Attributing Atmospheric Methane to Anthropogenic Emission Sources. *Acc. Chem. Res.* 49, 1344–1350. <https://doi.org/10.1021/acs.accounts.6b00081>
- Bergamaschi, P., Bräunlich, M., Marik, T., Brenninkmeijer, C.A.M., 2000. Measurements of the carbon and hydrogen isotopes of atmospheric methane at Izaña, Tenerife: Seasonal cycles and synoptic-scale variations. *J. Geophys. Res. Atmos.* 105, 14531–14546. <https://doi.org/10.1029/1999JD901176>
- Bergamaschi, P., Lubina, C., Königstedt, R., Fischer, H., Veltkamp, A.C., Zwaagstra, O., 1998. Stable isotopic signatures ($\delta^{13}\text{C}$, δD) of methane from European landfill sites. *J. Geophys. Res. Atmos.* 103, 8251–8265. <https://doi.org/10.1029/98JD00105>
- Bilek, R.S., Tyler, S.C., Kurihara, M., Yagi, K., 2001. Investigation of cattle methane production and emission over a 24-hour period using measurements of $\delta^{13}\text{C}$ and δD of emitted CH_4 and rumen water. *J. Geophys. Res. Atmos.* 106, 15405–15413. <https://doi.org/10.1029/2001JD900177>
- Brandt, A.R., Heath, G.A., Cooley, D., 2016. Methane Leaks from Natural Gas Systems Follow Extreme Distributions. *Environ. Sci. Technol.* 50, 12512–12520. <https://doi.org/10.1021/acs.est.6b04303>
- Bréas, O., Guillou, C., Reniero, F., Wada, E., 2001. The global methane cycle: Isotopes and mixing ratios, sources and sinks. *Isotopes Environ. Health Stud.* 37, 257–379. <https://doi.org/10.1080/10256010108033302>
- Chanton, J.P., Powelson, D.K., Abichou, T., Fields, D., Green, R., 2008. Effect of temperature and oxidation rate on carbon-isotope fractionation during methane oxidation by landfill cover materials. *Environ. Sci. Technol.* 42, 7818–7823. <https://doi.org/10.1021/es801221y>
- Chanton, J.P., Rutkowski, C.M., Mosher, B., 1999. Quantifying methane oxidation from landfills using stable isotope analysis of downwind plumes. *Environ. Sci. Technol.* 33, 3755–3760. <https://doi.org/10.1021/es9904033>
- Deng, J., McCalley, C.K., Frohling, S., Chanton, J., Crill, P., Varner, R., Tyson, G., Rich, V., Hines, M., Saleska, S.R., Li, C., 2017. Adding stable carbon isotopes improves model representation of the role of microbial communities in peatland methane cycling. *J. Adv. Model. Earth Syst.* 9, 1412–1430. <https://doi.org/10.1002/2016MS000817>
- Duffy, P., Hanley, E., Black, K., O'Brien, P., Hyde, B., Ponzi, J., Alam, S., 2015. Ireland's National Inventory Report 2015 - Greenhouse Gas Emissions 1990-2013. Environmental Protection Agency.
- Environment Agency, 2018. Historic Landfill Sites [WWW Document]. URL

<https://data.gov.uk/dataset/17edf94f-6de3-4034-b66b-004ebd0dd010/historic-landfill-sites> (accessed 2.11.19).

- Etminan, M., Myhre, G., Highwood, E.J., Shine, K.P., 2016. Radiative forcing of carbon dioxide, methane, and nitrous oxide: A significant revision of the methane radiative forcing. *Geophys. Res. Lett.* 43, 12,614–12,623.
<https://doi.org/10.1002/2016GL071930>
- Feinberg, A.I., Coulon, A., Stenke, A., Schwietzke, S., Peter, T., 2018. Isotopic source signatures: Impact of regional variability on the $\delta^{13}\text{C}_{\text{CH}_4}$ trend and spatial distribution. *Atmos. Environ.* 174, 99–111.
<https://doi.org/10.1016/j.atmosenv.2017.11.037>
- Fischer, J.C. von, Cooley, D., Chamberlain, S., Gaylord, A., Griebenow, C.J., Hamburg, S.P., Salo, J., Schumacher, R., Theobald, D., Ham, J., 2017. Rapid, Vehicle-Based Identification of Location and Magnitude of Urban Natural Gas Pipeline Leaks. *Environ. Sci. Technol.* 51, 4091–4099. <https://doi.org/10.1021/acs.est.6b06095>
- Hijmans, R.J., 2017. *geosphere: Spherical Trigonometry*.
- HSE, 2005. Enforcement Policy for the replacement of iron gas mains 2006 - 2013.
- Jackson, R.B., Down, A., Phillips, N.G., Ackley, R.C., Cook, C.W., Plata, D.L., Zhao, K., Philips, N.G., Ackley, R.C., Cook, C.W., Plata, D.L., Zhao, K., 2014. Natural gas pipeline leaks across Washington, DC. *Environ. Sci. Technol.* 48, 2051–8.
<https://doi.org/10.1021/es404474x>
- Janssens-Maenhout, G., Crippa, M., Guizzardi, D., Muntean, M., Schaaf, E., Dentener, F., Bergamaschi, P., Pagliari, V., Olivier, J.G.J., Peters, J.A.H.W., van Aardenne, J.A., Monni, S., Doering, U., Petrescu, A.M.R., 2017. EDGAR v4.3.2 Global Atlas of the three major Greenhouse Gas Emissions for the period 1970 - 2012. *Earth Syst. Sci. Data Discuss.* 1–55. <https://doi.org/10.5194/essd-2017-79>
- Kirschke, S., Bousquet, P., Ciais, P., Saunoy, M., Canadell, J.G., Dlugokencky, E.J., Bergamaschi, P., Bergmann, D., Blake, D.R., Bruhwiler, L., Cameron-Smith, P., Castaldi, S., Chevallier, F., Feng, L., Fraser, A., Heimann, M., Hodson, E.L., Houweling, S., Josse, B., Fraser, P.J., Krummel, P.B., Lamarque, J.-F., Langenfelds, R.L., Le Quéré, C., Naik, V., O'Doherty, S., Palmer, P.I., Pison, I., Plummer, D., Poulter, B., Prinn, R.G., Rigby, M., Ringeval, B., Santini, M., Schmidt, M., Shindell, D.T., Simpson, I.J., Spahni, R., Steele, L.P., Strode, S. A., Sudo, K., Szopa, S., van der Werf, G.R., Voulgarakis, A., van Weele, M., Weiss, R.F., Williams, J.E., Zeng, G., 2013. Three decades of global methane sources and sinks. *Nat. Geosci.* 6, 813–823. <https://doi.org/10.1038/ngeo1955>
- Levin, I., Bergamaschi, P., Dörr, H., Trapp, D., 1993. Stable isotopic signature of methane from major sources in Germany. *Chemosphere* 26, 161–177.
[https://doi.org/10.1016/0045-6535\(93\)90419-6](https://doi.org/10.1016/0045-6535(93)90419-6)

- Lopez, M., Sherwood, O.A., Dlugokencky, E.J., Kessler, R., Giroux, L., Worthy, D.E.J., 2017. Isotopic signatures of anthropogenic CH₄ sources in Alberta, Canada. *Atmos. Environ.* 164, 280–288. <https://doi.org/10.1016/j.atmosenv.2017.06.021>
- McEwing, K.R., Fisher, J.P., Zona, D., 2015. Environmental and vegetation controls on the spatial variability of CH₄ emission from wet-sedge and tussock tundra ecosystems in the Arctic. *Plant Soil* 388, 37–52. <https://doi.org/10.1007/s11104-014-2377-1>
- MET éireann, 2018. MET éireann [WWW Document]. URL <https://www.met.ie/climate/what-we-measure/wind> (accessed 8.31.18).
- Miller, J.B., Tans, P.P., 2003. Calculating isotopic fractionation from atmospheric measurements at various scales. *Tellus, Ser. B Chem. Phys. Meteorol.* 55, 207–214. <https://doi.org/10.1034/j.1600-0889.2003.00020.x>
- NAEI, 2018. National Atmospheric Emissions Inventory [WWW Document]. URL <http://naei.beis.gov.uk/> (accessed 9.5.18).
- Nakagawa, F., Tsunogai, U., Komatsu, D.D., Yamada, K., Yoshida, N., Moriizumi, J., Nagamine, K., Iida, T., Ikebe, Y., 2005. Automobile exhaust as a source of ¹³C- and D-enriched atmospheric methane in urban areas. *Org. Geochem.* 36, 727–738. <https://doi.org/10.1016/j.orggeochem.2005.01.003>
- Oil & Gas Authority, 2018. Oil & Gas Authority [WWW Document]. URL <https://www.ogauthority.co.uk/> (accessed 8.30.18).
- Phillips, N.G., Ackley, R., Crosson, E.R., Down, A., Hutyra, L.R., Brondfield, M., Karr, J.D., Zhao, K., Jackson, R.B., 2013. Mapping urban pipeline leaks: Methane leaks across Boston. *Environ. Pollut.* 173, 1–4. <https://doi.org/10.1016/j.envpol.2012.11.003>
- Rella, C.W., Hoffnagle, J., He, Y., Tajima, S., 2015. Local- and regional-scale measurements of CH₄, δ¹³CH₄, and C₂H₆ in the Uintah Basin using a mobile stable isotope analyzer. *Atmos. Meas. Tech.* 8, 4539–4559. <https://doi.org/10.5194/amt-8-4539-2015>
- Rowland, C.S., Morton, R.D., L., C., G., M., A.W., O., M, W.C., 2017. Land Cover Map 2015 (vector, GB). <https://doi.org/10.5285/6c6c9203-7333-4d96-88ab-78925e7a4e73>
- Saunois, M., Bousquet, P., Poulter, B., Peregón, A., Ciais, P., Canadell, J.G., Dlugokencky, E.J., Etiope, G., Bastviken, D., Houweling, S., Janssens-Maenhout, G., Tubiello, F.N., Castaldi, S., Jackson, R.B., Alexe, M., Arora, V.K., Beerling, D.J., Bergamaschi, P., Blake, D.R., Brailsford, G., Brovkin, V., Bruhwiler, L., Crevoisier, C., Crill, P., Covey, K., Curry, C., Frankenberg, C., Gedney, N., Höglund-Isaksson, L., Ishizawa, M., Ito, A., Joos, F., Kim, H.S., Kleinen, T., Krummel, P., Lamarque,

- J.F., Langenfelds, R., Locatelli, R., Machida, T., Maksyutov, S., McDonald, K.C., Marshall, J., Melton, J.R., Morino, I., Naik, V., O'Doherty, S., Parmentier, F.J.W., Patra, P.K., Peng, C., Peng, S., Peters, G.P., Pison, I., Prigent, C., Prinn, R., Ramonet, M., Riley, W.J., Saito, M., Santini, M., Schroeder, R., Simpson, I.J., Spahni, R., Steele, P., Takizawa, A., Thornton, B.F., Tian, H., Tohjima, Y., Viovy, N., Voulgarakis, A., Van Weele, M., Van Der Werf, G.R., Weiss, R., Wiedinmyer, C., Wilton, D.J., Wiltshire, A., Worthy, D., Wunch, D., Xu, X., Yoshida, Y., Zhang, B., Zhang, Z., Zhu, Q., 2016a. The global methane budget 2000-2012. *Earth Syst. Sci. Data* 8, 697–751. <https://doi.org/10.5194/essd-8-697-2016>
- Saunio, M., Jackson, R.B., Bousquet, P., Poulter, B., Canadell, J.G., 2016b. The growing role of methane in anthropogenic climate change. *Environ. Res. Lett.* 11, 1–5. <https://doi.org/10.1088/1748-9326/11/12/120207>
- Schwietzke, S., Sherwood, O.A., Bruhwiler, L.M.P., Miller, J.B., Etiope, G., Dlugokencky, E.J., Michel, S.E., Arling, V.A., Vaughn, B.H., White, J.W.C., Tans, P.P., 2016. Upward revision of global fossil fuel methane emissions based on isotope database. *Nature* 538, 88–91. <https://doi.org/10.1038/nature19797>
- Sherwood, O.A., Schwietzke, S., Arling, V.A., Etiope, G., 2017. Global inventory of gas geochemistry data from fossil fuel, microbial and burning sources, version 2017. *Earth Syst. Sci. Data* 9, 639–656. <https://doi.org/10.5194/essd-9-639-2017>
- Shindell, D., Kuylenstierna, J.C.I., Vignati, E., van Dingenen, R., Amann, M., Klimont, Z., Anenberg, S.C., Muller, N., Janssens-Maenhout, G., Raes, F., Schwartz, J., Faluvegi, G., Pozzoli, L., Kupiainen, K., Hoglund-Isaksson, L., Emberson, L., Streets, D., Ramanathan, V., Hicks, K., Oanh, N.T.K., Milly, G., Williams, M., Demkine, V., Fowler, D., 2012. Simultaneously Mitigating Near-Term Climate Change and Improving Human Health and Food Security. *Science* (80-.). 335, 183–189. <https://doi.org/10.1126/science.1210026>
- Stocker, T.F., Qin, D., Plattner, G.-K., Tignor, M.M.B., Allen, S.K., Boschung, J., Nauels, A., Xia, Y., Bex, V., Midgley, P.M., (eds.), 2013. *Climate Change 2013: The Physical Science Basis. Contribution of Working Group I to the Fifth Assessment Report of the Intergovernmental Panel on Climate Change.* Cambridge, United Kingdom and New York, NY, USA.
- Turner, A.J., Frankenberg, C., Wennberg, P.O., Jacob, D.J., 2017. Ambiguity in the causes for decadal trends in atmospheric methane and hydroxyl. *Proc. Natl. Acad. Sci.* 114, 5367–5372. <https://doi.org/10.1073/pnas.1616020114>
- UC Davis SIF, 2019. UC Davis Stable Isotope Facility [WWW Document]. UC Davis. URL <https://stableisotopefacility.ucdavis.edu/> (accessed 1.24.19).
- Vavrek, M.J., 2011. fossil: palaeoecological and palaeogeographical analysis tools. *Palaeontol. Electron.* 14, 1T.

- Vermeesch, P., 2018. IsoplotR: A free and open toolbox for geochronology. *Geosci. Front.* <https://doi.org/10.1016/j.gsf.2018.04.001>
- Wehr, R., Saleska, S.R., 2017. The long-solved problem of the best-fit straight line: application to isotopic mixing lines. *Biogeosciences* 14, 17–29. <https://doi.org/10.5194/bg-14-17-2017>
- Weller, Z.D., Roscioli, J.R., Daube, W.C., Lamb, B.K., Ferrara, T.W., Brewer, P.E., Von Fischer, J.C., 2018. Vehicle-Based Methane Surveys for Finding Natural Gas Leaks and Estimating Their Size: Validation and Uncertainty. *Environ. Sci. Technol.* 52, 11922–11930. <https://doi.org/10.1021/acs.est.8b03135>
- Whiticar, M.J., 1999. Carbon and hydrogen isotope systematics of bacterial formation and oxidation of methane. *Chem. Geol.* 161, 291–314. [https://doi.org/10.1016/S0009-2541\(99\)00092-3](https://doi.org/10.1016/S0009-2541(99)00092-3)
- Williams, E., 2011. Aviation Formulary v1.46 [WWW Document]. URL <http://www.edwilliams.org/avform.htm> (accessed 5.11.18).
- Yarnes, C., 2013. $\delta^{13}\text{C}$ and $\delta^2\text{H}$ measurement of methane from ecological and geological sources by gas chromatography/combustion/pyrolysis isotope-ratio mass spectrometry. *Rapid Commun. Mass Spectrom.* 27, 1036–1044. <https://doi.org/10.1002/rcm.6549>
- York, D., 1969. Least squares fitting of a straight line with correlated errors. *Earth Planet. Sci. Lett.* 5, 320–324. [https://doi.org/10.1016/S0012-821X\(68\)80059-7](https://doi.org/10.1016/S0012-821X(68)80059-7)
- Yoshida, H., Mønster, J.G., Scheutz, C., 2014. Plant-integrated measurement of greenhouse gas emissions from a municipal wastewater treatment plant. *Water Res.* 61, 108–18. <https://doi.org/10.1016/j.watres.2014.05.014>
- Zazzeri, G., Lowry, D., Fisher, R.E., France, J.L., Lanoisellé, M., Grimmond, C.S.B., Nisbet, E.G., 2017. Evaluating methane inventories by isotopic analysis in the London region. *Sci. Rep.* 7, 4854. <https://doi.org/10.1038/s41598-017-04802-6>
- Zazzeri, G., Lowry, D., Fisher, R.E., France, J.L., Lanoisellé, M., Nisbet, E.G., 2015. Plume mapping and isotopic characterisation of anthropogenic methane sources. *Atmos. Environ.* 110, 151–162. <https://doi.org/10.1016/j.atmosenv.2015.03.029>

3.7 Supplementary material

3.7.1 Supplementary tables

Table S 3.1 Land use statistics in study area excluding littoral.

Land use	Area (km ²)	%
Arable and horticulture	180	12.5
Improved grassland	757	52.6
Suburban	138	9.6
Urban	57	4.0
Acid grassland	60	4.2
Broadleaf woodland	123	8.5
Saltmarsh	83	5.8
Saltwater	40	2.7
Neutral grassland	24	1.7
Freshwater	9	0.7
Coniferous woodland	9	0.6
Heather	8	0.5
Heather grassland	3	0.2
Calcareous grassland	3	0.2
Inland rock	3	0.2
Bog	2	0.2
Total urban	195	4.0
Total agriculture	937	65.0
Total	1,441	69.0

Table S 3.2 Statistics for different land use types as measured by two instruments.**Background statistics are means \pm SE, peak statistics are medians.**

Land use	Peaks	Background CH ₄ (ppm)	Peak height (ppm)	Peak area (ppm m)	Background $\delta^{13}\text{C}$	Peak $\delta^{13}\text{C}$
<i>G2201-i</i>						
All	232	$1.97 \pm 1.02 \times 10^{-04}$	0.15	103.3	-45.47 ± 0.02 $-44.9945 \pm$	-44.9095
Urban	96	$1.97 \pm 2.11 \times 10^{-04}$	0.15	92.4	0.03	-44.2530
Agriculture	126	$1.97 \pm 1.61 \times 10^{-04}$	0.15	109.1	-45.986 ± 0.03	-44.7173
<i>UGGA</i>						
						km driven
All	707	$1.97 \pm 1.03 \times 10^{-04}$	0.15	53.6		557
Urban	271	$1.97 \pm 2.07 \times 10^{-04}$	0.23	61.7		72
Agriculture	268	$1.97 \pm 1.61 \times 10^{-04}$	0.18	78.5		238

3.7.2 Supplementary figures

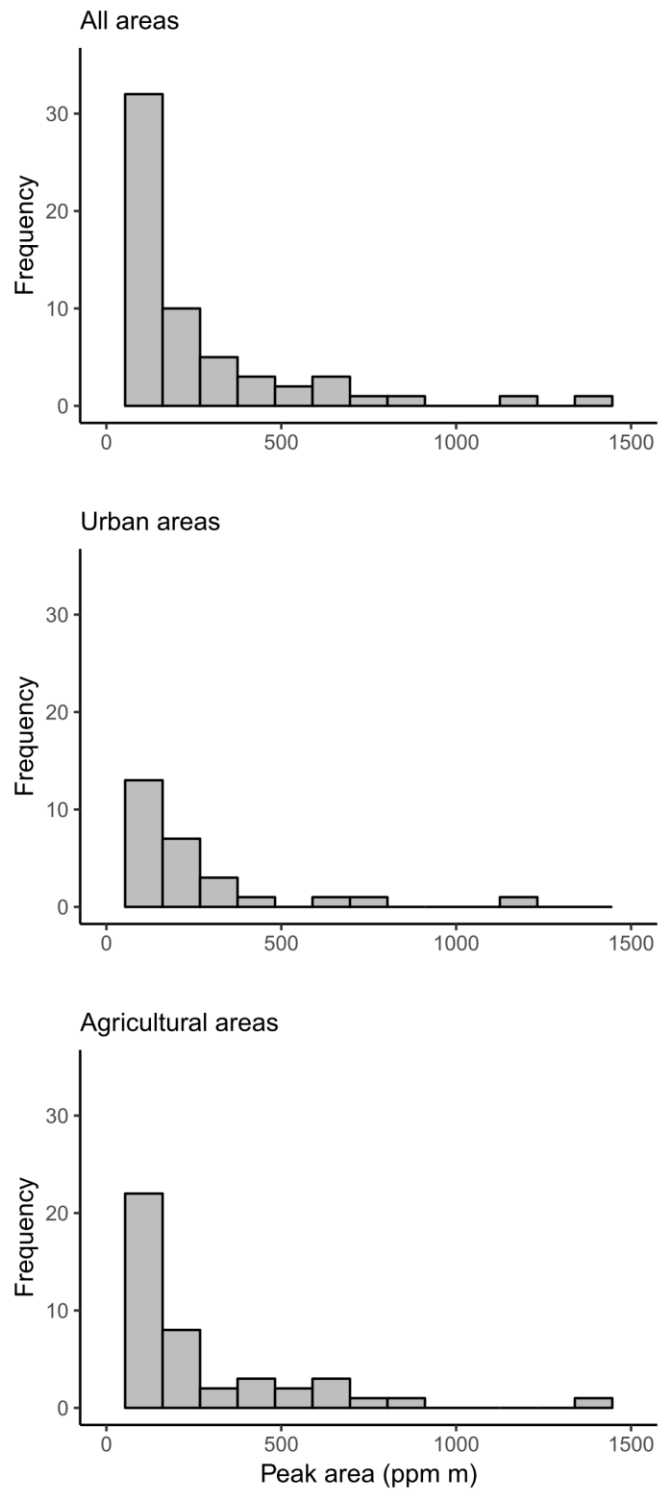


Figure S 3.1 Histograms of speed-corrected peak areas in study area.

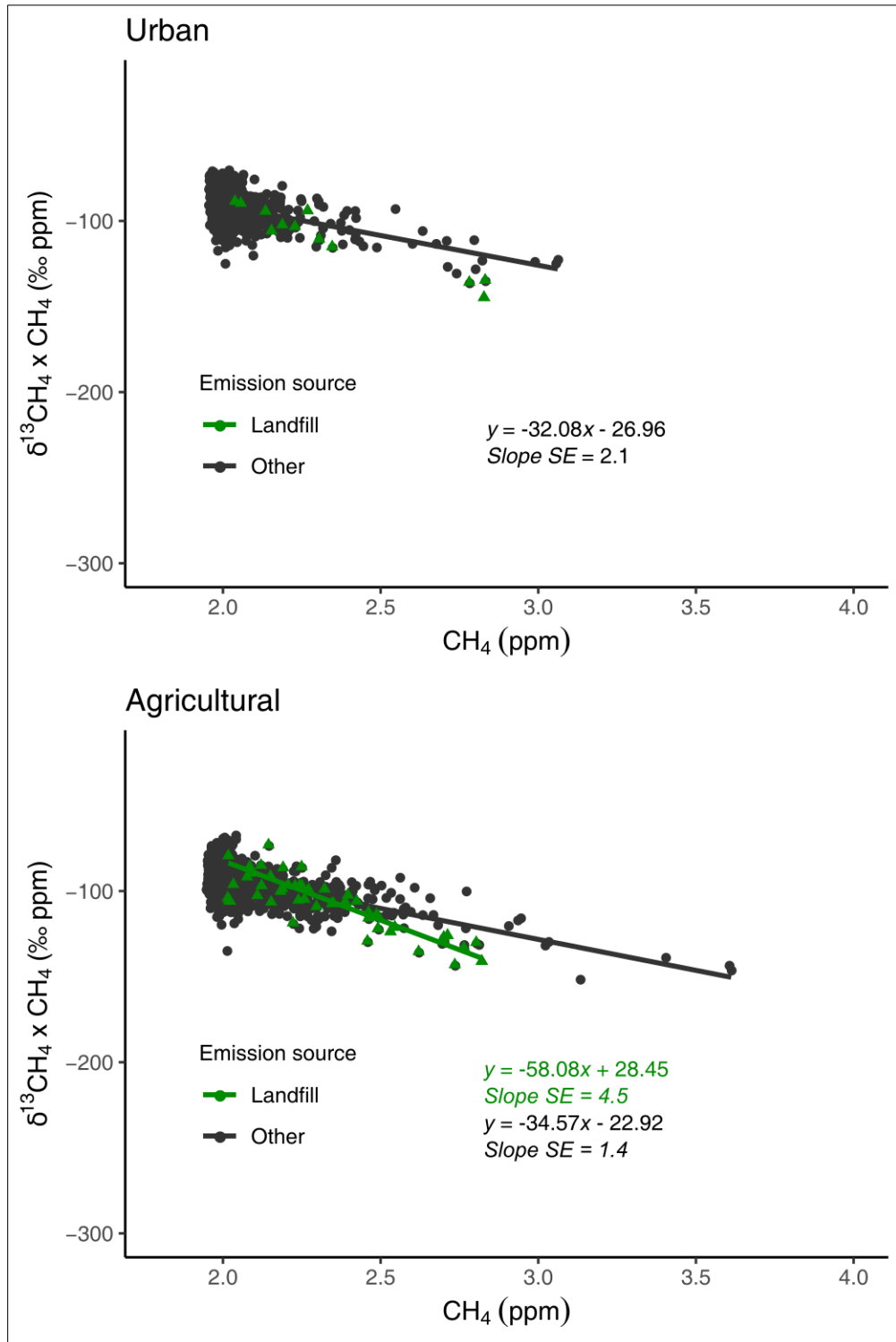


Figure S 3.2 Miller-Tans plot for elevated CH_4 data for different land use types, excluding stationary measurements. A separate regression was calculated for known emissions from landfill sites. No model was calculated for landfills in urban areas due to small number of data points. Due to proximity of land use types, peaks can span multiple land use types.

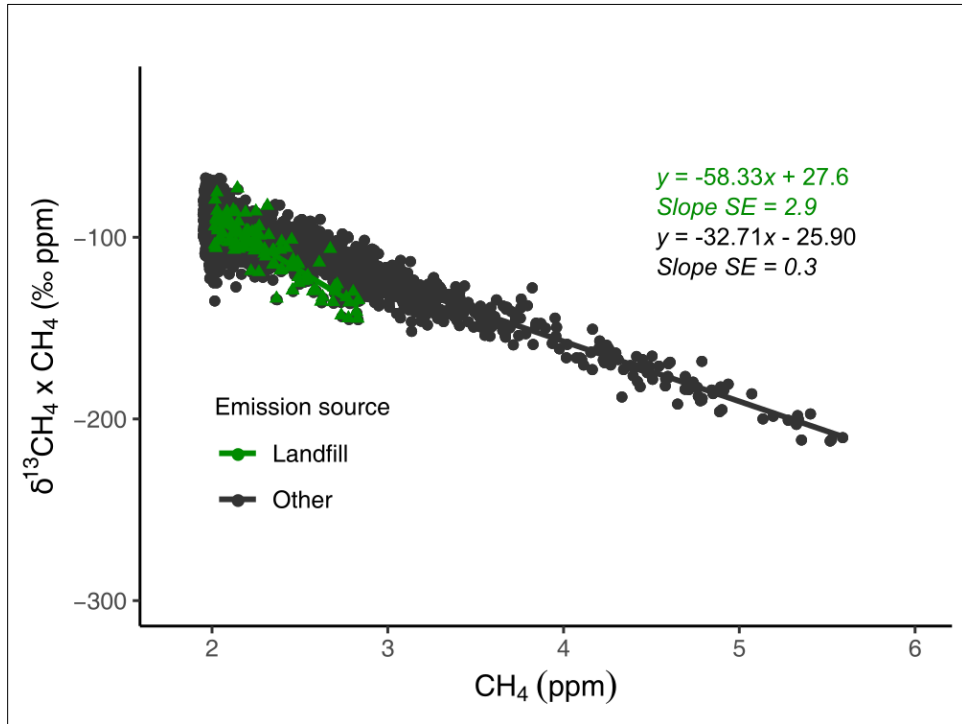


Figure S 3.3 Miller-Tans plot for all CH₄ data, including stationary measurements. A separate regression was calculated for known emissions from landfill sites. Note different X-axis range on this plot.

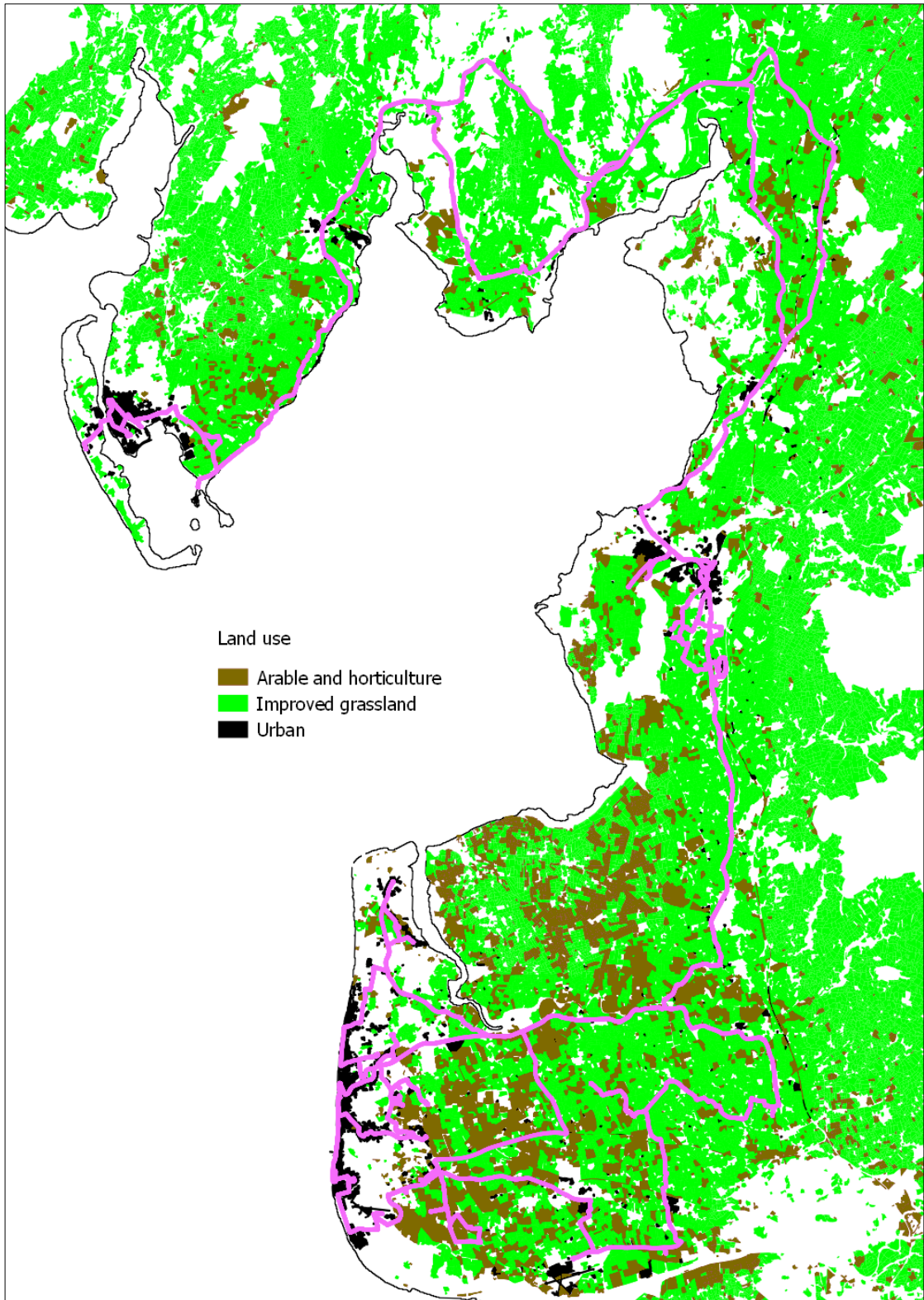


Figure S 3.4 Urban and agricultural land use in study area with the route taken during mobile measurements in purple. Land use data based on CEH Landcover Map 2015 (Rowland et al., 2017).

4

Large seasonal and interannual variations in methane emissions do not affect carbon and hydrogen isotopes from an ombrotrophic peat bog

Takriti, M., Chadwick, A., Rose, R., Dodd, B., Oakley, S., Wynn, P., McNamara, N., Ward, S.

4.1 Abstract

Natural wetlands contribute around 30 % to global emissions of CH₄, a significant part of which originate from northern peatlands. Understanding sources and drivers of CH₄ emissions from wetlands is therefore essential for modelling and potential mitigation. However, this is challenging because of high spatial and temporal variability. Atmospheric inversion models mainly rely on stable isotope signatures to constrain contributions from different sources. While CH₄ stable isotope signatures are often assumed to be constant, few studies have investigated the effects of seasonal changes in environmental conditions on emission signatures from peatland ecosystems. We here present results from a 2.5-year monitoring study investigating seasonal changes in CH₄ fluxes and dual stable isotope signatures in an ombrotrophic peat bog in Northern England, UK. We used a spectroscopic greenhouse gas analyser to perform dynamic flux chamber measurements as well as isotope ratio mass spectrometry to determine stable isotope signatures. We found

large seasonal and interannual variations in CH₄ fluxes, with uncharacteristically high emissions of over 100 mg CH₄ m⁻² h⁻¹ in the summer of 2016, contrasting with median fluxes across the sampling period of 0.14-1.5 mg CH₄ m⁻² h⁻¹. Fluxes showed strong relationships with abiotic conditions, increasing exponentially with soil temperature, and responding negatively to high and low water table levels.

Incubation experiments of peat cores showed that CH₄ production potential peaked below the water table at 30-40 cm depths, while oxidation potential decreased with depth. Despite the large seasonal and interannual variations in fluxes, stable isotope signatures remained constant throughout the study period indicating that methanogenic pathways and the proportion of CH₄ oxidised in the peat remained stable throughout the study despite changes in abiotic conditions and flux levels. Values of $\delta^{13}\text{C} = -83.99 \pm 0.04 \text{ ‰}$ and $\delta^2\text{H} = -310.69 \pm 1.21 \text{ ‰}$ indicate a relatively high contribution of hydrogenotrophic methanogenesis at the study site, which contrasts with previous studies in peatlands. Our results show that stable isotope signatures can be independent of flux rates and environmental conditions in peatlands and suggest that an improved understanding of microbial processes of CH₄ cycling on local and regional scales may be important to constraining wetland CH₄ emissions.

4.2 Introduction

Natural wetlands are the largest source of methane (CH₄) emissions globally, estimated to account for around 30 % of total emissions (Kirschke et al., 2013), and their contribution is projected to increase considerably under future climate scenarios (Dean et al., 2018; Z. Zhang et al., 2017). Despite a solid body of research, their contribution to changes in the global CH₄ budget over the last decades remains ambiguous, with annual and interannual uncertainties in emissions of around 50 % (Saunois et al., 2016a; Turner et al., 2017). Part of this uncertainty is due to the large seasonal and inter-annual variability in emissions, as well as high spatial heterogeneity (Lai, 2009; Limpens et al., 2008; Turetsky et al., 2014). Stable isotope analysis is a commonly employed method to constrain regional to global scale methane budgets (e.g. Deng et al., 2017; Dlugokencky et al., 2011; Kirschke et al., 2013; Umezawa et al., 2012) as source categories differ in their ¹³C/¹²C and ²H/¹H ratios (Levin et al., 1993; Sherwood et al., 2017; Whiticar, 1999). However, despite the knowledge that seasonal variations in CH₄ emissions exists, current biogeochemical models do not

consider potential seasonal variations in stable isotope signatures, which may lead to mis-estimation of emissions.

Northern peatlands are a major contributor to global wetland CH₄ emissions (Melton et al., 2013). Stable carbon isotope (C) ratios of peatland CH₄ emissions have been measured repeatedly, with $\delta^{13}\text{C}$ values in northern peatlands typically in the range of -59 ‰ to -74 ‰ (Feinberg et al., 2018). However, few studies have investigated their seasonal variations. In Finnish wetlands, Fisher et al. (2017) have found increasingly depleted values from summer to autumn while Sriskantharajah et al. (2012) have found slightly enriched values after the spring melt. Studies in other systems, such as rice paddies (Bergamaschi, 1997; Rao et al., 2008; G. Zhang et al., 2017), as well as landfill cover soils (Chanton and Liptay, 2000), have found that emission signatures in these systems can vary considerably over seasonal cycles. Data for $\delta^2\text{H}$ -CH₄ of peatlands are rarely reported. Kuhlmann et al. (1998) found values of -442 ± 142 ‰ for the Hudson Bay Lowland, while Wahlen et al. (1990) found a value of -300 ‰ for a peat bog in West Virginia. Atmospheric models therefore usually do not include $\delta^2\text{H}$ data, even though they may help to constrain source estimates (Dlugokencky et al., 2011). Moreover, isotopic measurements in wetlands are often limited to the growing season, while non-growing season CH₄ emissions contribute significantly to total annual emissions (Treat et al., 2018). This lack of understanding limits the ability to constrain peatland emissions and understand their responses to environmental drivers.

Peatland CH₄ fluxes and their isotope signatures are determined by a complex interplay of environmental factors and, compared to CO₂ fluxes, are still poorly predictable on local to global scales. Water tables and soil moisture are known to strongly affect CH₄ emissions as they determine the depth of the oxic and anoxic zones of the peat (Basiliko et al., 2007; Smith et al., 2003), and therefore CH₄ production and oxidation. When O₂ availability increases, e.g. due to a drop in water tables, CH₄ emissions decrease (Limpens et al., 2008; Updegraff et al., 2001). Lower water levels may also lead to an enrichment in CH₄ isotope signatures due to isotopic fractionation during CH₄ oxidation in aerated soil. The second main environmental driver of CH₄ emissions is temperature, with higher temperatures promoting microbial methanogenesis across a wide range of ecosystems (Yvon-Durocher et al., 2014). Temperature is also thought to change the relative activity between microbial CH₄ production and oxidation, with methanogens being more temperature sensitive than methanotrophs (Le Mer and Roger, 2001), thus potentially shifting CH₄ isotope signatures. Vegetation cover is also a major determinant of CH₄ fluxes from wetlands, as it affects

both inputs of carbon (C) into the peat and the potential pathways of CH₄ release into the atmosphere. In addition to diffusive release into the atmosphere and ebullition through bubbles, CH₄ can pass through the aerenchyma of vascular plants, which act as conduits for gases (Bridgman et al., 2013, Figure 4.1). Fractionation can occur in the aerenchyma, leading to isotopically lighter CH₄ being emitted to the atmosphere (Chanton, 2005; Vaughn et al., 2016). Plants also provide labile C to soil microbes, thus increasing microbial activity, changing microbial substrates, and microbial communities (Chowdhury and Dick, 2013).

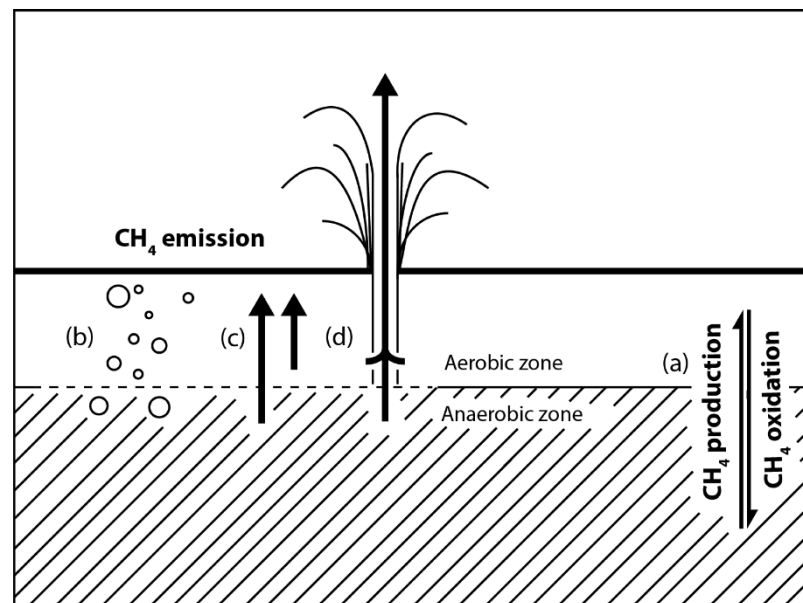


Figure 4.1 Pathways of CH₄ release to the atmosphere. (a) CH₄ production and oxidation in the peat profile, (b) ebullition, (c) diffusion, (d) plant-mediated transport. Modified from (Lai, 2009).

Microbial CH₄ in wetlands is produced by methanogenic archaea by one of two main metabolic pathways: acetoclastic methanogenesis, using acetate as substrate, and hydrogenotrophic methanogenesis, using CO₂ and H₂ as substrate. Both forms occur in freshwater wetland systems, with acetoclastic methanogenesis considered to dominate CH₄ emissions (Kotsyurbenko et al., 2004; Whiticar, 1999). These two pathways have distinct stable isotope signatures, with CH₄ formed through acetoclastic methanogenesis being more enriched in $\delta^{13}\text{C}$ and more depleted in $\delta^2\text{H}$ ($\delta^{13}\text{C} = -60\text{‰}$ to -50‰ and $\delta^2\text{H} = -400\text{‰}$ to -250‰) compared to hydrogenotrophic methanogenesis ($\delta^{13}\text{C} = -110\text{‰}$ to -60‰ and $\delta^2\text{H} = -250\text{‰}$ to -170‰) (McCalley et al., 2014).

The aim of our study was to combine emission measurements with dual stable isotope signatures to 1) investigate seasonal variations in wetland emission signatures, particularly $\delta^2\text{H}$, which is rarely measured; 2) investigate changes in underlying microbial processes, such as methane production and oxidation, in response to environmental drivers, inferred from isotope data and laboratory incubations. We hypothesised that 1) there would be a seasonal pattern in flux rates driven by changes in temperature, water levels, and season; 2) CH_4 production would be more temperature sensitive than CH_4 oxidation and $\delta^{13}\text{CH}_4$ and $\delta^2\text{H-CDH}_4$ would therefore be positively correlated with peat temperature; 3) Decreasing water table levels would increase CH_4 oxidation and lead to an enrichment in $\delta^{13}\text{CH}_4$ and $\delta^2\text{H-CDH}_4$ signatures.

4.3 Methods

4.3.1 Study area

The study was undertaken at a temperate ombrotrophic blanket peat bog in Northern England, UK (54°41'44.2"N, 2°23'16.5"W) within the Moor House National Nature reserve. An extensive amount of environmental data is available for the site (UK Environmental Change Network, data.ecn.ac.uk), and it has been shown to be an important source of CH_4 emissions in the UK (McNamara et al., 2008; Ward et al., 2013, 2007).

The mean annual temperature and precipitation are 5.8°C, and 2148 mm, respectively (UK Environmental Change Network). The study site is located on a level area on a hilltop at an elevation of 565 m. The vegetation community is classified as a *C. vulgaris*–*Eriophorum vaginatum* blanket mire, *Empetrum nigrum ssp. nigrum* sub-community M19b according to the UK National Vegetation Classification (NVC) (Rodwell, 1993). Plant species composition in the study plots was determined as approximate area of coverage according to the DAFOR scale (Hurford et al., 2006), see Table S 4.2.

4.3.2 Flux measurements

In June 2015 five locations were randomly selected from an area measuring around 100 m² as sampling plots. A 30 cm diameter 10 cm high gas sampling collar was permanently installed in each plot (1-5) to a depth of around 5 cm. Flux measurements were taken weekly from June 2015 to October 2016, after which flux measurements continued every two weeks until October 2017. Flux chamber measurements were conducted using a Los

Gatos Ultraportable Greenhouse Gas Analyzer (UGGA; Los Gatos Inc., San Jose, USA): Collars were sealed with opaque 19 L dome-shaped chambers and the CH₄ concentrations in the chamber were measured for a minimum of five minutes. Data was assessed according to the DEFRA SP1210 protocol (Evans et al., 2017) to ensure consistent treatment of data and exclusion of anomalous ebullition events. Flux rates were calculated from rate of CH₄ concentration change as described in McEwing et al. (2015) and based on a minimum of 30 s of continuous measurements.

4.3.3 Isotope measurements

Isotope samples were collected monthly from January 2016 to January 2017, with additional samples collected in September 2015, March 2017, and October 2017. At the end of the flux measurements, chambers were left on the collars for a total of 1 h to allow gas concentrations to build up to the necessary concentration for isotopic analysis. After 1 h, 20 mL samples of headspace gas were extracted with a syringe through septa in the chambers and filled into evacuated 12 mL Exetainer vials (Labco Ltd., Ceredigion, UK) for ¹³C/¹²C and ²H/¹H analysis. A further 10 mL gas were filled into 3 mL Exetainer vials for CO₂ and CH₄ concentration analysis. Syringes were purged with ambient air between each sample. Stable isotope analysis of CH₄ was performed at UC Davis stable isotope facility as described in Yarnes (2013). CH₄ concentrations were measured by gas chromatography using an Autosystem XL GC (Perkin Elmer, Waltham, MA, USA).

4.3.4 Soil moisture, water level, temperature, and water chemistry

Soil physical parameters were measured as part of a long-term monitoring programme (Centre for Ecology & Hydrology, 2018). Soil temperature was recorded using 108-LC temperature probes (Campbell Scientific, Loughborough, UK) at 30 cm depths in a topographically similar area around 20 m away from the flux chambers. Soil moisture at 18 cm depth was measured at the same location using a conductive soil moisture probe. Manual water table measurements were recorded at the time of the flux measurements. Samples for soil water dissolved organic carbon (DOC) and soil water colour were collected and analysed every two weeks. DOC concentration was measured by combustion, water colour by absorbance at wavelength 436 nm at CEH centralised analytical facility at Lancaster University.

4.3.5 Methane production and oxidation potential

To determine the CH₄ production and oxidation potential in the peat profile during the transition from non-growing to growing-season, laboratory incubations of peat cores collected monthly from March to September 2016 were performed: Three 100 cm cores were collected at each sampling event using a peat sampler. To reduce damage to the peat, each core was collected at 1 m distance from a central point and the sampling position rotated by 45° at each sampling event. Peat cores were divided into 10 cm segments, placed into self-seal bags and transported to the laboratory and stored at 4°C until incubation. Incubations were started within five days of sampling. Incubation experiments were conducted on core segments from seven depth intervals (0-10 cm, 10-20 cm, 20-30 cm, 30-40 cm, 50-60 cm, 70-80 cm, and 90-100 cm). Laboratory incubations to determine CH₄ production and oxidation potential were adapted from Sundh et al. (1995) and Kettunen et al. (1999). In brief, peat samples were homogenised and 25 g aliquots placed into 250 mL Kilner jars with septa in the lids and amended with 25 mL de-ionised water to achieve a slurry. Two sets of samples were prepared for CH₄ production and oxidation potential. For CH₄ production incubations, jars were flushed with N₂ gas for 120 s to remove oxygen and then immediately sealed and injected with 40 mL N₂ gas to obtain excess pressure to compensate for gas removed during headspace sampling. For CH₄ oxidation, incubation samples were treated similarly, but compressed air was used instead of N₂. In addition, oxidation samples were injected with 5 mL 100,000 ppm CH₄ gas (CK Special gases LTD, Leicestershire, England) to obtain an initial concentration of around 1600 ppm CH₄. During incubation, samples were stored on a rotary shaker at 20° in the dark. To assess the rate of change of CH₄ concentration, 5 mL headspace samples were collected at the start of the incubation and then at 1, 3, and 7 days using a syringe. Samples were transferred into evacuated 3 mL Exetainer vials and CH₄ concentrations measured by gas chromatography as above. Production and oxidation rates were calculated from linear regressions as described by Sundh et al. (1995).

4.3.6 Statistical analysis

Mean flux rates between sampling plots varied by up to three orders of magnitude. To make responses in flux rate comparable between plots, the standard scores of flux rates (i.e. the standard deviations from the mean of each measurement) for each plot were calculated.

To investigate seasonal variations across sampling plots and differences in emission fluxes between plots, non-parametric Friedman tests were used as the data violated the assumptions for one-way ANOVA with repeated measures. To determine differences between flux rates from individual plots, Fishers Least Significant Difference test was performed with Bonferroni correction on ranked data. For analysis of CH₄ production and oxidation potentials, one-way ANOVA followed by Tukey's HSD test was used. Where necessary, data were log-transformed to meet assumptions for ANOVA.

An exponential model was fitted for the relationship between standard scores of flux-rates and temperature. We used correlation tables to investigate the relationships between CH₄ fluxes and environmental variables. As several pairs of variables violated the assumptions of Pearson's correlation, Spearman's rank-correlations were used. A simple linear regression was fitted for the relationship between standard scores of flux-rates and soil moisture.

To determine isotope source signatures, Miller-Tans plots were used by plotting the product of CH₄ concentration and δ -value against CH₄ concentration and determining the source isotope signature from the slope of a regression (Miller and Tans, 2003). Compared to more commonly used Keeling plots these are insensitive to variations in background values over time. For the regression we used York's method to obtain unbiased estimates of the regression parameters that allow for errors in both variables and produce an uncertainty estimate that is based on the empirical instrument precision (Wehr and Saleska, 2017; York, 1969). All statistical analysis were performed in R version 3.5.1 (R Core Team, 2018) with the additional use of the *acricolae* (Mendiburu, 2017) and *IsoplotR* (Vermeesch, 2018) packages.

4.4 Results

4.4.1 Methane fluxes and environmental factors

Flux rates of CH₄ showed significant temporal variation over the seasons ($X^2(63)$, $p = 2.2 \times 10^{-16}$), with peak fluxes in all plots occurring between June and November. In 2016, fluxes from June to November were considerably higher than in the previous or following year with flux rates in all plots reaching values 2.5 to 8 standard deviations above their respective means in this year alone (Figure S 4.2). Flux rates also varied considerably across sampling plots, with values between -0.02 and 3.1 mg CH₄ m⁻² h⁻¹ observed in all plots in the winter

and spring, while fluxes above $10 \text{ mg CH}_4 \text{ m}^{-2} \text{ h}^{-1}$ were only observed in plots 1 and 5 during the summer and autumn (Figure 4.2). Plot 5 in particular showed fluxes of around 100 to $600 \text{ mg CH}_4 \text{ m}^{-2} \text{ h}^{-1}$ during several weeks in August and September 2016. Overall, however, plot 1 had the highest median fluxes of $1.5 \text{ mg CH}_4 \text{ m}^{-2} \text{ h}^{-1}$, followed by plot 4 with $0.60 \text{ mg CH}_4 \text{ m}^{-2} \text{ h}^{-1}$, and plots 2, 3, and 5 with 0.14, 0.24, and $0.35 \text{ mg CH}_4 \text{ m}^{-2} \text{ h}^{-1}$, respectively (Tukey HSD, $p < 0.05$, Figure 4.3).

Mean water table levels ranged from -19 cm in May 2016 to 7 cm in October 2017. Soil moisture at 18 cm depth was lowest at 91 % in September 2016, with maximum values of 97 % reached in winter periods.

Mean air temperatures for the three years were 5.8, 6.1, and $6.4 \text{ }^\circ\text{C}$, respectively, however, temperatures for both air and, in particular, soil were highest during the summer period of 2016 (Figure 4.4). When considering only the months of June-November with the highest flux rates, 2016 temperatures were slightly higher, while rainfall was considerably lower (Table S 4.1). However, the values were within the range of long-term observations at the site (Figure S 4.4).

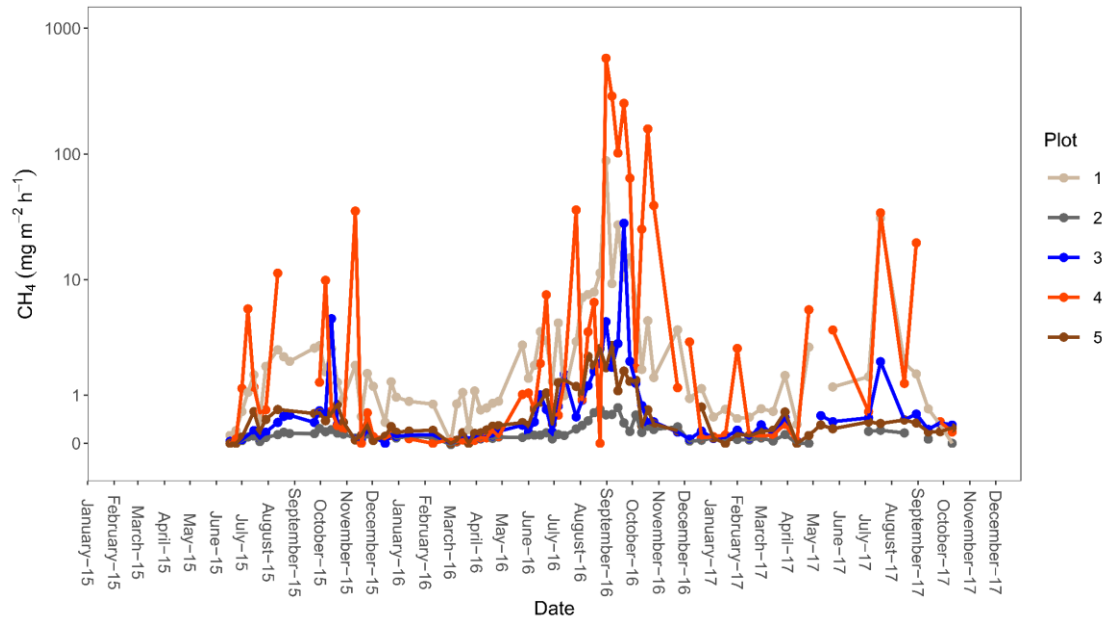


Figure 4.2 CH₄ flux rates from five sampling plots in an ombrotrophic peat bog.

Across all sampling points, 40% of the variation in CH₄ flux standard scores was explained by an exponential response to peat temperature at 30 cm (Figure 4.6). Water tables showed a unimodal relationship with CH₄ fluxes: emissions dropped when water tables were below around -7 cm and above 3 cm (Figure 4.7). Soil water colour showed a positive correlation with CH₄ flux and was highly correlated with soil temperature, while soil moisture showed a negative correlation and was also highly correlated with soil temperature (Table 4.1).

While mean air and soil temperatures in 2016 were only slightly higher than in the other two years, there are distinctly higher peak values in July to September 2016 (Figure 4.4). The combination of higher temperatures and low rainfall likely explain the lower levels of soil moisture and water levels in 2016, which in turn would affect the temperature regime of the peat.

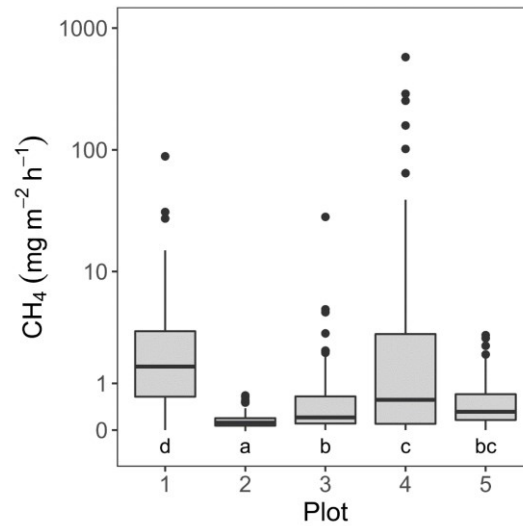


Figure 4.3 Box plot of CH₄ fluxes across five plots. Different letters below boxes indicate significantly different means at $p < 0.05$ (Tukey HSD) from the lowest mean (a) to the highest (d).

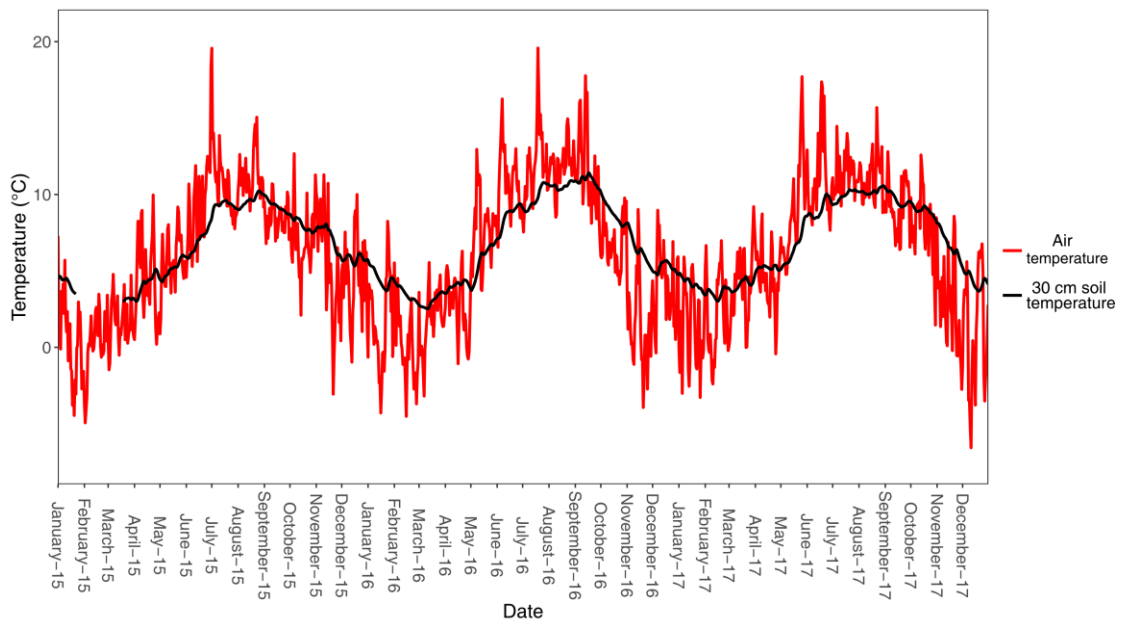


Figure 4.4 Mean air temperature and soil temperature at 30 cm depth. Soil temperature data missing from January 22 to March 18 2015 due to instrument failure.

Chapter 4: Large seasonal and interannual variations in methane emissions do not affect carbon and hydrogen isotopes from an ombrotrophic peat bog

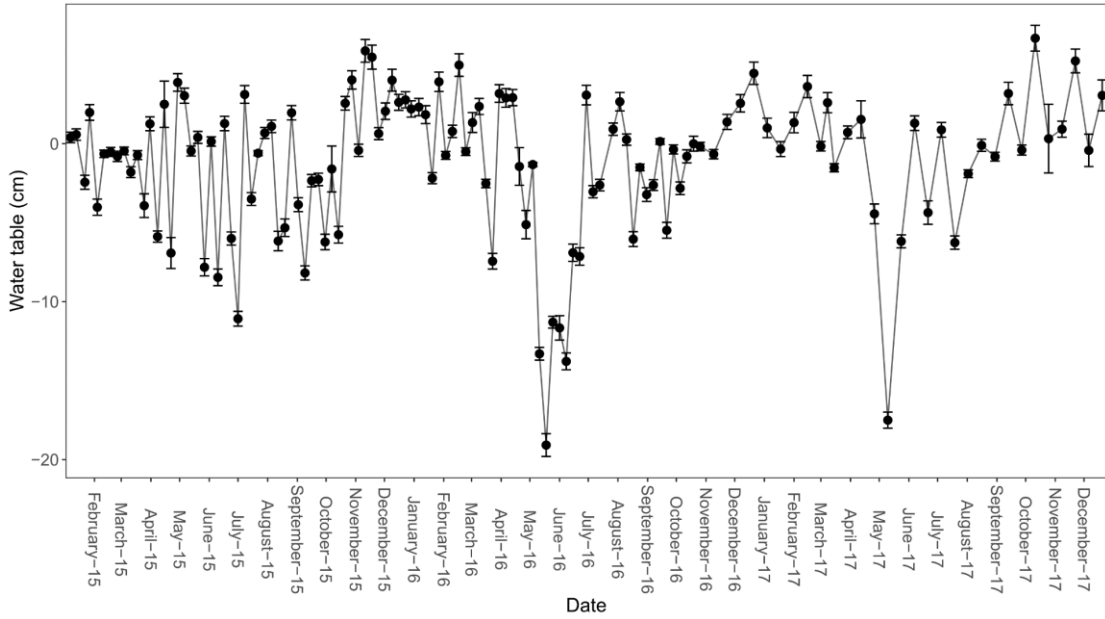


Figure 4.5 Mean water table levels from five dipwells located near the CH₄ flux sampling plots. Positive values indicate water levels above soil surface.

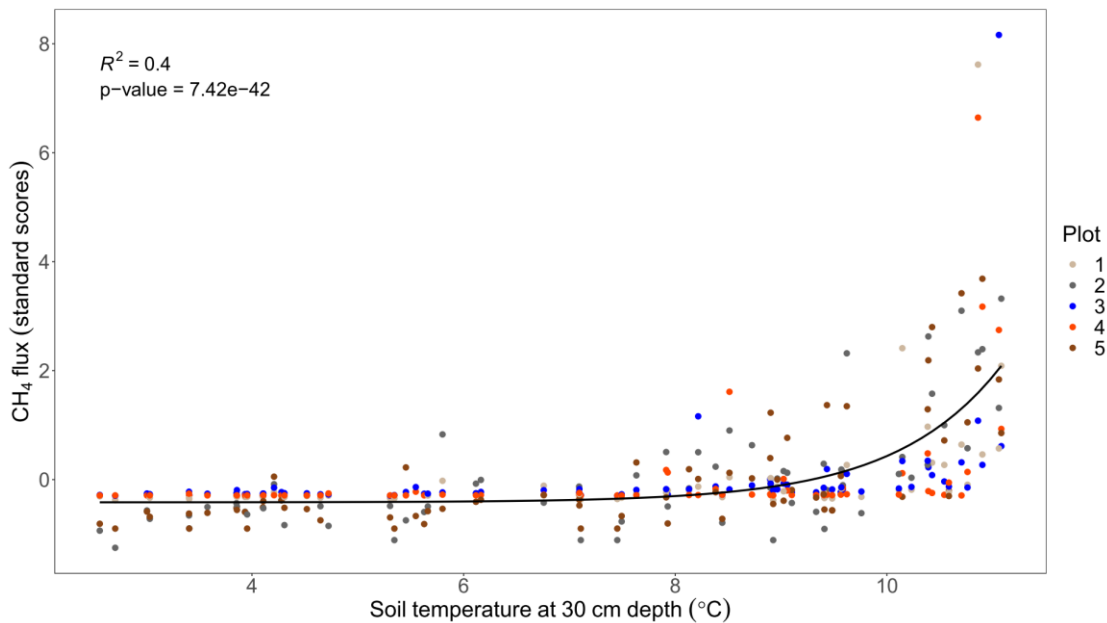


Figure 4.6 Relationship between CH₄ flux and soil temperature.

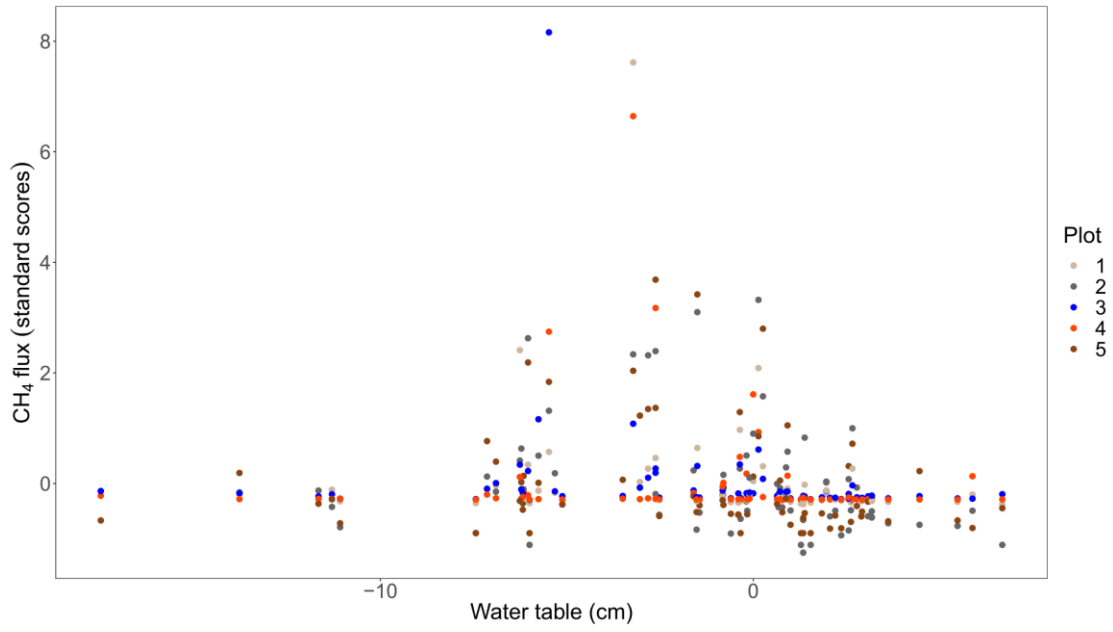


Figure 4.7 CH₄ flux rates and mean water table levels.

Table 4.1 Spearman rank correlations of CH₄ flux and soil parameters. * p < 0.05, ** p < 0.01, * p < 0.001, n.s. not significant, n.a. indicates non-monotonic relationships between variables.**

	CH ₄ flux	Soil temperature	Water table	Soil moisture	Soil water colour	Soil water DOC
CH ₄ flux						
Soil temperature	0.64***					
Water table	n.a.	n.a.				
Soil moisture	-0.52***	-0.96***	n.a.			
Soil water colour	0.68***	0.83***	-0.24***	-0.79***		
Soil water DOC	n.a.	0.41***	-0.21**	-0.3***	0.73***	
pH	n.a.	-0.32***	n.s.	0.31***	-0.63***	-0.56***

4.4.2 Isotope signatures

For both $\delta^{13}\text{C}$ and $\delta^2\text{H}$ measurements, the data fell on a single slope indicating that there were no variations in source signature across flux rates, seasons, or plots (Figure 4.8 & Figure 4.9). The source signatures for $\delta^{13}\text{C}$ and $\delta^2\text{H}$ were $-83.99 \pm 0.04 \text{ ‰ SE}$ and $-310.69 \pm 1.21 \text{ ‰}$, respectively. Removing data points that violated the regression assumption of normal distribution of residuals had a marginal influence on model parameters. The effects of plot, season and concentration range were investigated by subsetting the data. As no obvious trends were found, the analysis is presented from the whole data set.

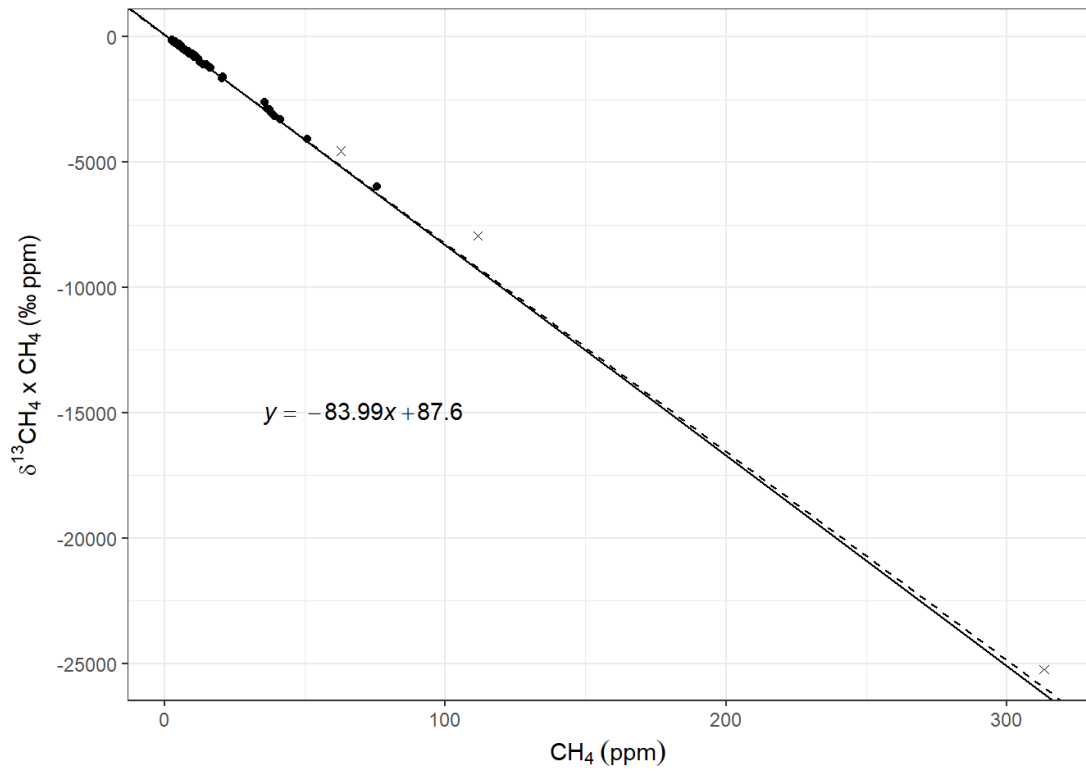


Figure 4.8 Miller-Tans plot showing the source signature of ¹³CH₄ in an ombrotrophic peat bog from 2015 to 2017. The source signature is the slope of a York-regression (n = 77). Three data points marked with x were excluded because of non-normality of residuals. Dashed line shows model with all data points included.

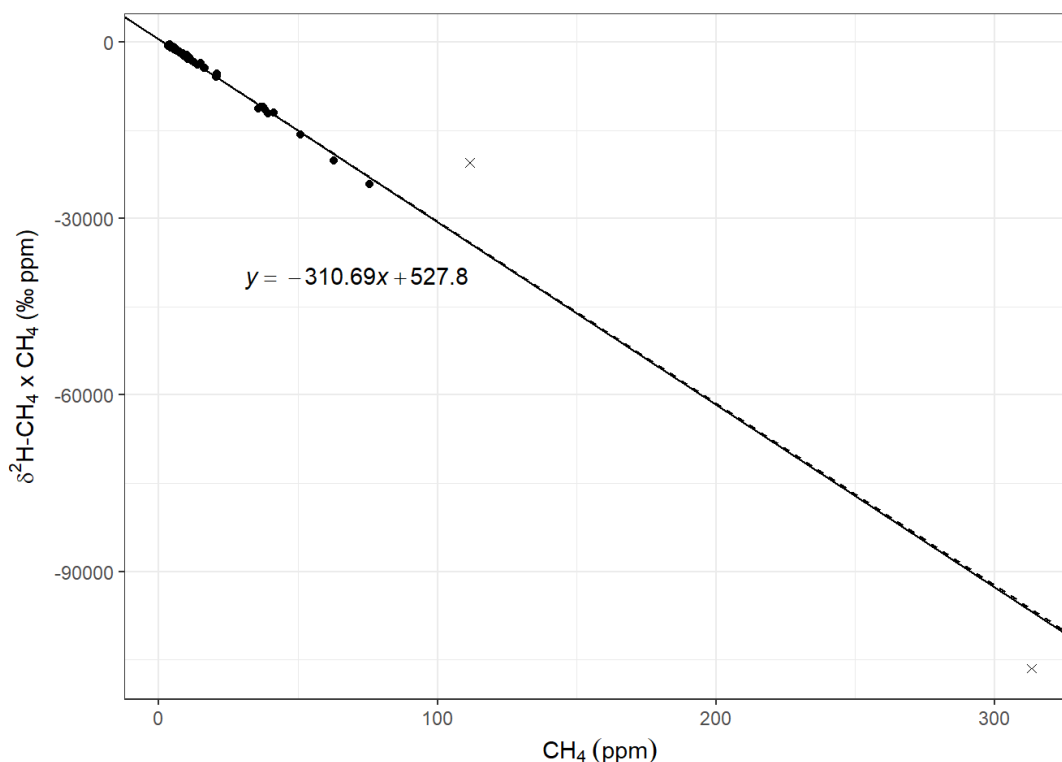


Figure 4.9 Miller-Tans plot showing the source signature of ²H-CH₄ in an ombrotrophic peat bog from 2015 to 2017. The source signature is the slope of a York-regression (n = 60). Two data points marked with x were excluded because of non-normality of residuals. Dashed line shows model with all data points included.

4.4.3 Peat incubations

Potential production rates of CH₄ were variable, ranging from 0.0 μg CH₄ m⁻² h⁻¹ to 5.2 μg CH₄ m⁻² h⁻¹. Rates varied over the seven months period, with rates in April significantly higher than those in other months, except for March and September (Tukey HSD, p < 0.05, Figure 4.10). When standardising measurements across sampling times by calculating standard scores, flux rates were seen to be significantly higher at 30-40 cm depth compared to other depths, except for 90-100 cm (Tukey HSD, p < 0.05, Figure S 4.3). Oxidation potentials did not significantly change throughout the study period but decreased significantly within the peat profile.

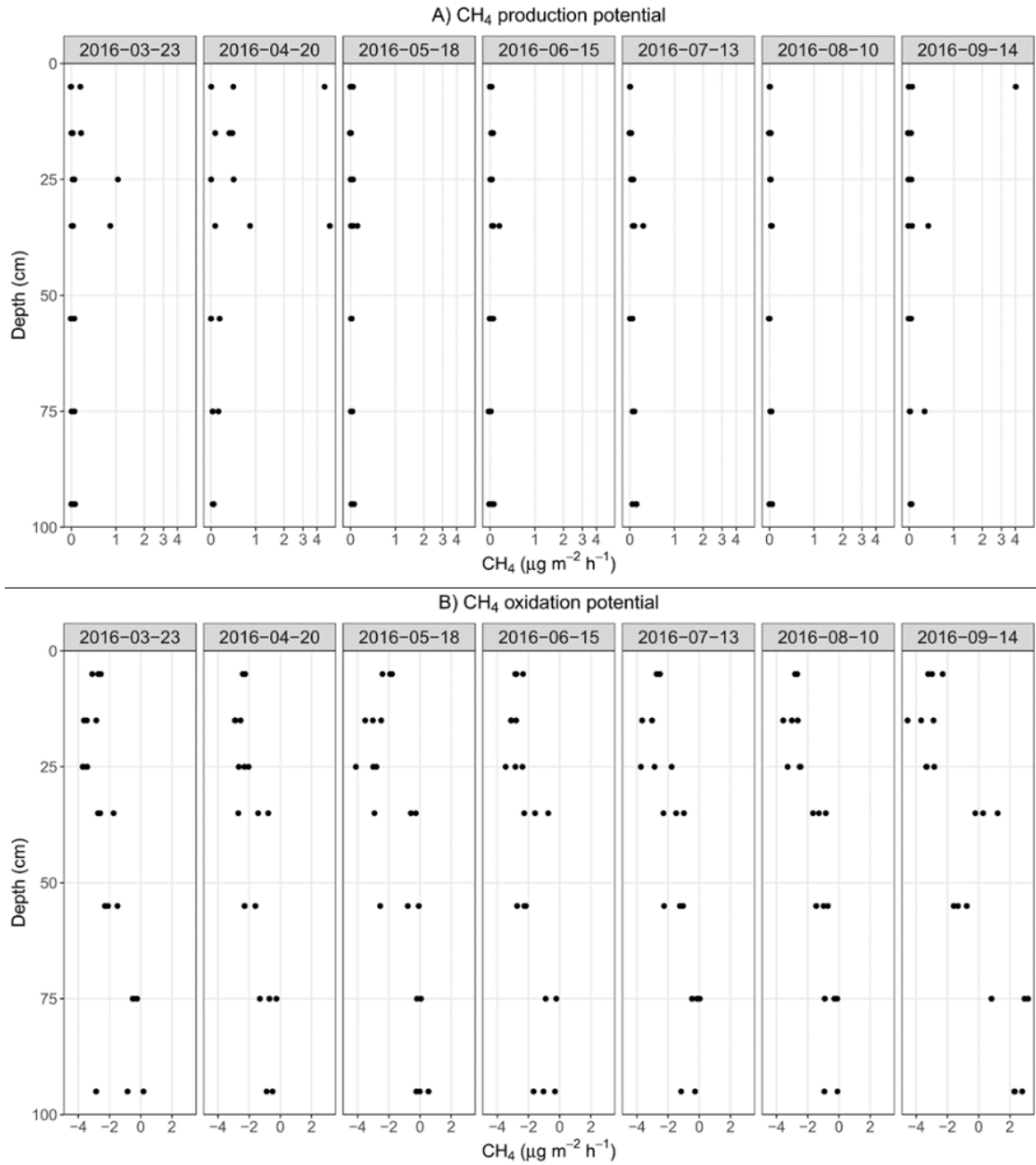


Figure 4.10 Potential CH₄ A) production and B) oxidation within the peat profile of three replicate peat cores. Sampling dates of peat cores shown at top of panels. Note that flux rates for A) are plotted on an inverse hyperbolic sine scale for comparability. Negative fluxes indicate CH₄ oxidation, positive fluxes CH₄ production.

4.5 Discussion

It is well understood that environmental factors influence CH₄ fluxes in peatlands. We hypothesised that both CH₄ emissions and their dual-isotope signatures would vary seasonally in response to changes in temperature and hydrology of the peat affecting microbial processes. Our flux and isotope measurements, collected over a 28 months period, showed that while there was high variability in fluxes between seasons and years, isotope signatures remained notably stable for both $\delta^{13}\text{C}$ and $\delta^2\text{H}$.

4.5.1 Fluxes and environmental drivers

We hypothesised that fluxes would vary seasonally with both temperature and water table levels. We found a significant non-linear relationship between CH₄ fluxes and temperature, as well as a correlation between CH₄ fluxes and soil moisture and soil water colour (Figure 4.6, Table 4.1). Our sampling covered a period of unusually high fluxes in 2016, with peak emissions around one order of magnitude above those of the years 2015 and 2017. Values of around 100 to 600 mg m⁻² h⁻¹ were recorded, which is in the top range of peatland emissions reported in the literature for temperate peatlands (e.g. Turetsky et al., 2014) and considerably higher than what has previously been found in UK peatlands (Levy et al., 2012). While highly unusual, similarly high fluxes have been found in other UK peatlands in 2016 (A Heinemeyer, 2018, personal communication, 2 July). An important driver behind the increased fluxes was likely the higher temperatures observed during the 2016 summer (Figure 4.4 & Figure 4.6). Temperature is well known to drive wetland CH₄ emissions (Yvon-Durocher et al., 2014) and increases in emission have previously been observed at a nearby site in response to increases in air and soil temperatures (Ward et al., 2013, 2007).

Water table levels are known to be an important determinant of CH₄ fluxes in peatlands (Dinsmore et al., 2009; Limpens et al., 2008; Updegraff et al., 2001). However, unlike often previously reported, we did not find a monotonic relationship between water tables and CH₄ fluxes. Instead, there appears to be an optimum range between -7 cm and 3 cm (Figure 4.7). A drop in CH₄ emissions during water table drawdown is possibly related to a reduction in the anoxic peat layer (Limpens et al., 2008). Strack et al. (2004) suggest that a reduction in CH₄ fluxes during conditions of standing water are likely related to a decrease in substrate availability due to reduced plant inputs, as well as changes in soil temperature. While total rainfall in 2016 was lower than in the other years, water tables never fell below

20 cm. In combination with higher temperatures, this may have led to higher microbial activity while keeping water levels in the range necessary for anaerobic decomposition. The correlation with soil water colour is ambiguous, as increases in soil water colour, resulting from the release of tannins during decomposition, may be a result of increased decomposer activity, which also drives methanogenesis, rather than a direct cause of increased methanogenesis.

Temperature and hydrology have likely contributed to the unusually high fluxes in 2016, however, meteorological measurements at the study site have been recorded since 1992 and mean 2016 temperatures of 6.08°C were not unusual compared to the long-term average of 5.94°C. Considering only the period from June to November of each year, where CH₄ emissions were consistently above the mean flux value, 2016 was dryer and warmer than the other sampling years, but within the range of values observed since 1992 (Figure S 4.4). Therefore, factors not investigated in this study may have contributed to the unusually high fluxes observed in our study and possibly other UK peatlands.

There was a high degree of variability in CH₄ fluxes between plots, particularly during the summer and autumn where fluxes varied by two orders of magnitude between plots (Figure 4.2). Median values across the sampling period were significantly different from each other but remained in a similar range (Figure 4.3) and within the range of values reported in the literature. Part of this variability may be due to the difference in vegetation in individual plots. Plots 1 and 4 consistently showed the highest fluxes and were the only ones with a high abundance of graminoids, notably the sedge *Eriophorum vaginatum* (Table S 4.2), which are known to correlate with higher levels of CH₄ fluxes (Gray et al., 2013; Limpens et al., 2008; Ward et al., 2013). Sedges can affect the release of CH₄ both by providing substrates to methanogens through root exudates and, more importantly, by mediating the transport of CH₄ through aerenchyma, bypassing the oxic peat layer (Green and Baird, 2012; Greenup et al., 2000).

The laboratory peat incubations revealed no clear seasonal pattern in CH₄ production potentials, although highest rates were observed in April, while oxidation potentials remained similar throughout the study period (Figure 4.10). However, across all incubations, production potentials were highest between 30-40 cm depth, while oxidation potentials decreased with depth (Figure S 4.3). While care has to be taken when extrapolating from such incubation experiments to field conditions, the results do suggest

that water table levels remained consistently above the main zone of methanogenesis in the peat profile.

The annual period of elevated CH₄ emissions during the study period lasted from around June to November each year, and therefore starts later than and extends beyond the annual summer or growing season (Figure S 4.2). The reason may be that CH₄ fluxes may be more dependent on soil temperatures, rather than air temperature or solar radiation, which affect plant productivity. There is a lag between air and soil temperatures (Figure 4.4), which increases with soil depth (Dawson and Fisher, 1964). Since CH₄ production at our study site mainly occurred at depth below 30 cm, this likely explains why seasonal variations in flux rates show a lag relative to meteorological conditions above ground.

4.5.2 Isotope signatures

We expected to find seasonal variations in stable isotope emission signatures of CH₄ which are the result of biological and physical processes interacting during formation and release: fractionation during acetoclastic or hydrogenotrophic methanogenesis leading to differential depletion in $\delta^{13}\text{C}$ and $\delta^2\text{H}$, fractionation during microbial oxidation leading to an enrichment in isotope signatures, and transport through aerenchyma which leads to a depletion in isotope signatures. The balance between production and oxidation in particular can be affected by factors such as temperature, substrate availability, and seasonal changes in plant mediated pathways (Le Mer and Roger, 2001). However, even though emissions varied by as much as two orders of magnitude across the sampling period and between sampling plots, isotopic signatures of $\delta^{13}\text{C}$ and $\delta^2\text{H}$ were notably consistent across all samples (Figure 4.8 & Figure 4.9). Moreover, the observed $\delta^{13}\text{C}$ source signature of -84.1 ‰ is considerably lower than the range of -48 ‰ to -70 ‰ often reported in the literature for wetland ecosystems (Sherwood et al., 2017). However, using continuous measurements with a quantum cascade laser spectrometer, McCalley et al. (2014) found average $\delta^{13}\text{C}$ values of -79.6 ‰ in a *Sphagnum* dominated Swedish mire due to hydrogenotrophic methanogenesis. Bowes and Hornibrook (2006) have found $\delta^{13}\text{C}$ values of -90 ‰ to 81.5 ‰ in a UK upland peatbog with comparable vegetation to Moor House, but did not find differences between vegetation types and flux rates. Fisher et al. (2017) have reported values as low as -112 ‰ for individual chamber measurements, while mean signature derived from diel sampling of ambient air revealed an integrated signature of -69.2 ‰. Data on $\delta^2\text{H}$ is more limited, but the observed signature of -310.8 ‰ is close to

the median value of -310 ‰ reported for a range of previous studies (Sherwood et al., 2017).

In peatlands, CH₄ production is considered to be predominantly the result of acetoclastic methanogenesis, contributing around two thirds of total emissions (Kotsyurbenko et al., 2004), with the proportion of hydrogenotrophic methanogenesis increasing with peat depth (Flanagan et al., 2005; Popp et al., 1999). While both pathways can produce a range of isotope signatures, our results suggest that there may be a higher contribution of hydrogenotrophic methanogenesis than is generally assumed for peatlands (Whiticar, 1999).

The lack of seasonal variation and low $\delta^{13}\text{C}$ signature might be indicative of low and stable methane oxidation in peat. The CH₄ oxidation potential in the peat incubations was found to be consistent across the seven-month experiment (Figure 4.10) under laboratory conditions. In the field, rates of methanotrophy are often closely correlated with CH₄ production (Limpens et al., 2008). This could indicate that while the methanotroph community in the peat profile may remain stable over time, their activity will be determined by substrate availability, consuming a constant fraction of produced CH₄.

It should be noted that the stable isotope signatures obtained by a set of chamber measurements are not necessarily representative of the total emissions of the ecosystem. Peatlands are heterogeneous systems, and emission signatures can vary not just over time but also with location. For example, Fisher et al. (2017) found differences of up to 64 ‰ $\delta^{13}\text{C}$ between chamber measurements from the same Swedish mire ecosystem. The consistency of the isotopic signatures in our study over time and large variations in emission rates suggests that, for the studied ecosystem, they are likely representative of more than just the immediate sampling site. However, future research could include integrated sampling techniques to put individual chamber measurements into the context of whole ecosystem emissions.

4.5.3 Conclusions

We have found CH₄ emissions in a temperate ombrotrophic peat bog to be highly variable, with unusually high fluxes in the summer and autumn of 2016. Such extreme events are difficult to capture in short term or infrequent sampling campaigns but understanding their causes may be important for predicting the response of peatlands to changing

environmental conditions and the large variation in annual wetland methane budgets. Long term measurement campaigns that can capture such rare events are therefore critical for understanding what are likely non-linear responses in peatland ecosystems and how they may relate to climate change. Unlike previous studies, we have found $\delta^{13}\text{C}$ and $\delta^2\text{H}$ isotope signatures to be unchanging over time and between sampling plots, despite high variations in flux rates over time and between sampling plots. In addition, heavily depleted $\delta^{13}\text{C}$ signatures suggest a high contribution of hydrogenotrophic methanogenesis, which are uncharacteristic for peatlands. The values and seasonal changes in wetland emission signatures have important consequences for atmospheric inversion models that use stable isotopes to constrain emission sources. Models generally assume constant emission signatures, both in time and space. The high variability in stable isotope signatures between study sites, as well as observed latitudinal trends (Feinberg et al., 2018) highlight the need to extend existing stable isotope databases, such as Sherwood et al. (2017), with regional data to improve model estimates.

4.6 References

- Basiliko, N., Blodau, C., Roehm, C., Bengtson, P., Moore, T.R., 2007. Regulation of decomposition and methane dynamics across natural, commercially mined, and restored northern peatlands. *Ecosystems* 10, 1148–1165. <https://doi.org/10.1007/s10021-007-9083-2>
- Bergamaschi, P., 1997. Seasonal variations of stable hydrogen and carbon isotope ratios in methane from a Chinese rice paddy. *J. Geophys. Res. Atmos.* 102, 25383–25393. <https://doi.org/10.1029/97JD01664>
- Bowes, H.L., Hornibrook, E.R.C., 2006. Emission of highly¹³C-depleted methane from an upland blanket mire. *Geophys. Res. Lett.* 33, 11–14. <https://doi.org/10.1029/2005GL025209>
- Bridgham, S.D., Cadillo-Quiroz, H., Keller, J.K., Zhuang, Q., 2013. Methane emissions from wetlands: biogeochemical, microbial, and modeling perspectives from local to global scales. *Glob. Chang. Biol.* 19, 1325–1346. <https://doi.org/10.1111/gcb.12131>
- Centre for Ecology & Hydrology, 2018. UK Environmental Change Network [WWW Document]. URL <http://www.ecn.ac.uk> (accessed 8.21.18).
- Chanton, J., Liptay, K., 2000. Seasonal variation in methane oxidation in a landfill cover soil as determined by an in situ stable isotope technique. *Global Biogeochem. Cycles* 14, 51–60. <https://doi.org/10.1029/1999GB900087>
- Chanton, J.P., 2005. The effect of gas transport on the isotope signature of methane in wetlands. *Org. Geochem.* 36, 753–768. <https://doi.org/10.1016/j.orggeochem.2004.10.007>
- Chowdhury, T.R., Dick, R.P., 2013. Ecology of aerobic methanotrophs in controlling methane fluxes from wetlands. *Appl. Soil Ecol.* 65, 8–22. <https://doi.org/10.1016/j.apsoil.2012.12.014>
- Dawson, G.B., Fisher, R.G., 1964. Diurnal and seasonal ground temperature variations at Wairakei. *New Zeal. J. Geol. Geophys.* 7, 144–154. <https://doi.org/10.1080/00288306.1964.10420166>
- Dean, J.F., Middelburg, J.J., Röckmann, T., Aerts, R., Blauw, L.G., Egger, M., Jetten, M.S.M., de Jong, A.E.E., Meisel, O.H., Rasigraf, O., Slomp, C.P., in't Zandt, M.H., Dolman, A.J., 2018. Methane Feedbacks to the Global Climate System in a Warmer World. *Rev. Geophys.* 56, 207–250. <https://doi.org/10.1002/2017RG000559>
- Deng, J., McCalley, C.K., Frohling, S., Chanton, J., Crill, P., Varner, R., Tyson, G., Rich, V., Hines, M., Saleska, S.R., Li, C., 2017. Adding stable carbon isotopes improves model representation of the role of microbial communities in peatland methane

- cycling. *J. Adv. Model. Earth Syst.* 9, 1412–1430.
<https://doi.org/10.1002/2016MS000817>
- Dinsmore, K.J., Skiba, U.M., Billett, M.F., Rees, R.M., Drewer, J., 2009. Spatial and temporal variability in CH₄ and N₂O fluxes from a Scottish ombrotrophic peatland: Implications for modelling and up-scaling. *Soil Biol. Biochem.* 41, 1315–1323.
<https://doi.org/10.1016/j.soilbio.2009.03.022>
- Dlugokencky, E.J., Nisbet, E.G., Fisher, R., Lowry, D., 2011. Global atmospheric methane: budget, changes and dangers. *Philos. Trans. R. Soc. A Math. Phys. Eng. Sci.* 369, 2058–2072. <https://doi.org/10.1098/rsta.2010.0341>
- Evans, C., Morrison, R., Burden, A., Williamson, J., Baird, A., Brown, E., Callaghan, N., Chapman, P., Cumming, A., Dean, H., Dixon, S., Dooling, G., Evans, J., Gauci, V., Grayson, R., Haddaway, N., He, Y., Heppel, K., Holden, J., Hughes, S., Kaduk, J., Jones, D., Matthews, R., Menichino, N., Misselbrook, T., Page, S., Pan, G., Peakock, M., Rayment, M., Ridley, L., Robinson, I., Rylett, D., Scowen, M., Stanley, K., Worrall, F., 2017. Final report on project SP1210: Lowland peatland systems in England and Wales – evaluating greenhouse gas fluxes and carbon balances.
- Feinberg, A.I., Coulon, A., Stenke, A., Schwietzke, S., Peter, T., 2018. Isotopic source signatures: Impact of regional variability on the $\delta^{13}\text{C}_{\text{CH}_4}$ trend and spatial distribution. *Atmos. Environ.* 174, 99–111.
<https://doi.org/10.1016/j.atmosenv.2017.11.037>
- Fisher, R.E., France, J.L., Lowry, D., Lanoisellé, M., Brownlow, R., Pyle, J.A., Cain, M., Warwick, N., Skiba, U.M., Drewer, J., Dinsmore, K.J., Leeson, S.R., Bauguitte, S.J., Wellpott, A., Shea, S.J.O., Allen, G., Gallagher, M.W., Pitt, J., Percival, C.J., Bower, K., George, C., Hayman, G.D., Aalto, T., Lohila, A., Aurela, M., Laurila, T., Crill, P.M., McCalley, C.K., Nisbet, E.G., 2017. Measurement of the ¹³C isotopic signature of methane emissions from northern European wetlands. *Global Biogeochem. Cycles* 31, 605–623. <https://doi.org/10.1002/2016GB005504>
- Flanagan, L.B., Ehleringer, J.R., Pataki, D.E., Chanton, J., Chaser, L., Glasser, P., Siegel, D., 2005. Carbon and Hydrogen Isotopic Effects on Microbial Methane from Terrestrial Environments, in: *Stable Isotopes and Biosphere Atmosphere Interactions*. Elsevier, pp. 85–105. <https://doi.org/10.1016/B978-012088447-6/50006-4>
- Gray, A., Levy, P.E., Cooper, M.D.A., Jones, T., Gaiawyn, J., Leeson, S.R., Ward, S.E., Dinsmore, K.J., Drewer, J., Sheppard, L.J., Ostle, N.J., Evans, C.D., Burden, A., Zieliński, P., 2013. Methane indicator values for peatlands: a comparison of species and functional groups. *Glob. Chang. Biol.* 19, 1141–1150.
<https://doi.org/10.1111/gcb.12120>
- Green, S.M., Baird, A.J., 2012. A mesocosm study of the role of the sedge *Eriophorum*

- angustifolium in the efflux of methane—including that due to episodic ebullition—from peatlands. *Plant Soil* 351, 207–218. <https://doi.org/10.1007/s11104-011-0945-1>
- Greenup, A. L., Bradford, M. A., Mcnamara, N.P., Ineson, P., Lee, J. A., 2000. The role of *Eriophorum vaginatum* in CH₄ flux from an ombrotrophic peatland. *Plant Soil* 227, 265–272. <https://doi.org/10.1023/A:1026573727311>
- Hurford, C., Rowell, T., Allen, D., Brown, A., 2006. *Monitoring Nature Conservation in Cultural Habitats*. Springer Netherlands, Dordrecht, The Netherlands. <https://doi.org/10.1007/1-4020-3757-0>
- Kettunen, A., Kaitala, V., Lehtinen, A., Lohila, A., Alm, J., Silvola, J., Martikainen, P.J., 1999. Methane production and oxidation potentials in relation to water table fluctuations in two boreal mires. *Soil Biol. Biochem.* 31, 1741–1749. [https://doi.org/10.1016/S0038-0717\(99\)00093-0](https://doi.org/10.1016/S0038-0717(99)00093-0)
- Kirschke, S., Bousquet, P., Ciais, P., Saunio, M., Canadell, J.G., Dlugokencky, E.J., Bergamaschi, P., Bergmann, D., Blake, D.R., Bruhwiler, L., Cameron-Smith, P., Castaldi, S., Chevallier, F., Feng, L., Fraser, A., Heimann, M., Hodson, E.L., Houweling, S., Josse, B., Fraser, P.J., Krummel, P.B., Lamarque, J.-F., Langenfelds, R.L., Le Quéré, C., Naik, V., O'Doherty, S., Palmer, P.I., Pison, I., Plummer, D., Poulter, B., Prinn, R.G., Rigby, M., Ringeval, B., Santini, M., Schmidt, M., Shindell, D.T., Simpson, I.J., Spahni, R., Steele, L.P., Strode, S. A., Sudo, K., Szopa, S., van der Werf, G.R., Voulgarakis, A., van Weele, M., Weiss, R.F., Williams, J.E., Zeng, G., 2013. Three decades of global methane sources and sinks. *Nat. Geosci.* 6, 813–823. <https://doi.org/10.1038/ngeo1955>
- Kotsyurbenko, O.R., Chin, K.J., Glagolev, M. V., Stubner, S., Simankova, M. V., Nozhevnikova, A.N., Conrad, R., 2004. Acetoclastic and hydrogenotrophic methane production and methanogenic populations in an acidic West-Siberian peat bog. *Environ. Microbiol.* 6, 1159–1173. <https://doi.org/10.1111/j.1462-2920.2004.00634.x>
- Kuhlmann, A.J., Worthy, D.E.J., Trivett, N.B.A., Levin, I., 1998. Methane emissions from a wetland region within the Hudson Bay Lowland: An atmospheric approach. *J. Geophys. Res. Atmos.* 103, 16009–16016. <https://doi.org/10.1029/98JD01024>
- Lai, D.Y.F., 2009. Methane Dynamics in Northern Peatlands : A Review. *Pedosphere* 19, 409–421. [https://doi.org/10.1016/S1002-0160\(09\)00003-4](https://doi.org/10.1016/S1002-0160(09)00003-4)
- Le Mer, J., Roger, P., 2001. Production, oxidation, emission and consumption of methane by soils: A review. *Eur. J. Soil Biol.* 37, 25–50. [https://doi.org/10.1016/S1164-5563\(01\)01067-6](https://doi.org/10.1016/S1164-5563(01)01067-6)
- Levin, I., Bergamaschi, P., Dörr, H., Trapp, D., 1993. Stable isotopic signature of methane from major sources in Germany. *Chemosphere* 26, 161–177.

[https://doi.org/10.1016/0045-6535\(93\)90419-6](https://doi.org/10.1016/0045-6535(93)90419-6)

- Levy, P.E., Burden, A., Cooper, M.D.A., Dinsmore, K.J., Drewer, J., Evans, C., Fowler, D., Gaiawyn, J., Gray, A., Jones, S.K., Jones, T., McNamara, N.P., Mills, R., Ostle, N., Sheppard, L.J., Skiba, U., Sowerby, A., Ward, S.E., Ziełiński, P., 2012. Methane emissions from soils: synthesis and analysis of a large UK data set. *Glob. Chang. Biol.* 18, 1657–1669. <https://doi.org/10.1111/j.1365-2486.2011.02616.x>
- Limpens, J., Berendse, F., Blodau, C., Canadell, J.G., Freeman, C., Holden, J., Roulet, N., Rydin, H., Schaepman-Strub, G., 2008. Peatlands and the carbon cycle: from local processes to global implications - a synthesis. *Biogeosciences* 5, 1475–1491. <https://doi.org/10.5194/bgd-5-1379-2008>
- McCalley, C.K., Woodcroft, B.J., Hodgkins, S.B., Wehr, R. A., Kim, E.-H., Mondav, R., Crill, P.M., Chanton, J.P., Rich, V.I., Tyson, G.W., Saleska, S.R., 2014. Methane dynamics regulated by microbial community response to permafrost thaw. *Nature* 514, 478–481. <https://doi.org/10.1038/nature13798>
- McEwing, K.R., Fisher, J.P., Zona, D., 2015. Environmental and vegetation controls on the spatial variability of CH₄ emission from wet-sedge and tussock tundra ecosystems in the Arctic. *Plant Soil* 388, 37–52. <https://doi.org/10.1007/s11104-014-2377-1>
- McNamara, N.P., Plant, T., Oakley, S., Ward, S.E., Wood, C., Ostle, N., 2008. Gully hotspot contribution to landscape methane (CH₄) and carbon dioxide (CO₂) fluxes in a northern peatland. *Sci. Total Environ.* 404, 354–360. <https://doi.org/10.1016/j.scitotenv.2008.03.015>
- Melton, J.R., Wania, R., Hodson, E.L., Poulter, B., Ringeval, B., Spahni, R., Bohn, T., Avis, C.A., Chen, G., Eliseev, A. V., Hopcroft, P.O., Riley, W.J., Subin, Z.M., Tian, H., van Bodegom, P.M., Kleinen, T., Yu, Z.C., Singarayer, J.S., Zürcher, S., Lettenmaier, D.P., Beerling, D.J., Denisov, S.N., Prigent, C., Papa, F., Kaplan, J.O., 2013. Present state of global wetland extent and wetland methane modelling: methodology of a model inter-comparison project (WETCHIMP). *Geosci. Model Dev.* 6, 617–641. <https://doi.org/10.5194/gmd-6-617-2013>
- Mendiburu, F. De, 2017. Package ‘agricolae.’
- Miller, J.B., Tans, P.P., 2003. Calculating isotopic fractionation from atmospheric measurements at various scales. *Tellus, Ser. B Chem. Phys. Meteorol.* 55, 207–214. <https://doi.org/10.1034/j.1600-0889.2003.00020.x>
- Popp, T.J., Chanton, J.P., Whiting, G.J., Grant, N., 1999. Methane stable isotope distribution at a Carex dominated fen in north central Alberta. *Global Biogeochem. Cycles* 13, 1063–1077. <https://doi.org/10.1029/1999GB900060>
- Rao, D.K., Bhattacharya, S.K., Jani, R.A., 2008. Seasonal variations of carbon isotopic

- composition of methane from Indian paddy fields. *Global Biogeochem. Cycles* 22, n/a-n/a. <https://doi.org/10.1029/2006GB002917>
- Rodwell, J.S., 1993. *British Plant Communities, Vol. 2, Mires and Heaths*. Cambridge University Press. <https://doi.org/10.2307/2261244>
- Saunois, M., Bousquet, P., Poulter, B., Peregon, A., Ciais, P., Canadell, J.G., Dlugokencky, E.J., Etiope, G., Bastviken, D., Houweling, S., Janssens-Maenhout, G., Tubiello, F.N., Castaldi, S., Jackson, R.B., Alexe, M., Arora, V.K., Beerling, D.J., Bergamaschi, P., Blake, D.R., Brailsford, G., Brovkin, V., Bruhwiler, L., Crevoisier, C., Crill, P., Covey, K., Curry, C., Frankenberg, C., Gedney, N., Höglund-Isaksson, L., Ishizawa, M., Ito, A., Joos, F., Kim, H.S., Kleinen, T., Krummel, P., Lamarque, J.F., Langenfelds, R., Locatelli, R., Machida, T., Maksyutov, S., McDonald, K.C., Marshall, J., Melton, J.R., Morino, I., Naik, V., O'Doherty, S., Parmentier, F.J.W., Patra, P.K., Peng, C., Peng, S., Peters, G.P., Pison, I., Prigent, C., Prinn, R., Ramonet, M., Riley, W.J., Saito, M., Santini, M., Schroeder, R., Simpson, I.J., Spahni, R., Steele, P., Takizawa, A., Thornton, B.F., Tian, H., Tohjima, Y., Viovy, N., Voulgarakis, A., Van Weele, M., Van Der Werf, G.R., Weiss, R., Wiedinmyer, C., Wilton, D.J., Wiltshire, A., Worthy, D., Wunch, D., Xu, X., Yoshida, Y., Zhang, B., Zhang, Z., Zhu, Q., 2016. The global methane budget 2000-2012. *Earth Syst. Sci. Data* 8, 697–751. <https://doi.org/10.5194/essd-8-697-2016>
- Sherwood, O.A., Schwietzke, S., Arling, V.A., Etiope, G., 2017. Global inventory of gas geochemistry data from fossil fuel, microbial and burning sources, version 2017. *Earth Syst. Sci. Data* 9, 639–656. <https://doi.org/10.5194/essd-9-639-2017>
- Smith, K. A., Ball, T., Conen, F., Dobbie, K.E., Massheder, J., Rey, A., 2003. Exchange of greenhouse gases between soil and atmosphere: interactions of soil physical factors and biological processes. *Eur. J. Soil Sci.* 54, 779–791. <https://doi.org/10.1046/j.1365-2389.2003.00567.x>
- Sriskantharajah, S., Fisher, R.E., Lowry, D., Aalto, T., Hatakka, J., Aurela, M., Laurila, T., Lohila, A., Kuitunen, E., Nisbet, E.G., 2012. Stable carbon isotope signatures of methane from a Finnish subarctic wetland. *Tellus B* 64, 1–8. <https://doi.org/10.3402/tellusb.v64i0.18818>
- Strack, M., Waddington, J.M., Tuittila, E.-S., 2004. Effect of water table drawdown on northern peatland methane dynamics: Implications for climate change. *Global Biogeochem. Cycles* 18, n/a-n/a. <https://doi.org/10.1029/2003GB002209>
- Sundh, I., Mikkela, C., Nilsson, M., Svensson, B.H., 1995. Potential aerobic methane oxidation in a sphagnum-dominated peatland - controlling factors and relation to methane emission. *Soil Biol. Biochem.* 27, 829–837. [https://doi.org/10.1016/0038-0717\(94\)00222-M](https://doi.org/10.1016/0038-0717(94)00222-M)
- Treat, C.C., Bloom, A.A., Marushchak, M.E., 2018. Nongrowing season methane emissions-a significant component of annual emissions across northern ecosystems.

Glob. Chang. Biol. 24, 3331–3343. <https://doi.org/10.1111/gcb.14137>

Turetsky, M.R., Kotowska, A., Bubier, J., Dise, N.B., Crill, P., Hornibrook, E.R.C., Minkinen, K., Moore, T.R., Myers-Smith, I.H., Nykänen, H., Olefeldt, D., Rinne, J., Saarnio, S., Shurpali, N., Tuittila, E.-S., Waddington, J.M., White, J.R., Wickland, K.P., Wilmking, M., 2014. A synthesis of methane emissions from 71 northern, temperate, and subtropical wetlands. *Glob. Chang. Biol.* 20, 2183–97. <https://doi.org/10.1111/gcb.12580>

Turner, A.J., Frankenberg, C., Wennberg, P.O., Jacob, D.J., 2017. Ambiguity in the causes for decadal trends in atmospheric methane and hydroxyl. *Proc. Natl. Acad. Sci.* 114, 5367–5372. <https://doi.org/10.1073/pnas.1616020114>

Umezawa, T., Machida, T., Aoki, S., Nakazawa, T., 2012. Contributions of natural and anthropogenic sources to atmospheric methane variations over western Siberia estimated from its carbon and hydrogen isotopes. *Global Biogeochem. Cycles* 26, n/a-n/a. <https://doi.org/10.1029/2011GB004232>

Updegraff, K., Bridgman, S.D., Pastor, J., Weishampel, P., Harth, C., 2001. Response of CO₂ and CH₄ emissions from peatlands to warming and water table manipulation. *Ecol. Appl.* 11, 311–326. [https://doi.org/10.1890/1051-0761\(2001\)011\[0311:ROCACE\]2.0.CO;2](https://doi.org/10.1890/1051-0761(2001)011[0311:ROCACE]2.0.CO;2)

Vaughn, L.J.S., Conrad, M.E., Bill, M., Torn, M.S., 2016. Isotopic insights into methane production, oxidation, and emissions in Arctic polygon tundra. *Glob. Chang. Biol.* 22, 3487–3502. <https://doi.org/10.1111/gcb.13281>

Vermeesch, P., 2018. IsoplotR: A free and open toolbox for geochronology. *Geosci. Front.* <https://doi.org/10.1016/j.gsf.2018.04.001>

Wahlen, M., Tanaka, N., Henry, R., Deck, B., Broeker, W., Shemesh, A., Fairbanks, R., Vogel, J.S., Southon, J., 1990. ¹³C, ¹⁸O, and ¹⁴C in methane, in: *NASA Upper Atmosphere Research Program: Research Summaries 1988-1989*.

Ward, S.E., Bardgett, R.D., McNamara, N.P., Adamson, J.K., Ostle, N.J., 2007. Long-term consequences of grazing and burning on northern peatland carbon dynamics. *Ecosystems* 10, 1069–1083. <https://doi.org/10.1007/s10021-007-9080-5>

Ward, S.E., Ostle, N.J., Oakley, S., Quirk, H., Henrys, P. a, Bardgett, R.D., 2013. Warming effects on greenhouse gas fluxes in peatlands are modulated by vegetation composition. *Ecol. Lett.* 1285–1293. <https://doi.org/10.1111/ele.12167>

Wehr, R., Saleska, S.R., 2017. The long-solved problem of the best-fit straight line: application to isotopic mixing lines. *Biogeosciences* 14, 17–29. <https://doi.org/10.5194/bg-14-17-2017>

Whiticar, M.J., 1999. Carbon and hydrogen isotope systematics of bacterial formation and

oxidation of methane. *Chem. Geol.* 161, 291–314. [https://doi.org/10.1016/S0009-2541\(99\)00092-3](https://doi.org/10.1016/S0009-2541(99)00092-3)

Yarnes, C., 2013. $\delta^{13}\text{C}$ and $\delta^2\text{H}$ measurement of methane from ecological and geological sources by gas chromatography/combustion/pyrolysis isotope-ratio mass spectrometry. *Rapid Commun. Mass Spectrom.* 27, 1036–1044. <https://doi.org/10.1002/rcm.6549>

York, D., 1969. Least squares fitting of a straight line with correlated errors. *Earth Planet. Sci. Lett.* 5, 320–324. [https://doi.org/10.1016/S0012-821X\(68\)80059-7](https://doi.org/10.1016/S0012-821X(68)80059-7)

Yvon-Durocher, G., Allen, A.P., Bastviken, D., Conrad, R., Gudas, C., St-Pierre, A., Thanh-Duc, N., del Giorgio, P.A., 2014. Methane fluxes show consistent temperature dependence across microbial to ecosystem scales. *Nature* 507. <https://doi.org/10.1038/nature13164>

Zhang, G., Ma, J., Yang, Y., Yu, H., Shi, Y., Xu, H., 2017. Variations of Stable Carbon Isotopes of CH_4 Emission from Three Typical Rice Fields in China. *Pedosphere* 27, 52–64. [https://doi.org/10.1016/S1002-0160\(15\)60096-0](https://doi.org/10.1016/S1002-0160(15)60096-0)

Zhang, Z., Zimmermann, N.E., Stenke, A., Li, X., Hodson, E.L., Zhu, G., Huang, C., Poulter, B., 2017. Emerging role of wetland methane emissions in driving 21st century climate change. *Proc. Natl. Acad. Sci.* 114, 9647–9652. <https://doi.org/10.1073/pnas.1618765114>

4.7 Supplementary material

4.7.1 Supplementary tables

Table S 4.1 Mean temperatures and total rainfall in study years.

	2015		2016		2017	
	Jan-May,		Jan-May,		Jan-May,	
	Dec	Jun-Nov	Dec	Jun-Nov	Dec	Jun-Nov
Air temp. (°C)	2.9	8.7	3.1	9.1	3.7	9.0
30 cm soil temp. (°C)	4.7*	8.4	4.4	9.2	4.7	9.1
Rainfall (mm)	1250	967	860	848	747	1270

* Soil temperature data missing from January 22 to March 18 2015 due to instrument failure.

Table S 4.2 Species composition within each static chamber collar. Abundance is measured using the DAFOR scale, with dominant (D), abundant (A), frequent (F), occasional (O) and rare (R) composition categories; (-) marks species absence.

Plot number	Dwarf shrub		Graminoid		Moss					Monocot	Litter
	<i>Calluna vulgaris</i>	<i>Erica tetralix</i>	<i>Eriophorum cespitosum</i>	<i>Trichophorum cespitosum</i>	<i>Sphagnum papillosum</i>	<i>Sphagnum capillifolium</i>	<i>Sphagnum magellanicum</i>	<i>Hypnum jutlandicum</i>	<i>Plagiothecium undulatum</i>	<i>Narthecium ossifragum</i>	
1	A	-	A	-	-	O	O	F	R	R	F
2	F	-	F	-	-	D	-	O	R	O	O
3	O	O	F	-	O	F	-	O	-	-	F
4	D	-	A	-	D	O	-	O	-	-	F
5	F	A	F	F	-	-	-	-	-	-	A

4.7.2 Supplementary figures

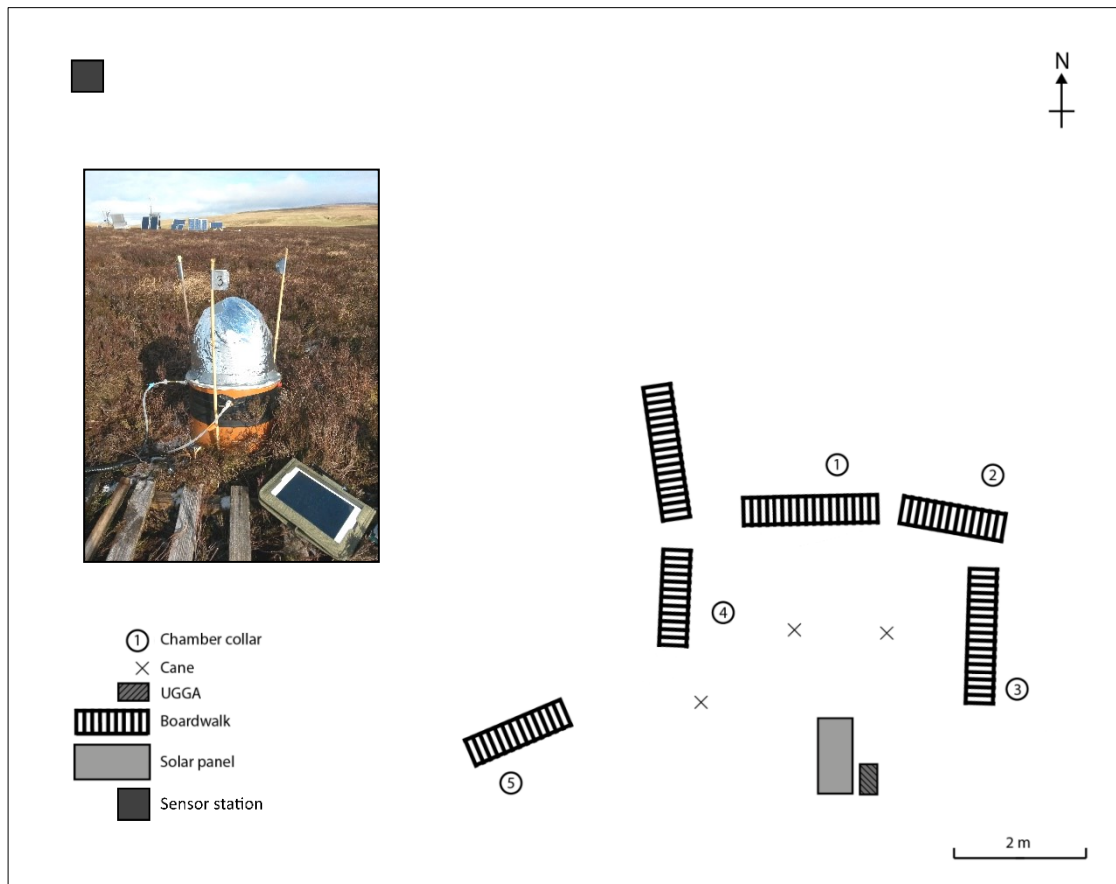


Figure S 4.1 Illustration of sampling setup. Boardwalks were placed next to chamber collars to minimise disturbance of the peat (see insert). For flux measurements, the UGGA was powered by a deep cycle battery charged with a solar panel. For peat core sampling, samples were collected around a centre point marked with a cane. Soil temperature, moisture, water table, and soil water chemistry measurements were performed at the sensor station.

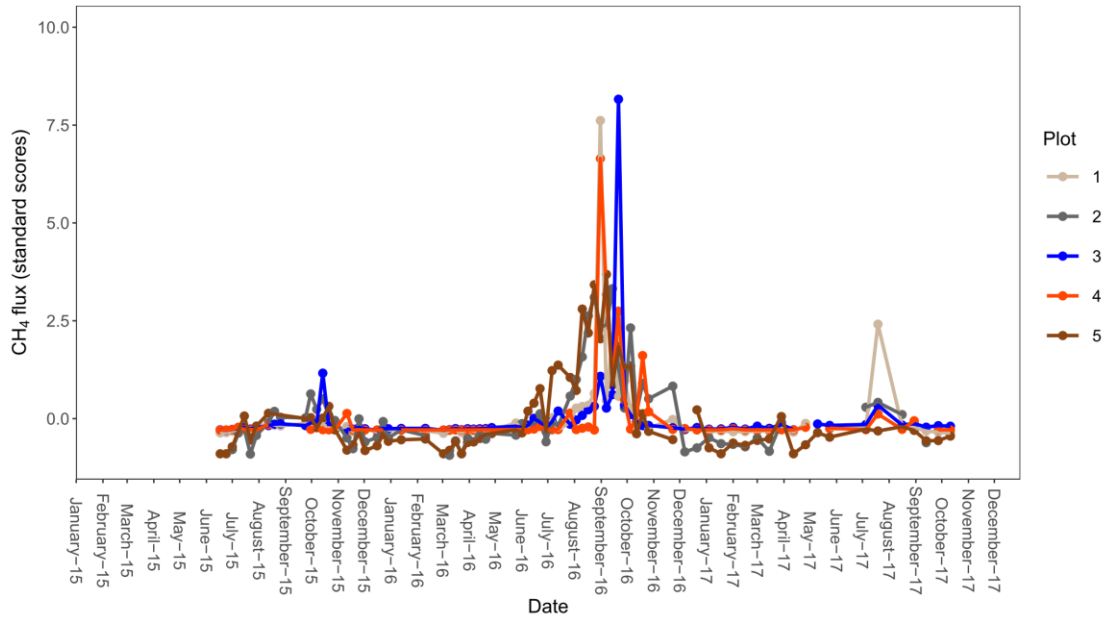


Figure S 4.2 Scaled CH₄ flux values obtained by subtracting the mean and dividing by the standard deviation for each chamber.

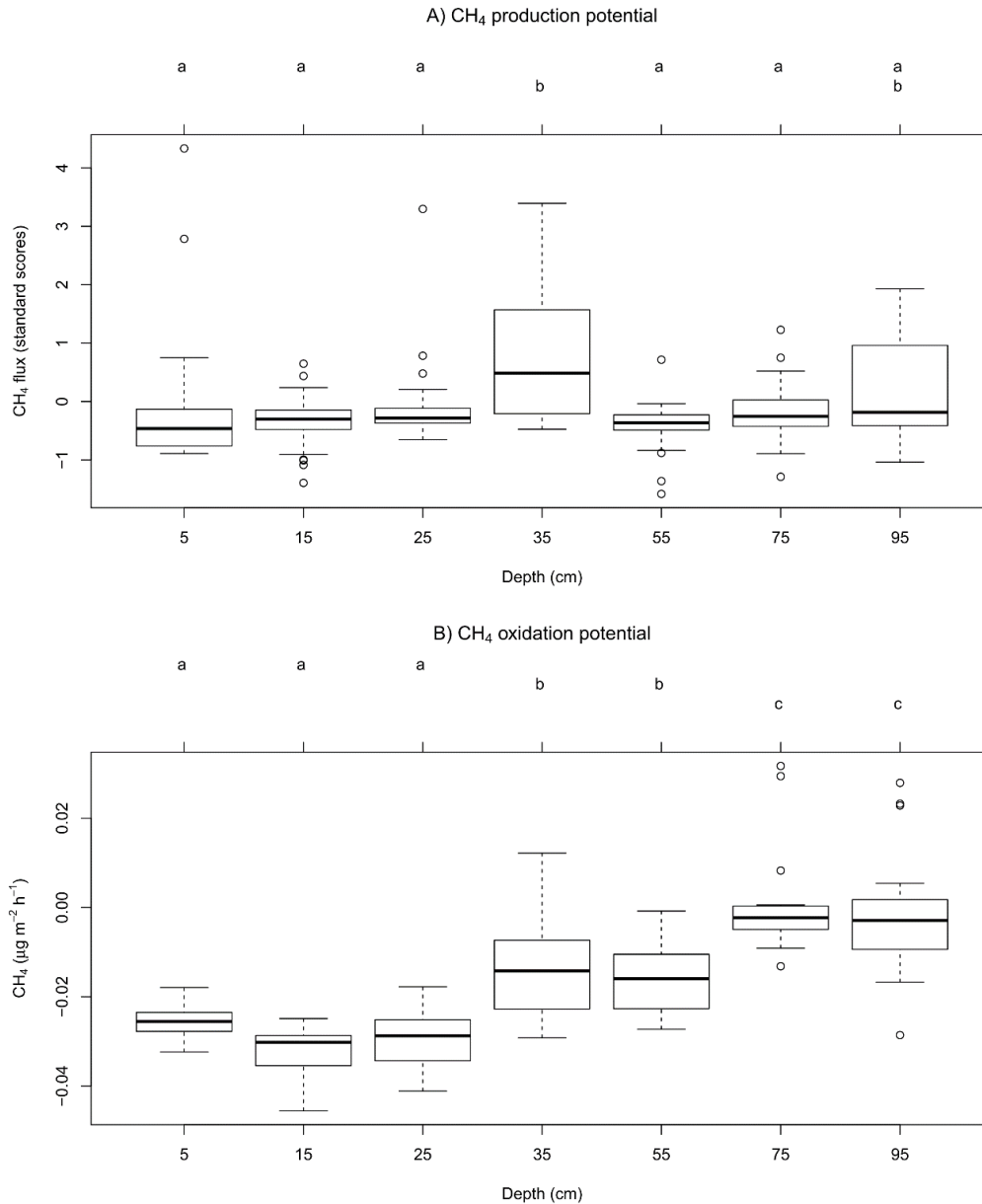


Figure S 4.3 Potential CH₄ production A) and potential CH₄ oxidation B) at different mean depth. Data is combined from seven individual incubation experiments. Different letters below box-plots indicate significant differences between groups. Note that for A) flux rates were standardised to account for seasonal differences in production rates. Note that negative fluxes indicate CH₄ oxidation, positive fluxes CH₄ production.

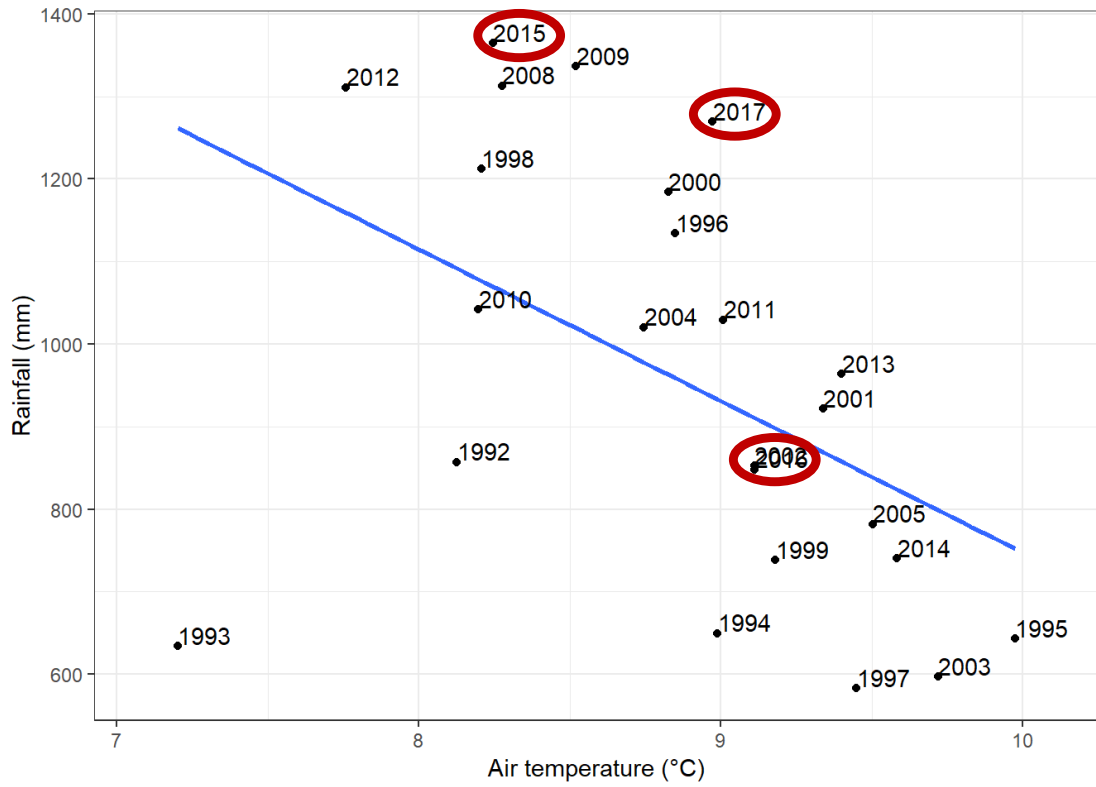


Figure S 4.4 June to November rainfall plotted against mean temperature at Moor House National Nature Reserve from 1992 to 2017. Study years circled. Years 2006 and 2007 removed due to missing data.



Figure S 4.5 Vegetation within each sampling plot.

5

General discussion

Improving our understanding of the CH₄ cycle depends on investigating its key processes, improving the data available to constrain emissions estimates, as well as improving the methods used to obtain such data. In this PhD, I have employed a variety of methods across temporal and spatial scales, with the aim to further our understanding in some of the key research areas around CH₄ emissions: 1) the development and critical evaluation of new measurement technologies for identifying and characterising emissions; 2) dual-isotope characterisation of regional emission categories; 3) baseline identification and attribution of emission sources, before the start of shale gas extraction in North West England; and 4) investigation of seasonal changes in wetland emissions and their stable isotope signatures.

5.1 Mobile measurements

When comparing the performance of CH₄ gas analysers in a mobile system, I found that slower instrument response times lead to greater underestimation of atmospheric concentrations, both while driving, and during static measurements. This limits the comparability of concentration measurements obtained with different instrumental setups or collected at different driving speeds. However, for mobile measurements, the integral of concentration with respect to distance is constant, regardless of instrument speed. For mobile isotopic measurements with a given instrument, the precision of the measurement depends primarily on the concentration range measured and, to a certain extent, the duration of the measurement. The model I wrote to simulate mobile isotopic measurements can predict achievable isotopic precision under given sampling conditions.

These findings can inform sampling strategies and choice of instruments and provide a framework to interpret the results obtained from different instrumental setups.

Mobile measurements in the Fylde and Morecambe bay area detected emissions from landfills, multiple gas leaks, and a gas terminal. For these larger emission sources, it was possible to determine the $\delta^{13}\text{C}$ signature with sufficient accuracy to unambiguously attribute them as microbial or thermogenic emissions. For more diffuse or distant sources, such as agricultural emissions, sampling conditions did not allow for sufficiently precise estimates, while background $\delta^{13}\text{C}$ signatures were more depleted overall in areas with agricultural land use. Overall, there are notable emission sources in the study area, and care must be taken when attributing any additional emissions which may arise from shale gas extraction. This is particularly true for gas leaks, which have a thermogenic emission signature, and can be found randomly in areas with gas distribution pipelines, which were a significant source of emissions in the study area.

5.2 Emission source characterisation

5.2.1 Dual isotope source signatures

For this PhD project, I collected CH_4 samples for dual-isotope analysis from a range of emission sources. Plotting the dual isotope data against the classic $^{13}\text{C}/^2\text{H}$ plot by Whiticar (1999), we can observe broad agreement with the main formation mechanisms of CH_4 , and their relation to different source categories (Figure 5.1). There are, however, some notable patterns. The atmospheric samples collected at coastal and inland locations clearly deviate from the global atmospheric background and are shifted towards the range of thermogenic emissions with regards to both $\delta^{13}\text{C}$ and $\delta^2\text{H}$. This indicates an influence of natural gas emissions in air reaching the English coast from the Irish Sea. The natural gas samples cluster within the thermogenic range, as natural gas in the UK originates primarily from the North Sea and has a small microbial component (Lowry et al., 2001). As such, natural gas emissions are clearly distinguishable from all microbial sources in the region. Agricultural and landfill gas emissions form distinct clusters and are mainly distinguishable by their ^2H signatures. Wetland emissions show contrasting trends depending on ecosystem type. The two peat bogs, Moor House and Roudsea Wood, are most depleted in ^{13}C with δ -values around -80 ‰. The samples from the coastal reed bed, Leighton Moss, are more enriched in ^{13}C , but are more depleted in ^2H , suggesting differences in the underlying microbial formation and oxidation as well as transport processes. Relatively few studies on

CH₄ isotopes perform ²H analysis in addition to ¹³C analysis. Due to higher variability and the overlap between $\delta^2\text{H}$ values of microbial and thermogenic emissions, ²H in isolation is less useful in distinguishing emission sources (Whiticar, 1999). However, the comprehensive data set I have collected demonstrates that performing dual-isotope analysis can distinguish between emission sources that overlap in their $\delta^{13}\text{C}$ ratios and provide valuable insights into the dynamics underlying CH₄ emissions.

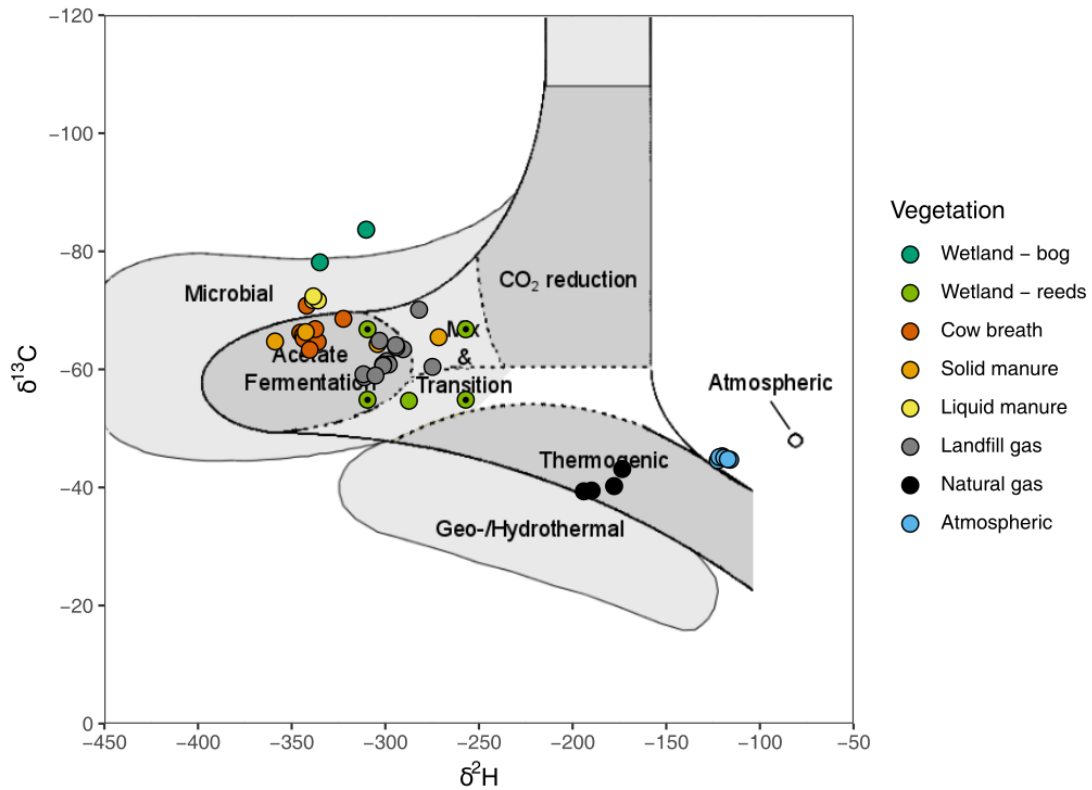


Figure 5.1 Dual-isotope samples collected during this PhD project from different sources plotted against CH₄ formation mechanisms as adapted from Whiticar (1999). Data points with a black dot represent possible combinations of $\delta^{13}\text{C}$ and $\delta^2\text{H}$ shown in Figure 4.8 & Figure 4.9.

5.3 Future research

5.3.1 Wetland ecosystems

The isotopic data collected from emissions at Moor House, Leighton Moss, and Roudsea Wood provides a nuanced picture of wetland CH₄ emissions. To better represent CH₄ emissions in earth system models, and to predict their response under a changing climate, requires an improved mechanistic understanding of the biotic and abiotic processes that

drive these emissions. The uncommonly high emissions found in 2016 at Moor House represent an event that is challenging to fully evaluate because of its rarity and therefore limited data. However, such rare events have the potential to provide important insights into the functioning of ecosystems, and how they might respond to environmental change. Expanding the use of long-term monitoring programs using either manual or automated methods, such as automated chamber measurements or eddy covariance, could capture such events and provide critical insights into the functioning of wetland ecosystems. The use of experimental studies manipulating environmental variables, and often simulating extreme events, such as heatwaves, drought, or heavy rainfall, are also crucially important to develop such understanding, but need to be informed by, and their findings tested against, observational studies in uncontrolled settings.

For an accurate representation of wetland emissions in atmospheric inversion models, knowledge of bulk emission signatures is key. However, as wetlands are the largest source of uncertainty in the global CH₄ budget, a thorough understanding of what drives isotopic emission signatures is needed to understand and predict changes over time and space. My research at Moor House has shown that emission signatures can be stable over a multi-year period and changing environmental conditions within a site, despite variable plant composition in each plot. Conversely, measurements at Leighton Moss and Roudsea Wood indicate that changes in vegetation structure and location lead to considerable variation in emission signatures at these sites. Other studies have also found evidence for seasonal variations in emissions signatures (Fisher et al., 2017; Sriskantharajah et al., 2012). For a better understanding of CH₄ emission signatures in wetlands, research that covers a variety of vegetation types and locations is required. Elucidating the underlying biotic and abiotic mechanisms will likely require comprehensive approaches, combining isotopic measurements with microbiological and molecular analysis, as well as vegetation and physical processes in wetlands, involved in the production and oxidation of CH₄.

5.3.2 Mobile emission measurements and isotopic characterisation

The field of mobile CH₄ measurements is rapidly developing as new, faster, cheaper, and more portable devices are developed, as well as those which can identify multiple species of gases. Mobile measurements of CH₄ are a comparatively efficient way to investigate emissions and may be one of the most effective methods to routinely investigate fugitive emissions from industrial sources and gas distribution pipelines. If such monitoring were more widely adopted, it could also provide data for more general monitoring of CH₄

emissions from other sources, while use of multi-species analysers could simultaneously inform on emissions of other air pollutants (Kapsalidis et al., 2018). A key challenge currently is to develop suitable sampling protocols and modelling applications to fully utilise such data such that it can inform regional emission estimates.

My results in this PhD project have demonstrated the value of dual-isotope analysis for attributing CH₄ emissions, and adding ²H ratios to atmospheric models may improve model performance (Warwick et al., 2016). Use of mobile systems to collect samples for dual-isotope analysis may provide an efficient way to build databases of integrated emission signatures. While the utility of δ²H measurements in atmospheric inversion models is currently limited by the paucity of atmospheric ²H records (Rice et al., 2016; Warwick et al., 2016), it could aid future efforts to constrain the global CH₄ cycle.

5.4 References

- Fisher, R.E., France, J.L., Lowry, D., Lanoisellé, M., Brownlow, R., Pyle, J.A., Cain, M., Warwick, N., Skiba, U.M., Drewer, J., Dinsmore, K.J., Leeson, S.R., Bauguitte, S.J., Wellpott, A., Shea, S.J.O., Allen, G., Gallagher, M.W., Pitt, J., Percival, C.J., Bower, K., George, C., Hayman, G.D., Aalto, T., Lohila, A., Aurela, M., Laurila, T., Crill, P.M., Mccalley, C.K., Nisbet, E.G., 2017. Measurement of the ^{13}C isotopic signature of methane emissions from northern European wetlands. *Global Biogeochem. Cycles* 31, 605–623. <https://doi.org/10.1002/2016GB005504>
- Kapsalidis, F., Shahmohammadi, M., Süess, M.J., Wolf, J.M., Gini, E., Beck, M., Hundt, M., Tuzson, B., Emmenegger, L., Faist, J., 2018. Dual-wavelength DFB quantum cascade lasers: sources for multi-species trace gas spectroscopy. *Appl. Phys. B Lasers Opt.* 124, 1–17. <https://doi.org/10.1007/s00340-018-6973-2>
- Lowry, D., Holmes, C.W., Rata, N.D., O'Brien, P., Nisbet, E.G., 2001. London methane emissions: Use of diurnal changes in concentration and $\delta^{13}\text{C}$ to identify urban sources and verify inventories. *J. Geophys. Res. Atmos.* 106, 7427–7448. <https://doi.org/10.1029/2000JD900601>
- Rice, A.L., Butenhoff, C.L., Teama, D.G., Röger, F.H., Khalil, M.A.K., Rasmussen, R.A., 2016. Atmospheric methane isotopic record favors fossil sources flat in 1980s and 1990s with recent increase. *Proc. Natl. Acad. Sci. U. S. A.* 113, 10791–6. <https://doi.org/10.1073/pnas.1522923113>
- Sriskantharajah, S., Fisher, R.E., Lowry, D., Aalto, T., Hatakka, J., Aurela, M., Laurila, T., Lohila, A., Kuitunen, E., Nisbet, E.G., 2012. Stable carbon isotope signatures of methane from a Finnish subarctic wetland. *Tellus B* 64, 1–8. <https://doi.org/10.3402/tellusb.v64i0.18818>
- Warwick, N.J., Cain, M.L., Fisher, R., France, J.L., Lowry, D., Michel, S.E., Nisbet, E.G., Vaughn, B.H., White, J.W.C., Pyle, J.A., 2016. Using $\delta^{13}\text{C}\text{-CH}_4$ and $\delta\text{D}\text{-CH}_4$ to constrain Arctic methane emissions. *Atmos. Chem. Phys.* 16, 14891–14908. <https://doi.org/10.5194/acp-16-14891-2016>
- Whiticar, M.J., 1999. Carbon and hydrogen isotope systematics of bacterial formation and oxidation of methane. *Chem. Geol.* 161, 291–314. [https://doi.org/10.1016/S0009-2541\(99\)00092-3](https://doi.org/10.1016/S0009-2541(99)00092-3)